STRUCTURE/FUNCTION OF THE GAMMA REGULATORY DITHIOL DOMAIN OF THE CHLOROPLAST ATP SYNTHASE

By

Hardeep S. Samra

B.S., University of Kansas, 2001
B.S., University of Kansas, 2001

Submitted to the Department of Molecular Biosciences and the
Faculty of the Graduate School of the University of Kansas
In partial fulfillment of the requirements for the degree of
Doctor of Philosophy

_____
Chairperson – Mark Richter

Committee members: _____
Paul Kelly

_____
Cindy Berrie

_____
Audrey Lamb

_____
Krzyzstof Kuczera

Date defended: 4/10/2007

The Dissertation Committee for Hardeep Samra certifies
that this is the approved version of the following dissertation:

STRUCTURE/FUNCTION OF THE GAMMA REGULATORY DITHIOL DOMAIN OF THE CHLOROPLAST ATP SYNTHASE

Committee:

_____
Chairperson – Mark Richter

_____
Paul Kelly

_____
Cindy Berrie

_____
Audrey Lamb

_____
Krzyzstof Kuczera

Date approved: 4/13/2007

Abstract

Strategically-placed dithiols act as photo-switches regulating the catalytic rates of several key enzymes in higher plants, thereby governing photosynthetic output. One such dithiol within the γ subunit of the chloroplast ATP synthase acts in concert with the inhibitory ε subunit to block nonproductive ATP hydrolysis, preventing depletion of essential ATP pools in the dark when photosynthetic electron transport is inactive. The critical γ dithiol is located within a special regulatory domain in the γ subunit of the F_1 segment of the photosynthetic ATP synthase. We recently published a homology model of the three-dimensional structure of the γ subunit from higher plants that provides significant new insight into how the redox state of the dithiol may regulate catalysis. Studies described in this dissertation elucidate the mechanism by which this critical regulatory process occurs.

A series of deletion mutants were designed to structurally map the regulatory domain of the γ subunit as well as an additional extra loop region in the homology model identified as having a possible involvement in dithiol regulation. Deleting major regions of the regulatory domain, as well as the central portion of the extra loop, relieved the inhibition of ATPase activity normally observed after oxidation of the regulatory dithiol. Deletions within the regulatory domain did not affect inhibition of ATPase activity by the epsilon subunit, whereas deletions of the extra loop region severely impaired the ability of ε to inhibit ATPase activity. The data suggest a model by which the C-terminal arm of ε subunit binds across both the regulatory domain and the extra loop region of the γ subunit.

To determine the role of interdomain motion within the γ subunit, cysteines were engineered at locations expected to lead to cross-linking between the N- and C-terminal helices, and between the C-terminal helix and the central domain of the γ subunit. Cross-

links formed in all cases but did not interfere with catalysis, suggesting certain large-scale domain movements are not necessary for dithiol regulation. The $\gamma^{V31C,A276C}$ mutant reduced MgATPase activity and ATP synthesis, suggesting certain γ-β interactions are critical for proton coupled activation.

Single molecule fluorescence experiments were designed to characterize the dynamic motion of the regulatory domain by measuring changes in fluorescence amplitude of a thiol reactive probe placed on one of the two γ dithiols that form the regulatory disulfide. Autocorrelation time constants were generated from surface immobilized, labeled protein samples. Inhibiting the enzyme with AMP-PNP resulted in a significant increase in the frequency of fluorescence amplitude shifts indicating the presence of a nucleotide-dependent change in the conformation of the regulatory domain.

Acknowledgements

I would like to thank all of those who helped me with my research and education during my graduate career. I would like to acknowledge Drs. Fei Gao and Zugen Chen for creating and characterizing some of the deletion mutations within the regulatory domain presented in Chapter 2. Drs. Ward Tucker and Ray Hein provided guidance in learning all of the standard procedures used in the Richter lab during my time as an undergraduate research associate in the lab. I would also like to acknowledge Andrew Giessel who, under the guidance of Dr. Krzyzstof Kuczera, created the γ subunit homology model and conducted the molecular dynamics simulations discussed throughout this dissertation. I would like to thank Etter Hoang for creating several of the deletions characterized in Chapter 2. Nick Degner was also a great help in assembly of the mutant hybrid protein enzymes characterized in Chapter 3.

I also would like to acknowledge Dr. Carey Johnson and his research group for significant guidance in the single-molecule experiments described in Chapter 4. Specifically, I would like to thank Jay Unruh, Brian Slaughter, and Shane Price, who were very helpful in the data collection and analysis in Chapter 4.

I would also like to thank my committee members for reading this dissertation, especially Drs. Audrey Lamb and Krzyzstof Kuczera who served as the readers. For his continued support and friendship throughout our time in graduate school, as well as significant contributions to the research in this dissertation, I would like to thank Feng He. Lastly, a very special thank you goes to my advisor, Dr. Mark Richter. His scientific expertise and advice throughout the course of my graduate career contributed significantly to the success I have experienced while at KU.

TABLE OF CONTENTS

List of Figures

List of Tables

Chapter 1. Introduction

A. An Overview of the F_1F_0-ATP Synthase

Adenosine triphosphate (ATP) is synthesized by oxidative or photosynthetic phosphorylation in most living cells. The newly synthesized ATP is subsequently hydrolyzed to do cellular work and eventually resynthesized. The F_1F_0-ATP synthase can be found on bacterial membranes, the thylakoid membranes of chloroplasts and the inner membranes of the mitochondria. Mitchell's chemiosmotic theory stated that proton-motive force is generated by the movement of protons across the inner membrane of mitochondria to form an electrochemical gradient during photosynthetic and respiratory electron transport (Mitchell, 1961). This proton motive force is used by the F_1F_0-ATP synthase by coupling the movement of protons down the electrochemical gradient to the synthesis of adenosine triphosphate from adenosine diphosphate (ADP) and inorganic phosphate. The primary function of the ATP synthase in most cells is to synthesize ATP; however, it can function as an ATPase in some cells to provide a proton gradient for metabolite transport (Senior, 1990).

The F_1F_0-ATP synthases demonstrate substantial structural similarity, as well as a large degree of amino acid sequence homology within structurally and functionally important regions, indicating that all ATP synthases share a common ancestry. These sequence and structural similarities also suggest that these enzymes use the same basic catalytic mechanism for ATP synthesis and hydrolysis. The ATP synthases of bacteria, mitochondria and chloroplasts are made up of two physical segments, F_0 (coupling factor 0) which is an integral membrane-spanning proton channel, and F_1 (coupling factor 1) which is peripheral to the membrane and contains the catalytic sites for ATP synthesis/hydrolysis. Figure 1 depicts the subunit structures shared by the enzymes from differing organisms. The F_1 segment, also

Figure 1. ***General structure of the Chloroplast ATP synthase.*** The cartoon depicts the subunit structure of the Chloroplast F_1F_0 ATP synthase.

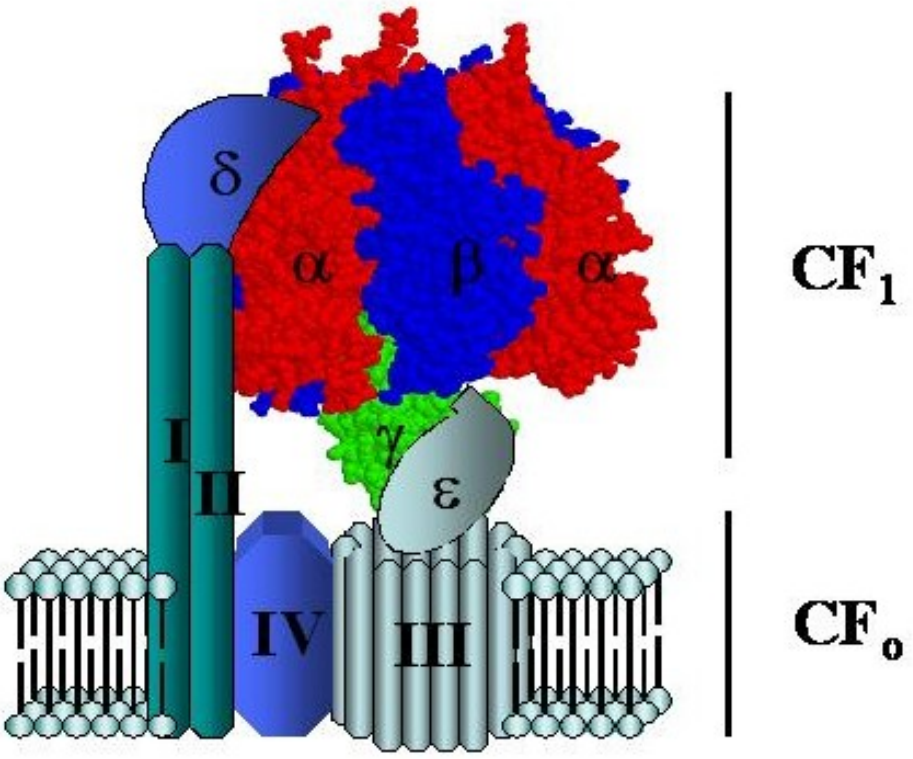
δ
α
β
α
γ
ε
I
II
IV
III
CF1
CFo

known as the catalytic segment, has been isolated and studied from a variety of different sources. The soluble F_1 segment has been widely characterized independently due to its intrinsic ATPase activity.

The F_1 segment is comprised of five different polypeptide subunits, labeled α through ε in order of decreasing molecular weight. Early work defined the F_1 subunit stoichiometry as $\alpha_3\beta_3\gamma_1\delta_1\varepsilon_1$ (Racker, 1961), and the first high resolution crystal structure solved of an F_1 segment from bovine heart mitochondrial F_1 (MF_1) (Abrahams et al., 1994) confirmed that the α and β subunits alternate to form an $\alpha_3\beta_3$ hexamer. The crystal structure indicated the presence of the six different nucleotide binding sites, three of which are catalytic and three are non-catalytic, located at each αβ subunit interface of the hexamer. Each of the catalytic sites is located on the β subunit, while each of the non-catalytic sites is located on the α subunit. The structures of the α and β subunits are similar, each consisting of an N-terminal β-barrel domain, a central nucleotide binding domain, and a C-terminal domain located on the underside (membrane side) of the hexamer in the assembled enzyme.

Less than 50% of the structure of the γ subunit was resolved in the MF_1 structure, but the electron density was sufficient to identify the N- and C-terminal ends of the γ subunit which form a twisted helical pair that extended through the center of the $\alpha_3\beta_3$ hexamer. The structure also indicated several contact points between residues of the $\alpha_3\beta_3$ hexamer and the γ subunit (Figure 2). These contact regions include a foot region on the β subunit as well as a loop region which interacts with the C-terminus of the γ subunit. The extended twisted-helices of the γ subunit extend well beyond the base of the $\alpha_3\beta_3$ hexamer where they connect with a central domain within the γ subunit. This extended portion of the γ subunit forms a central element of the enzyme that bridges the F_1 and F_0 segments. Further crystal structures

Figure 2. ***Subunit Interactions Within the MF_1.*** Three dimensional structure of the bovine F_1-ATPase (PBD accession code: #1BMF). The α subunit (red), β subunit (blue), and the γ subunit (grey) are indicated. Of note are the specific sites of interaction between the β and γ subunits identified in the crystal structure. Hydrophobic resides from loops on the α and β subunits form a "bearing" structure through which the C-terminus of the γ subunit extends. The first catch involves interactions between an anionic loop on a β subunit with C-terminal residues of the γ subunit, whereas the second catch involves interactions between N-terminal residues of the γ subunit and a conserved DELSEED motif on a loop of the β subunit. Figure generated using Rastop (GeneInfinity, New York).

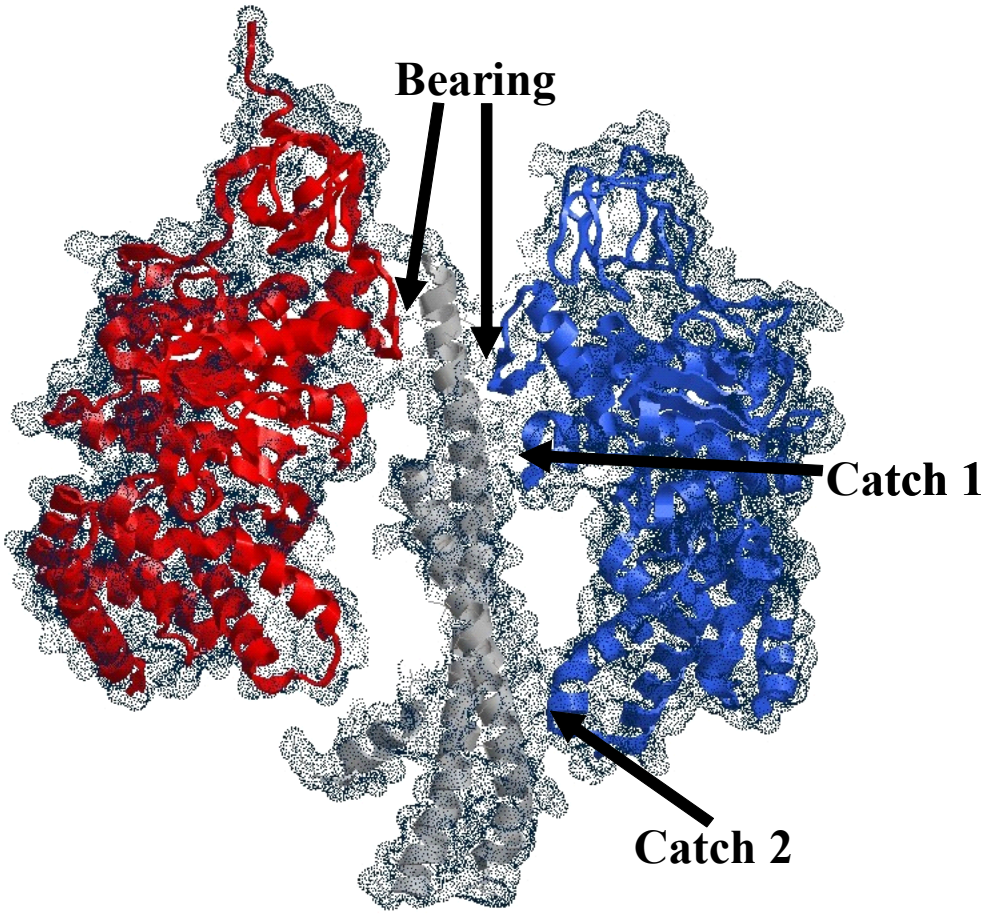
Bearing
Catch 1
Catch 2

show a very similar arrangement of the $\alpha_3\beta_3$ hexamer in the thermophilic F_1 (TF_1) (Shirakihara et al., 1997), the *E.coli* F_1 (EcF_1) (Hausrath et al., 1999), the rat liver MF_1 (Bianchet et al., 1998), and the chloroplast F_1 (CF_1) (Groth and Pohl, 2001). However, the γ subunits were not resolved in these systems. A partial structure of the EcF_1 γ subunit complexed with the ε subunit has been obtained (Rodgers and Wilce, 2000) and is remarkably similar to the corresponding part of MF_1, confirming the structural homology that exists among the different ATP synthases.

The δ subunit has been shown to form contacts with the α subunit and the b subunit of the F_0 (Bragg and Hou, 1986; Bragg and Hou, 1986; Ogilvie et al., 1997; Rodgers et al., 1997; Tozer and Dunn, 1986) consistent with its proposed role in forming part of "stator" element of the F_1F_0 motor. Crystallization and NMR studies of the MF_1 and EcF_1 ε subunits determined that the structure is comprised of an N-terminal β-barrel with ten strands and a C-terminal hairpin comprised of two alpha helices (Uhlin et al., 1997; Wilkens et al., 1995). However, the crystal structure of the MF_1 complex (Gibbons et al., 2000) revealed that the ε subunit was bound in a very different conformation than that observed in the EcF_1. These two different conformations have led to the theory that the ε subunit oscillates between two different conformations, acting as a "rachet" to prevent futile ATP hydrolysis (Capaldi and Schulenberg, 2000). The ε subunit binds directly to the γ subunit (Richter et al., 1985) and also plays a role in bridging the F_1 and F_0 segment.

The number of subunits comprising the F_0 segment varies depending on its origin. The F_0 is comprised of at least three different subunit types in bacteria, four subunits in chloroplasts, and up to ten subunits in mitochondria. In the chloroplast ATP synthase, the F_0 has four different subunits, denoted I-IV. The subunit composition of the F_0 in chloroplasts is $I_1II_1III_{14}IV_1$. In photosynthetic bacteria the a-subunit is analogous to subunit IV, the b-

subunit is analogous to subunit I, the c-subunit is analogous to subunit III, and the b'-subunit is analogous to subunit II (Richter and Gao, 1996). Multiple copies of the hydrophobic III subunit (c-subunit in EcF_1) form a large ring in the lipid bilayer, with the apical interior surface of the ring interacting with the N- and C-termini of the γ subunit and possibly with the epsilon subunit. The hydrophobic subunit IV (or the a-subunit in EcF_1) is also membrane spanning and located adjacent to the subunit III ring. While no structure is available for subunit IV, extensive cross-linking experiments have demonstrated that it has several contact regions with subunits I, II, and III (Fillingame et al., 1998; Fillingame et al., 1998; Schwem and Fillingame, 2006). Further studies indicate that subunit IV is critical for proton translocation and that it is responsible for loading individual protons on to the c subunit ring (Hatch et al., 1995). The N-terminal regions of the b and b' subunits contain a transmembrane domain and the polar C-terminus interacts with the δ subunit of the F_1 segment (Rodgers et al., 1997). The interaction of the subunits I and II with the δ subunit results in formation of the second stalk of the enzyme which connects the F_1 and F_0 segments, forming part of the proposed "stator".

B. The Binding Change Mechanism and Rotational Catalysis

Even after decades of study, the precise mechanism by which the ATP synthase synthesizes and hydrolyzes ATP has yet to be determined. The most remarkable aspect of the bovine MF_1 structure is that it clearly identified three different catalytic sites located primarily on the β subunits: an empty site, a site containing ADP, and one site that contained AMP-PNP, a non-hydrolyzable ATP analogue (Abrahams et al., 1994). The three sites indicated by the crystal structure result from asymmetric interactions between the γ subunit and the $\alpha_3\beta_3$ hexamer. These interactions induce conformational changes within the catalytic

sites located on the β subunits. The $\alpha_3\beta_3$ hexamer, independently, has little appreciable ATPase activity until assembled into the functional core catalytic complex (Gao et al., 1995).

The bovine MF_1 crystal structure supported a model derived from Paul Boyer's *binding change* mechanism, the model of rotational catalysis. Boyer hypothesized that during ATP synthesis the catalytic sites of the enzyme alternate between three different conformational states (Boyer, 1993; Boyer, 1997). The three states are denoted open (empty), loose (ADP bound), and tight (ATP bound), referring to sequential binding and release of substrates and products during energy dependent ATP synthesis (Figure 3). The overall process is highly cooperative: the binding of ADP and inorganic phosphate to one catalytic site initiates the release of ATP at another site.

The model of rotational catalysis suggests that the conformational changes occurring in the catalytic sites during ATP synthesis or hydrolysis are a direct result of the asymmetrical rotation of the γ subunit relative to the $\alpha_3\beta_3$ hexamer. Evidence for this type of catalysis driven by γ subunit rotation was first provided under conditions of ATP hydrolysis (Duncan et al., 1995) and later under conditions of ATP synthesis (Zhou et al., 1997). These experiments involved a series of reversible cross-links introduced between cysteines on both the γ and β subunits. Each β subunit was, in turn, cross-linked individually to the γ subunit during catalysis, demonstrating that the γ subunit changes position relative to each β subunit during the catalytic cycle.

Studies directly demonstrating rotation of the γ subunit were first published by Noji et al (Noji et al., 1997). A fluorescently labeled actin filament was attached to a cysteine residue introduced into the central domain of the γ subunit of TF_1 by a biotin-streptavidin linkage. The enzyme was immobilized onto a glass coverslip prior to attachment of the actin filament, and fluorescence microscopy was used to visualize filament rotation. The

Figure 3. ***Binding Change Mechanism***. Nucleotide binding sites alternate between a low affinity loose (L) site (pink), a high affinity tight (T) site (yellow), and an open (O) site (green) that contains no nucleotide. Protons (H^+) drive rotation of the γ (N-terminal helix in black, C-terminal helix in grey), inducing conformational changes in the three nucleotide binding sites. ATP binding drives γ subunit rotation in the reverse direction.

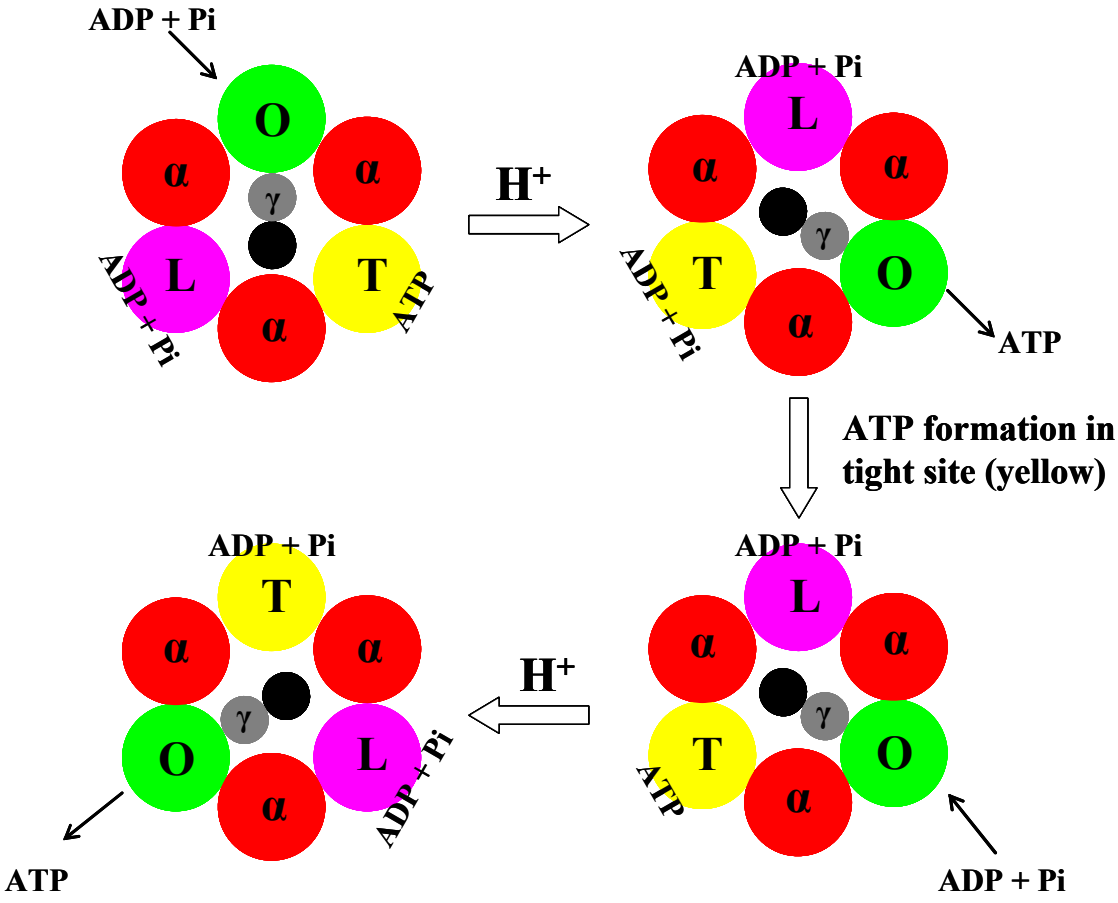
ADP + Pi
O
α
α
γ
L
T
α
ADP + Pi
ATP
H+
ADP + Pi
L
α
α
γ
T
O
α
ADP + Pi
ATP
ATP formation in
tight site (yellow)
ADP + Pi
T
α
α
γ
O
L
α
ADP + Pi
ATP
H+
ADP + Pi
L
α
α
γ
T
O
α
ATP
ADP + Pi

observed actin filament rotation was found to be ATP dependent and could be inhibited by several known F_1 inhibitors. These initial rotation experiments have been further refined and are now used as a standard method for observing γ subunit rotation in the ATP synthases.

During proton-driven rotation (Junge et al., 2001), protons are loaded onto the c-subunit ring through a proton channel on the a-subunit, subsequently resulting in the protonation of an aspartate residue on each c-subunit (Cross, 2000). Using an example of a c-subunit ring of 14 subunits, the loading of each proton is expected to result in a 26° rotation of the c-subunit ring relative to the a subunit. Every proton must travel through the remaining 334° before it is ejected on the opposite side of the membrane via an interaction with the a-subunit. Each 26° rotation exposes another aspartate residue on the lumen side of the membrane and another proton is loaded. The rotational torque generated by the c-subunit ring during proton translocation is transferred to the γ subunit via the ε subunit, resulting in the rotation of the γ subunit and subsequent synthesis of ATP. This model of rotational catalysis has yet to be confirmed experimentally.

The rotation of the γ subunit as a necessary component of catalysis has led to the identification of the ATP synthase as a "rotary engine" (Gumbiowski et al., 2001; Yoshida et al., 2001). Essentially, this name refers to the suggestion that the rotational torque generated by the rotation of the γ subunit can be coupled to perform nanoscale work.

C. Overview of the Chloroplast ATP Synthase

1. Regulation of Catalysis and Activation

One of the remarkable features of the chloroplast ATP synthase is the presence of a special regulatory domain on the γ subunit that most likely evolved to prevent futile hydrolysis of newly synthesized ATP, during dark periods when the electron transport chain

Figure 4. ***Structures of the γ Subunit from bacterial (Ec), mitochondrial (M), and homology model of chloroplast (C) F_1 enzymes***. The N and C-terminal helices of the *E.coli* γ subunit are not solved in the crystal structure. The ε subunit is shown in red and the γ subunit in blue. The regulatory domain (cyan) and the extra loop (green) of the CF_1 γ are also shown. The space-filled residues (yellow) in the chloroplast γ subunit represent γCys199 and γCys205. Figure generated using Rastop (GeneInfinity, New York). (PBD accession codes: #1BMF:MF_1 and #1FSO:EcF_1).

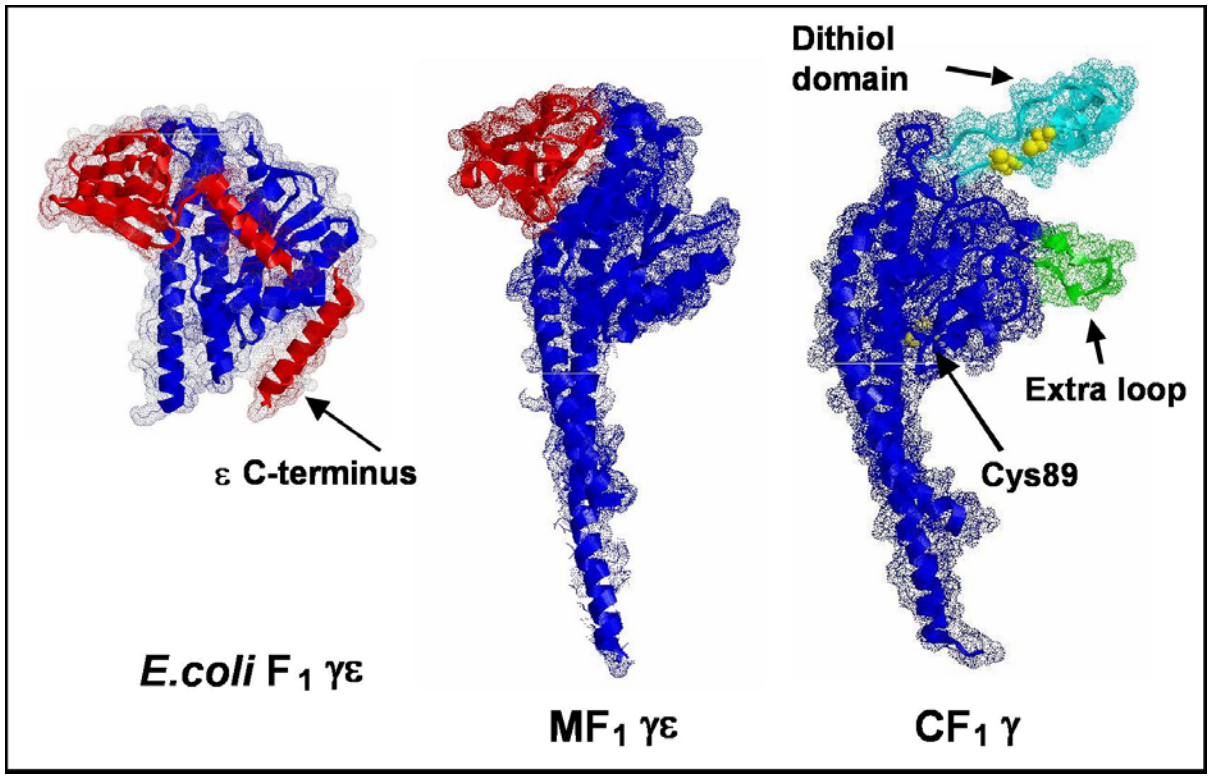
Dithiol
domain
ε C-terminus
Extra loop
Cys89
E.coli F1 γε
MF1 γε
CF1 γ

is inactive (Ort, 1992). A high resolution structure is not available for the chloroplast ATP synthase γ subunit. Recently, however, a homology model of the CF_1 γ subunit was created based on the known structures of the analogous subunits from MF_1 and EcF_1 (Figure 4).

The chloroplast γ subunit contains 4 native cysteines: γCys89, γCys199, γCys205, and γCys322. The chloroplast ATP synthase contains a regulatory domain comprised of 40 amino acids (196-242) that is highly conserved in higher plants (Figure 5). This regulatory domain contains γCys199 and γCys205 which, when oxidized to form a disulfide bond, reduce the catalytic function of the chloroplast enzyme by half at 37°C. The homology model not only provided a working template for the structure of the regulatory domain, but it also identified the presence of another smaller loop structure (residues 65-78) below the regulatory domain (Richter et al., 2005). Molecular dynamics simulations predict that a large amount of movement, upwards of 10Å, between the center of mass of the extra loop domain and the regulatory domain can potentially occur. The simulations also predict that considerable structural rearrangement occurs in the regulatory domain upon disulfide formation (Figure 6). The simulations predict that during disulfide formation, the regulatory domain becomes more compact and associates tightly with the extra loop region. This structure is supported by the observation that the γ subunit, upon oxidation, exhibits an apparent shift in molecular weight during gel electrophoresis (Ketcham et al., 1984).

The chloroplast ATP synthase differs from enzymes in other organisms because it is a latent ATPase. In the absence of a membrane potential or some form of activation, no significant amount of ATP synthesis or hydrolysis is observed. Activation of isolated CF_1 occurs through two events; 1) by reduction of the disulfide bond located in the regulatory domain of the γ subunit, 2) removal of the ε subunit from the enzyme. Both of these

Figure 5. ***Sequence Alignments of the γ subunits from bacterial, mitochondrial, and chloroplast F_1 enzymes.*** The sequence alignments indicate the regulatory domain ($\gamma^{196-242}$) residues (in grey) of the chloroplast γ subunit. Indicated in yellow are the residues comprising the extra loop region ($^{\gamma 65-78}$) of the chloroplast γ subunit.

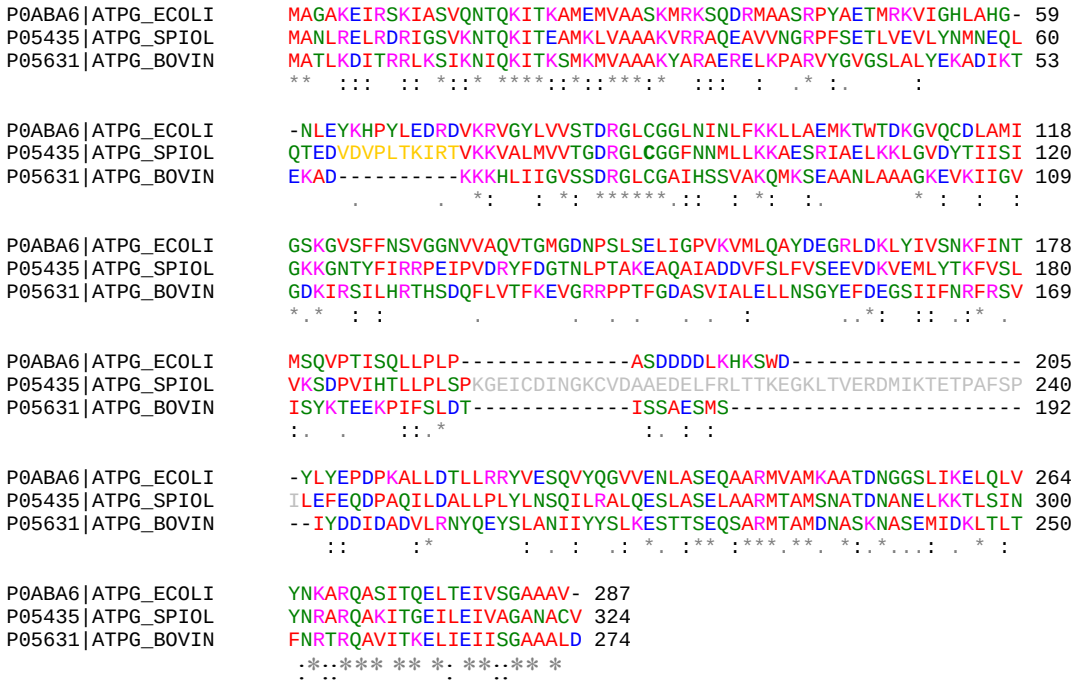
P0ABA6|ATPG_ECOLI MAGAKEIRSKIASVQNTQKITKAMEMVAASKMRKSQDRMAASRPYAETMRKVIGHLAHG- 59
P05435|ATPG_SPIOL MANLRELRDRIGSVKNTQKITEAMKLVAAAKVRRAQEAVVNGRPFSETLVEVLYNMNEQL 60
P05631|ATPG_BOVIN MATLKDITRRLKSIKNIQKITKSMKMVAAAKYARAERELKPARVYGVGSLALYEKADIKT 53
P0ABA6|ATPG_ECOLI -NLEYKHPYLEDRDVKRVGYLVVSTDRGLCGGLNINLFKKLLAEMKTWTDKGVQCDLAMI 118
P05435|ATPG_SPIOL QTEDVDVPLTKIRTVKKVALMVVTGDRGLCGGFNNMLLKKAESRIAELKKLGVDYTIISI 120
P05631|ATPG_BOVIN EKAD----------KKKHLIIGVSSDRGLCGAIHSSVAKQMKSEAANLAAAGKEVKIIGV 109
P0ABA6|ATPG_ECOLI GSKGVSFFNSVGGNVVAQVTGMGDNPSLSELIGPVKVMLQAYDEGRLDKLYIVSNKFINT 178
P05435|ATPG_SPIOL GKKGNTYFIRRPEIPVDRYFDGTNLPTAKEAQAIADDVFSLFVSEEVDKVEMLYTKFVSL 180
P05631|ATPG_BOVIN GDKIRSILHRTHSDQFLVTFKEVGRRPPTFGDASVIALELLNSGYEFDEGSIIFNRFRSV 169
P0ABA6|ATPG_ECOLI MSQVPTISQLLPLP--------------ASDDDDLKHKSWD------------------- 205
P05435|ATPG_SPIOL VKSDPVIHTLLPLSPKGEICDINGKCVDAAEDELFRLTTKEGKLTVERDMIKTETPAFSP 240
P05631|ATPG_BOVIN ISYKTEEKPIFSLDT-------------ISSAESMS------------------------ 192
P0ABA6|ATPG_ECOLI -YLYEPDPKALLDTLLRRYVESQVYQGVVENLASEQAARMVAMKAATDNGGSLIKELQLV 264
P05435|ATPG_SPIOL ILEFEQDPAQILDALLPLYLNSQILRALQESLASELAARMTAMSNATDNANELKKTLSIN 300
P05631|ATPG_BOVIN --IYDDIDADVLRNYQEYSLANIIYYSLKESTTSEQSARMTAMDNASKNASEMIDKLTLT 250
P0ABA6|ATPG_ECOLI YNKARQASITQELTEIVSGAAAV- 287
P05435|ATPG_SPIOL YNRARQAKITGEILEIVAGANACV 324
P05631|ATPG_BOVIN FNRTRQAVITKELIEIISGAAALD 274

Figure 6. ***Molecular Dynamics Simulations of the Modeled CF_1 γ Subunit***. The regulatory dithiol domain (green) shown in the open (left) and closed (right) conformations. The C-terminal helix (cyan) and the N-terminal helix (red) are also shown. The two cysteines of the regulatory dithiol are shown in yellow. The molecular dynamics simulations identified over 10,000 different structures. The two shown are those in which the thiols are closest and farthest apart (Richter et al., 2005).

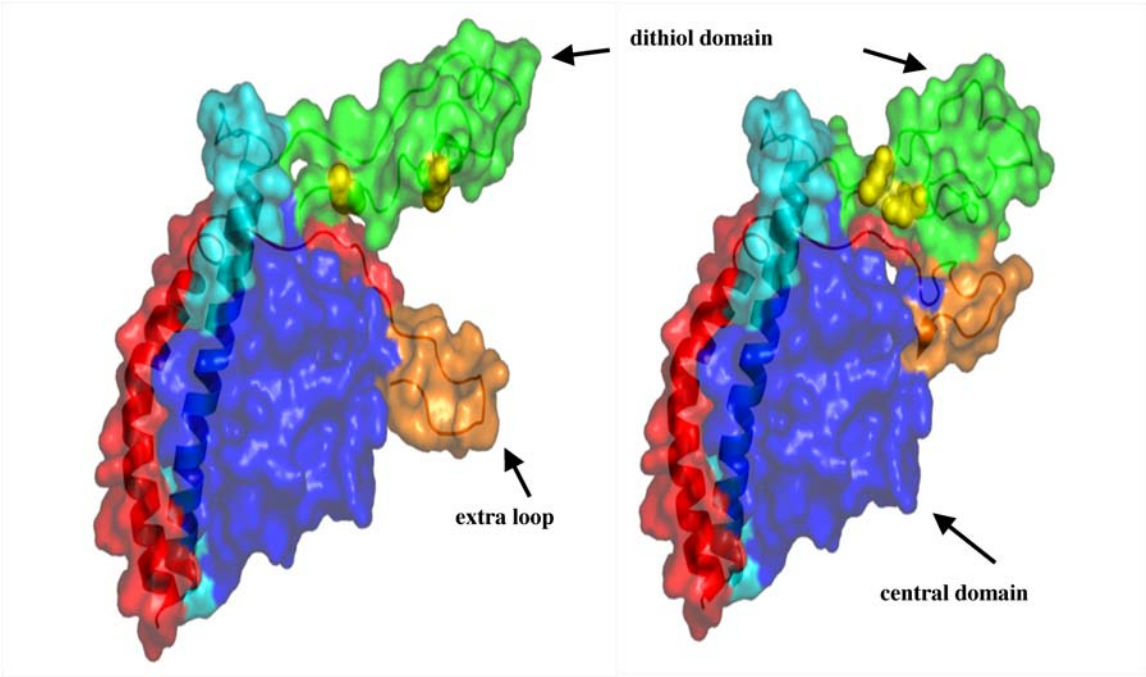
dithiol domain
extra loop
central domain

activation events are related and additive. Reduction of the disulfide bond reduces the affinity of the epsilon subunit by 20-fold, whereas removal of the ε subunit makes the disulfide more accessible to oxidizing and reducing agents (Snyder and Hammes, 1985; Soteropoulos et al., 1992).

Activation of CF_1 when bound to the membrane also requires the reduction of the regulatory disulfide bond which can be achieved artificially by adding a reducing agent, or under physiological conditions by the enzyme thioredoxin. Activation of CF_1 on the membrane not only requires the reduction of the disulfide bond, but also requires a low membrane potential generated by the movement of protons across the membrane (Ketcham et al., 1984). In isolated CF_1, the ε subunit plays an inhibitory role in regulation; however, for membrane bound CF_1, the ε subunit is essential for both ATP synthesis and hydrolysis activities. Both of these processes are proton-coupled on the thylakoid membrane and the ε subunit most likely plays a dual role in bridging the CF_1 and CF_0 segments, as well as regulating hydrolysis.

2. Cation Specificity

One major requirement for both ATP synthesis and hydrolysis by the chloroplast enzyme is the presence of divalent cations. Isolated CF_1 has the ability to hydrolyze both MgATP and CaATP; however, CF_1 coupled to the membrane is specific for magnesium nucleotides (MgADP and MgATP). The rate of ATP hydrolysis of isolated CF_1 in the absence of the ε subunit is 20-40 times greater in the presence of Ca^{2+} than in the presence of Mg^{2+}. This low rate of MgATP hydrolysis can be enhanced by the presence of oxyanions such as bicarbonate or sulfite (Larson, 1989).

The low MgATPase activity stems from the observation that Mg^{2+} is a strong inhibitor of the ATPase activity of CF_1 (Hochman et al., 1976). The mechanism of Mg^{2+} inhibition is complex and depends on nucleotide binding site occupancy as well as the levels of free Mg^{2+} present in the assay medium (Digel et al., 1998). The most likely scenario for the magnesium inhibition is that Mg^{2+} stabilizes binding of product ADP in the catalytic site thus limiting catalytic turnover. Release of MgADP is known to be the rate-limiting step in MgATP hydrolysis. The binding and hydrolysis of ATP at another catalytic site helps destabilize the MgADP bound (Nadanaciva et al., 1999), and release of the MgADP is aided by the presence of oxyanions. The presence of Mg^{2+} inhibits ATP hydrolysis by partially inhibiting nucleotide exchange, while the presence of Ca^{2+} during ATP hydrolysis stimulates nucleotide exchange. The inhibitory MgADP effects observed during ATP hydrolysis are a hallmark of all photosynthetic F_1-ATPases, whereas the inhibition observed in enzymes from other organisms is less pronounced (Hochman et al., 1976). While MgADP inhibition is observed during ATP hydrolysis, it is not a factor in ATP synthesis, which can occur in the presence of very high levels of free Mg^{2+}. The loss of Mg^{2+} inhibition during ATP synthesis is not fully understood, but it is likely due in part to the presence of a trans-membrane proton gradient (Richter et al., 2000). Another interesting facet of this process is that the membrane bound CF_1 is only capable of synthesis of ATP in the presence of Mg^{2+}. The inability of CF_1 to synthesize ATP in the presence of Ca^{2+} is not fully understood.

3. Catalytic structural changes in the γ subunit

Early fluorescence accessibility experiments involving γCys89 and γCys322 have led to insight into a potential structural reorganization of the γ subunit in the chloroplast ATP synthase that occurs during catalysis. γCys89 is known as the "light site" cysteine due to the

observation that it can be labeled with a thiol reactive maleimide probe only when bound to the CF_0 segment and in the presence of a light-induced transmembrane potential (Moroney et al., 1980). γCys322, known as the "dark site" cysteine, can be labeled with a thiol reactive probe while bound to the CF_0 segment on the membrane, or in isolated CF_1 in the dark or light (Moroney et al., 1984). Initially, due to the lack of a high resolution structure of the γ subunit, the cysteine residues of the γ subunit were used to map the location of the γ subunit relative to other parts of CF_1 and CF_0 using fluorescence resonance energy transfer (FRET) (Moroney and McCarty, 1982; Moroney and McCarty, 1982; Moroney et al., 1982; Schumann et al., 1985).

A recently constructed homology model of the chloroplast γ subunit has aided in predicting the position of γCys89 (Figure 7) (Richter et al., 2005). The homology model indicates that γCys89 is located at the interface between a central domain of the γ subunit and a C-terminal alpha helix. It is hypothesized that the exposure of γCys89 during coupled ATP synthesis could be achieved by rotation of the central domain of the gamma subunit relative to the N- and C-terminal twisted helices. This would also support a model in which different domains of the gamma subunit move relative to each other during rotational catalysis. Previous experiments have discovered that labeling γCys89 with thiol reactive maleimide probes in the light strongly inhibits the ATP synthesis and hydrolysis activities of CF_1 (Moroney et al., 1980; Nalin et al., 1983). Additional experiments demonstrated that exposure of membrane-bound CF_1 to bifunctional maleimides during proton driven ATP synthesis resulted in cross-linking between γCys89 and γCys322 (Cerione et al., 1983). The formation of this cross-link not only disrupted the proton permeability of the membrane, but also resulted in inhibition of ATP hydrolysis and synthesis (Moroney and McCarty, 1979).

Figure 7. ***Proposed Orientation of Cys89 in the CF1 γ Subunit.*** γCys89 (yellow) is shown residing in a position adjacent to the N- and C-terminal helices (blue) of the γ subunit (Richter et al., 2005). Also shown in yellow on the left are γCys199 and γCys205.

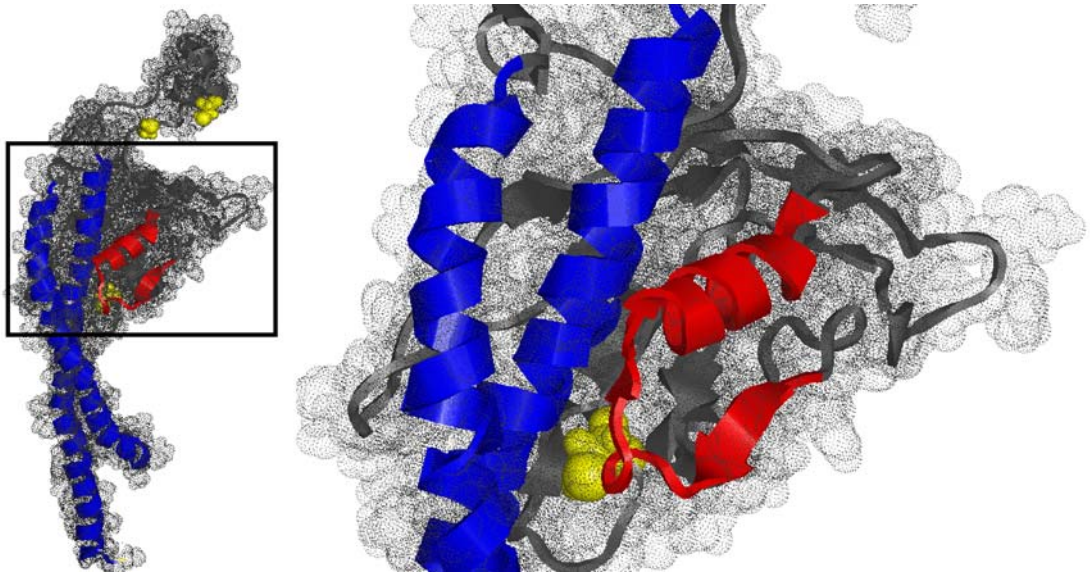

D. Current Research Objectives

Even after decades of study into the catalytic mechanism and the processes of regulation of the F-type ATP synthases, there are a number of questions that remain unanswered. Recent advances in biophysical techniques will hopefully allow more advanced study of these complex enzymes. In regards to the chloroplast ATP synthase, one of the major difficulties is the lack of high resolution structures of the γ and ε subunits. The process of rotational catalysis during ATP synthesis has yet to be fully demonstrated, and the exact subunit interactions of the core catalytic complex that lead to generation of rotational torque are still being elucidated. The main focus of this research is to investigate subunit interactions within the γ subunit during catalysis, and to further characterize the mechanism of redox regulation of the critically-placed dithiol in the γ subunit. The specific objectives of the studies described in this dissertation are:

1. To structurally characterize the dithiol-containing regulatory domain of the γ subunit of the chloroplast ATP synthase.

2. To determine if intra-domain structural changes in the γ subunit of CF1 are necessary for rotational catalysis and regulation.

3. To determine the time-scale of inter-domain movement within the γ subunit, and the role of domain motion in the catalytic cycle and regulation.

Chapter 2. Structural analysis of the regulatory dithiol–containing domain of the chloroplast ATP synthase Gamma subunit

A. Introduction

The two small CF_1 subunits, γ and ε, are involved in regulating CF_1 activity and in coupling the movement of protons across the membrane via CF_O to conformational changes at the catalytic sites on CF_1 during catalysis. Freshly isolated CF_1 is a latent ATPase and can be activated in two ways. First, reduction of the only disulfide bond in the enzyme, formed between Cys199 and Cys205 of the γ subunit, gives rise to partial activation of CF_1 (Nalin et al., 1983). Second, removal of the ε subunit also results in partial activation of the enzyme (Richter et al., 1984). These two effects are additive (Richter and McCarty, 1987).

Either removing ε from CF_1 or reducing the γ disulfide results in exposure of several sites on γ in close proximity to the regulatory dithiol domain that are hypersensitive to trypsin. Concurrent with tryptic cleavage of γ at these sites is the complete loss of inhibition by the ε subunit (Hightower and McCarty, 1996; Richter et al., 1985). A close physical proximity between the ε and γ subunits has also been shown (Richter et al., 1985; Schulenberg et al., 1997), consistent with the current view that these two subunits form part of a rotating spindle (Oster et al., 2000; Richter et al., 2005). Rotation of the γ subunit of CF_1 has been directly observed (Hisabori et al., 1999; Tucker et al., 2004).

On the membrane, the γ and ε subunits of CF_OF_1 both undergo significant conformational changes in response to an imposed transmembrane potential (Ketcham et al., 1984; Richter and McCarty, 1987; Schumann et al., 1985). In the presence of ATP and reducing agents such as dithiothreitol, the imposed potential results in activation of the latent ATPase activity of the enzyme. The conformational state of CF_1 under these activating

conditions closely resembles the ε-deficient state of the soluble enzyme. For example, the same trypsin-sensitive sites on γ as those exposed upon removal of ε from soluble CF_1 become exposed (Hightower and McCarty, 1996; Schumann et al., 1985). At the same time, epitopes on the C-terminus of the ε subunit become exposed to antibodies present in the medium (Nowak and McCarty, 2004; Nowak et al., 2002; Richter and McCarty, 1987), and Lys109 on ε becomes solvent-exposed (Komatsu-Takaki, 1992). Trypsin cleavage of γ in light-energized CF_1 results in uncoupling of ATP synthesis from electron transport (Moroney and McCarty, 1982). The cleaved enzyme, when isolated from thylakoids, is partially deficient in the ε subunit, indicating that ε binding is weakened (Soteropoulos et al., 1992). These studies have led to the hypothesis that the ε subunit may bind in the immediate vicinity of the disulfide bridge on γ where binding masks the disulfide bridge and the trypsin-sensitive sites on γ (Hightower and McCarty, 1996).

To obtain a clearer picture of the relationship between ε and γ in regulation and coupling in CF_1 methods were developed to reconstitute structurally altered γ subunits with isolated $\alpha_3\beta_3$ hexamers resulting in functional $\alpha_3\beta_3\gamma$ core enzyme assemblies (Gao et al., 1995; Hu et al., 1993). In this study, the reconstitution system was used to examine mutant γ subunits with deletions within the dithiol-containing regulatory domain and within an additional loop segment (the extra loop) predicted by modeling studies to interact directly with the dithiol domain. The results identify potential structural requirements for dithiol regulation and provide new insight into how the ε subunit simultaneously couples proton movement to γ rotation and ATP synthesis while blocking the reverse reaction driven by ATP hydrolysis.

B. Experimental Procedures

1. Materials

ATP (grade II) and antibiotics (ampicillin, tetracycline) were purchased from Sigma. Tryptone and yeast extract were obtained from DIFCO. Urea (ultrapure) was purchased from Fluka and hydroxylapatite (HTP) from Bio Rad. All other chemicals were of the highest quality reagent grade available.

CF_1 and CF_1 deficient in the δ and ε subunits, $CF_1(-\delta\varepsilon)$, were prepared from fresh market spinach as described previously (Hu et al., 1993; Penefsky, 1977) and stored as ammonium sulfate precipitates. Prior to use the proteins were desalted on Sephadex G-50 centrifuge columns (Hu et al., 1993; Penefsky, 1977). An $\alpha_3\beta_3$ complex devoid of the γ subunit was isolated from $CF_1(-\delta\varepsilon)$ as described previously (Gao et al., 1995). The $\alpha_3\beta_3$ subunit complex was recycled through the isolation procedure to ensure that trace amounts of contaminating γ subunit were removed.

2. Production and assembly of γ and ε subunits

The *atpG* and *atpE* genes encoding the full length γ (γ^{WT}) and ε subunits respectively were cloned into pET expression vectors as described previously (Chen et al., 1992; Cruz et al., 1995; Johnson and McCarty, 2002) and the constructs were used to transform *E.coli* BL21 host cells for over-expression of the γ and ε proteins. Protein over-expression was induced by addition of isopropylthiogalactoside (Cruz et al., 1995). Inclusion bodies containing the γ protein were solubilized with urea, the protein folded during slow dialysis into urea free buffer and assembled with the isolated, native $\alpha_3\beta_3$ complex as described

previously (Sokolov et al., 1999). Unreconstituted subunits were separated from the reconstituted $\alpha_3\beta_3\gamma$ by anion exchange chromatography (Gao et al., 1995). Similarly, the ε protein was solubilized from inclusion bodies in 8 M urea and folded by the dilution method of Cruz and McCarty (Cruz et al., 1995). The cloned ε subunit was reconstituted with the $\alpha_3\beta_3\gamma$ complex using the same procedure for reconstituting the native ε subunit with $CF_1(-\varepsilon)$ (Richter et al., 1984).

3. Generation of γ mutants

Mutant γ subunits were constructed by enzymatic amplification of the expression plasmid pET8c-gamma.BB1 (Sokolov et al., 1999) using a pair of "inverse" primers with abutting 5' ends. Deletions were generated with primers whose 5' termini defined the endpoints of the deletion. Oligonucleotides were generated with the aid of the Primer Design program (SciEd Software). Primers (obtained from Macromolecular Resources, Colorado State University) were 24-31 nucleotides long and were chemically phosphorylated at the 5' termini. A mutant containing a deletion of γ amino acid residues 197 to 205 ($\gamma^{\Delta 197\text{-}205}$) was constructed using a forward primer with the base sequence corresponding to bases +616 to +640 and a reverse primer with the base sequence corresponding to bases +564 to 568 of the *wild-type atpG* gene. A second mutant containing alanine in place of both of the cysteines at positions 199 and 205 was prepared by substituting GCT in the forward primer for the two Cys codons TGC and TCT starting at positions +622 and +637, respectively. The reverse primer contained the sequence +591 to +615 of the *atpC* coding sequence.

A third γ mutant containing a deletion of amino acid residues from 224 to 240 ($\gamma^{\Delta 224\text{-}240}$) was constructed with the forward primer, 5'-pTA CGA ATT CGA ACA AGA TCC

TGC TC (bases from +721 to +745 with respect to the *atpC* coding sequence), and the reverse primer, 5'-pTA GCT TAC CTT CTT TTG TTG TGA GAC G (bases from +643 to +669 with respect to the *atpC* coding sequence). In this mutant, 51 bps (17 amino acid residues) were deleted relative to the wild-type template (pET8c-gammaBB$_1$) and at the same time γL241 was mutated to Y241. A fourth mutant with the entire region between residues 196 and 241 deleted ($\gamma^{\Delta 197-240}$) was constructed using the forward primer: 5'-pATG ATG TAC TAA TTC GAA CAA GAT (bases +715 to +739 with respect to the *atp*G coding sequence) and the reverse primer: 5'-pTT CGG CGG ATC CTT TTA CTT CTT C (bases +572 to +596 with respect to the *atpG* coding sequence). In this mutant 114 bps (38 amino acid residues) were deleted relative to the wild-type γ template and at the same time γ197-EIC-199 were mutated to 197-SAE-199 and 239-PIL-241 were mutated to 239-MSY-241. An N-terminal γ fragment containing residues 1 to 196 and a C-terminal fragment containing amino acid residues 206 to 322 were generated by restriction nuclease cleavage of pET8cgam-bb1 using NcoI and SalI (the C-terminal fragment) and EcoR1 (the N-terminal fragment). In a series of additional mutants, γ residues V65 to P68, V65-R73, P68-73 and T74-V78 and the entire region V65-V78 were deleted using abutting primers of 24 nucleotides in length.

Plasmid DNA for PCR was prepared either by ethanol precipitation after phenol:chloroform extraction (Sambrook et al., 1989) or using the QIAprep Spin Miniprep kit (Qiagen, Valencia CA). PCR was carried out in 50 μl of cloned *Pfu* DNA polymerase reaction buffer also containing 60 ng of the pET8c-gammaBB$_1$ plasmid as described in detail elsewhere (Sambrook et al., 1989; Tucker et al., 2001). PCR products were purified using the QIAquick gel extraction kit (Qiagen, Valencia CA). The purified DNA was precipitated with ethanol and circularized by incubating 100-200 ng of the DNA with 3 U of T4 DNA ligase

(Promega) in T4 DNA ligase buffer overnight at room temperature. The resulting plasmid was transformed into competent *E.coli* XL1-blue cells. Cloned plasmid was isolated and transformed into the expression host *E.coli* BL21(DE3)/pLysS (Sambrook et al., 1989). The entire sequence of each mutant γ gene was confirmed using the fluorescent dideoxy method (Averboukh et al., 1996).

4. Other procedures

ATPase activities were determined by measuring phosphate release (Taussky and Shorr, 1953) for 5 minutes at 37^{o}C. The assay mixture for calcium-dependent ATPase activity contained 50 mM Tris-HCl (pH 8.0), 5 mM ATP and 5 mM $CaCl_2$. That for magnesium-dependent ATPase activity contained 40 mM Tricine-NaOH (pH 8.0), 4 mM ATP, 2 mM $MgCl_2$ and 50 mM Na_2SO_3 (Hu et al., 1993). Protein concentrations were determined by the Bradford method (Bradford, 1976). Gel electrophoresis was performed under reducing conditions on pre-cast 4-20% gradient gels (Nupage®; Invitrogen, San Diego).

C. Results

1. Mutations within the dithiol domain of the γ subunit.

The recently published (Richter et al., 2005) modeled structure of the CF_1 γ subunit shown in Figure 8 was used as the basis for preparing several mutant forms of the γ subunit (Table 1), partially to examine the structural requirements for the regulatory function of this region of γ, and partially to probe the structural requirement for ε binding and inhibition. There are three recognizable sub-domains within the γ subunit as indicated in Figure 8, a twisted helical domain formed by the extreme N- and C-terminal elements shown in blue, a

Figure 8. ***Structural elements of the CF1 γ subunit.*** The homology-modeled (11) CF_1 γ subunit shows the component structural elements in different colors. Two long N- and C-terminal helices form a twisted helical element that extends into the $\alpha_3\beta_3$ hexamer, acting as a rotating spindle imparting structural asymmetry to the catalytic sites (Abrahams et al., 1994). The regulatory dithiol domain shown in red contains the dithiol sulfhydryls shown in yellow and space-filled. Oxidation of the dithiol to form a disulfide bridge is thought to induce a downward movement of this domain such that it forms a tight (closed) association with the central domain (coloured green) leading to inhibition of catalysis (Richter et al., 2005). A short extra loop element shown in cyan is part of the central domain in the chloroplast γ subunit but is not present in the MF_1 γ subunit. Molecular dynamic simulations suggested that the extra loop forms a close association with the dithiol domain in the closed conformation (Richter et al., 2005).

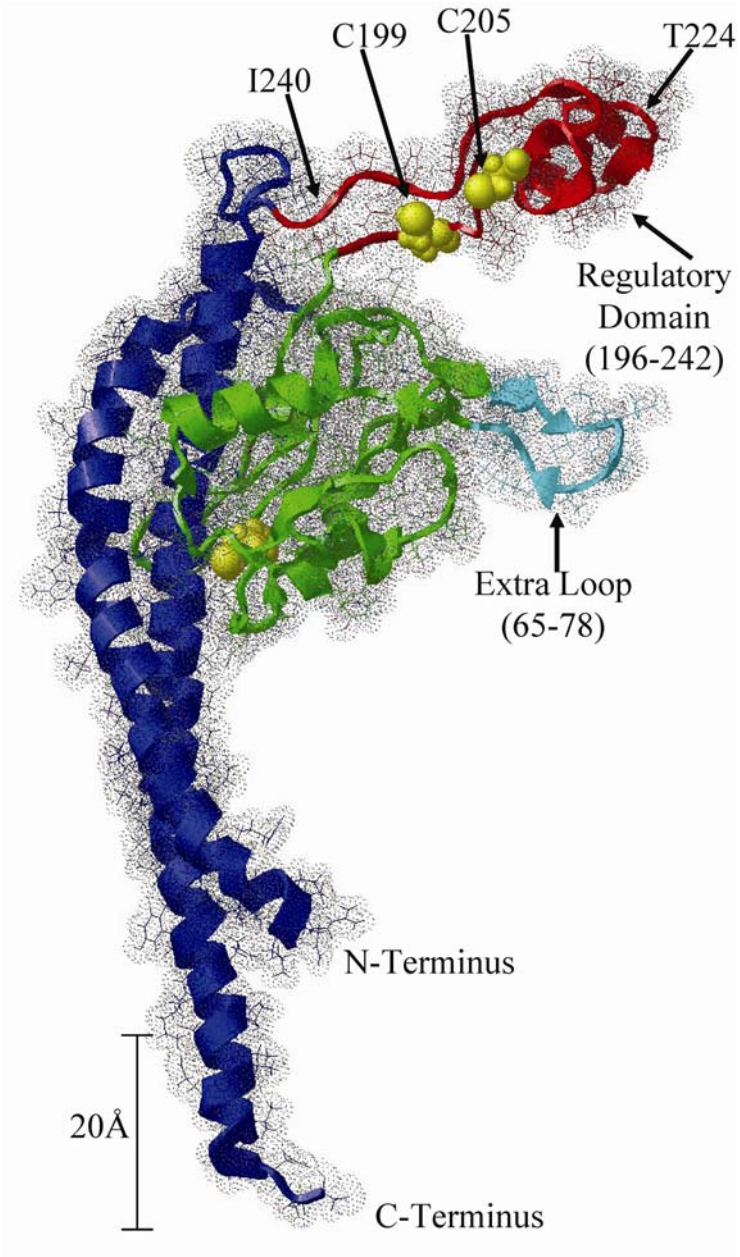
C199
C205
T224
I240
Regulatory
Domain
(196-242)
Extra Loop
(65-78)
N-Terminus
20Å
C-Terminus

Table 1. Recombinant CF_1 γ subunit constructs.

γ Structural element	Mutant γ subunit[1]	Assembly competence[2]
Dithiol domain	$\gamma^{C199A,C205A}$	+
	$\gamma^{\Delta 197\text{-}205}$	+
	$\gamma^{\Delta 224\text{-}240}$	+
	$\gamma^{\Delta 197\text{-}240}$	+
Subfragments	γ^{N}	-
	γ^{C}	-
	$\gamma^{N}+\gamma^{C}$	+
Extra loop	$\gamma^{\Delta 65\text{-}78}$	-
	$\gamma^{\Delta 74\text{-}78}$	+/-
	$\gamma^{\Delta 65\text{-}68}$	+
	$\gamma^{\Delta 65\text{-}73}$	+
	$\gamma^{\Delta 68\text{-}73}$	+

[1]Recombinant γ mutants were reconstituted with native $\alpha_3\beta_3$ and the assemblies purified as described in the *Experimental Procedures*. In the $\gamma^{C199A,C205A}$ mutant, both of the dithiol cysteines were substituted for alanines. In other mutants, the Δ symbol indicates that the residues indicated were deleted from the γ subunit. γ^{N}, is the N-terminal γ fragment comprised of residues 1 to 197; γ^{C} is the C-terminal γ fragment comprised of residues 206 to 323.

[2]Assembly competence was judged by the yield of purified assembly relative to *wild-type*: +, normal yield; +/-, low yield, -, failed to assemble.

central domain that links the two helical elements forming the twisted helical domain shown in green, and the regulatory dithiol-containing domain shown in red. A small loop structure that is present in the chloroplast γ but not in the homologous mitochondrial subunit is highlighted in cyan.

Molecular dynamic studies predicted that the dithiol domain exists in a range of conformations between two extreme states; the fully open state, shown in Figure 8, with the dithiol reduced, and a fully closed state with the dithiol oxidized to form a disulfide bridge. When the dithiol is oxidized, the regulatory domain becomes more compact and moves downwards to come into close contact with the central domain (Richter et al., 2005). Thus, the open conformation is predicted to represent the activated state and the closed conformation the inactivated state (Richter et al., 2005). The model further predicts a close interaction between the dithiol domain and the extra loop in the closed state. In one mutant, alanine was substituted for each of the two disulfide-forming cysteine residues at positions 199 and 205 ($\gamma^{C199A/C205A}$). In a second mutant, a small stretch of nine amino acids containing Glu197 through Cys205 was deleted ($\gamma^{\Delta 197\text{-}205}$). This sequence, containing the two disulfide-forming sulfhydryls, is unique to chloroplast F_1 and is highly-conserved among higher plant species. We hypothesized that both of these mutants would result in permanent activation of the enzyme with loss of oxido-reductive regulation, without compromising the functional integrity of the γ subunit.

In a third mutant, the seventeen-residue section spanning Thr224 through Ile240 was deleted while at the same time Leu241 was changed to tyrosine ($\gamma^{\Delta 224\text{-}240}$). The rationale for the substitution came from an amino acid sequence alignment which indicated that organisms naturally missing these seventeen amino acids have tyrosine in the equivalent position to

Lys241 in CF_1 γ. Thus the deletion mutant recreated a natural variant of the F_1 γ subunit with respect to the central domain. Residues 224 to 240, which flank the dithiol-containing segment, are present in both higher plants and cyanobacteria but are missing in other organisms. In the fourth mutant, the entire regulatory domain including Glu197 through Ile240, was deleted. At the same time, a short segment of six amino acids, SerAlaGluSerMetSer, was incorporated back into the deleted region. The construct exactly matched the central section sequence of bovine MF_1 γ in which the six amino acid segment acts as a connecting loop between the twisted helical domain and the central domain (Abrahams et al., 1994). In addition, two DNA fragments, one (γ^N) encoding the N-terminal residues of γ from 1 to 196, the other (γ^C) the C-terminal residues from 207 to 323, were constructed independently and individually over-expressed in the *E.coli* host.

The mutant γ subunits were tested for their ability to assemble with the $\alpha_3\beta_3$ complex and to reconstitute a functional ATPase. All of the constructs, including the combined N- and C-terminal fragments, successfully assembled with the α and β subunits to produce stable complexes which could be purified by anion exchange chromatography under conditions used to purify the assembly containing the wild-type γ subunit (Table 1). The gel electrophoresis profiles of representative mutant γ assemblies are shown in Figure 9. The relative staining densities qualitatively indicated that the mutant γ subunits had been assembled in the same ratio as the wild-type subunit with respect to the α and β subunits. Neither the N-terminal nor the C-terminal fragment of γ termini alone could assemble with the α and β subunits to form an active enzyme. When un-reconstituted subunits were separated from stable $\alpha_3\beta_3\gamma$ complexes by ion exchange chromatography (Gao et al., 1995), we found no evidence of an $\alpha_3\beta_3\gamma$ assembly formed in the presence of either γ fragment alone. However, when both N-

Figure 9. ***Sodium dodecylsulfate gel electrophoresis of protein assemblies.*** Proteins were separated by electrophoresis on 10 to 20% gradient polyacrylamide gels and stained with Coomassie brilliant blue G. Lane 1, $\alpha_3\beta_3\gamma^{WT}$ assembly; Lane 2, native $\alpha_3\beta_3$ complex; Lane 3, recombinant γ^{WT} subunit; Lane 4, $\alpha_3\beta_3\gamma^{\Delta 197-240}$ assembly; Lane 5, $\alpha_3\beta_3\gamma^{N}+\gamma^{C}$ assembly. The protein assemblies were purified by DEAE cellulose chromatography prior to electrophoresis. The γ^{C} fragment stains poorly with Coomassie blue and is only visible during the early stages of destaining.

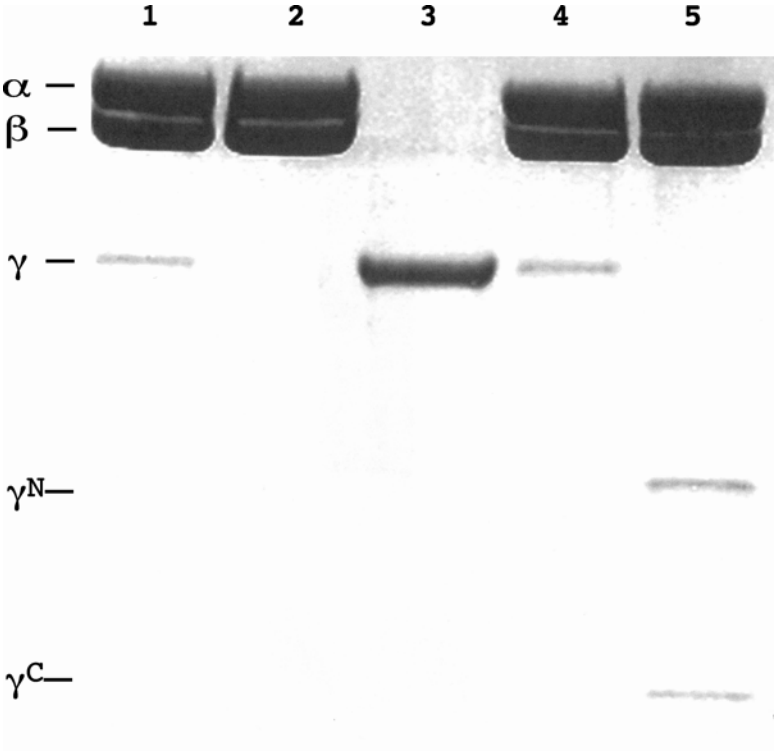
1
2
3
4
5
α
β
γ
γN
γC

Table 2. ATPase activities of regulatory domain γ mutant enzyme assemblies.

Protein Preparation[1]	ATPase Activity (μmole per min per mg protein)	
	Mg^{2+}	Ca^{2+}
$\alpha_3\beta_3\gamma^{WT}$	31.1 ± 4.0	19.5 ± 1.5
$\alpha_3\beta_3\gamma^{C199A,C205A}$	53.4 ± 5.2	30.5 ± 1.5
$\alpha_3\beta_3\gamma^{\Delta 197-205}$	54.7 ± 5.1	33.9 ± 1.5
$\alpha_3\beta_3\gamma^{\Delta 224-240}$	52.5 ± 2.4	34.9 ± 2.1
$\alpha_3\beta_3\gamma^{\Delta 197-240}$	45.15±3.15	30.6 ± 1.1
$\alpha_3\beta_3\gamma^{N}\gamma^{C}$	23.9 ± 0.5	13.4 ± 0.4

[1]Core F_1 enzymes were assembled with the wild type γ mutants as indicated, purified and assayed as described in the *Experimental* section.
Errors are standard deviations with n = 4.

and C-terminal fragments of γ were added together to the reconstitution mixture, a stable quaternary complex was produced (Figure 9, Lane 5) which eluted from DEAE cellulose at the same salt concentration as the normal $\alpha_3\beta_3\gamma$ complex.

The Ca^{2+}- and the Mg^{2+}-dependent ATPase activities of the mutant assemblies, immediately following isolation, were comparable to those of the wild-type assembly with the exception of the $\gamma^{C199A,C205A}$ and $\gamma^{\Delta 197\text{-}205}$ mutants, both of which were ~60% higher than wild-type (Table 2). The assemblies were exposed to conditions that either promote oxidation (100 μM $CuCl_2$, 30 min., RT) or promote reduction (10 mM DTT, 30 min at RT) of the γ disulfide (Richter et al., 1985). The enzyme containing the wild-type γ subunit, possessing the two disulfide-forming thiols, was significantly activated by reduction with DTT as shown in Table 3. In contrast, the $\gamma^{C199A,C205A}$ mutant and the $\gamma^{\Delta 197\text{-}205}$ mutant both exhibited maximal rates of ATPase activity without reduction by DTT which is the expected consequence of permanently blocking formation of the γ disulfide bond. Interestingly, the MgATPase activity of the $\gamma^{\Delta 197\text{-}205}$ mutant consistently showed an approximately 16% decrease in activity following exposure to DTT, whereas the $\gamma^{C199A/C205A}$ mutant did not. Exposure of the $\gamma^{\Delta 197\text{-}205}$ mutant to the alkylating agent N-ethylmaleimide, which selectively alkylates the C-terminal γCys322 of γ under these conditions (Richter and McCarty, 1987), blocked the DTT–induced inhibition (Table 3). The reason for this effect is unclear. The activity of the $\gamma^{\Delta 224\text{-}240}$ mutant was within 20% that of wild type but was not further enhanced by thiol reducing conditions. Similarly, removal of the entire regulatory domain in the $\gamma^{\Delta 197\text{-}240}$ mutant resulted in an assembly with a similar activity to wild-type that was

Table 3. Response of γ regulatory domain mutants to oxidizing/reducing conditions.

Protein preparation[1]	ATPase Activity[2]		red/ox[3]
	oxidized	reduced	
$\alpha_3\beta_3\gamma^{WT}$	30.0±0.9	50.3±3.7	1.7
$\alpha_3\beta_3\gamma^{C199A,C205A}$	53.4±5.2	55.7±5.7	1.0
$\alpha_3\beta_3\gamma^{\Delta 197\text{-}205}$	54.7±5.1	46.1±1.4	0.8
$\alpha_3\beta_3\gamma^{\Delta 197\text{-}205\ alkylated_4}$	54.7±5.1	54.9±0.7	1.0
$\alpha_3\beta_3\gamma^{\Delta 224\text{-}240}$	53.6±1.7	51.4±1.1	1.0
$\alpha_3\beta_3\gamma^{\Delta 197\text{-}240}$	44.7±0.8	45.6±1.5	1.0

[1]Core F_1 assemblies were purified and assayed as described in the *Experimental* section.
[2]MgATPase activites are expressed as μmoles per min per mg of protein.
[3]Ratio of activity of the reduced assembly to that of the oxidized assembly. The enzyme assembly was pre-treated with either 10 mM DTT (reduced) or 100 μM $CuCl_2$ (oxidized) prior to assay.
[4]$\alpha_3\beta_3\gamma^{\Delta 197\text{-}205}$ was exposed to 2 mM N-ethylmaleimide for 10 min prior to incubation with DTT.

insensitive to thiol reducing conditions (Tables 2 and 3).

2. Epsilon binding to mutant $\alpha_3\beta_3\gamma$ assemblies containing substitutions or deletions within the dithiol domain.

To assess the role of the modified or deleted segments of the γ subunit in mediating ATPase inhibition by the ε subunit, reconstituted $\alpha_3\beta_3\gamma$ complexes were titrated with purified recombinant ε subunit. Representative titration data are shown in Figures 10 and 11. The ε preparations were diluted from the ethanol/glycerol mixture in which they were isolated and stored (approximately 1 part ε with 2 parts assay buffer) such that the final concentrations of ethanol and glycerol maintains ε solubility while allowing ε to bind to $\alpha_3\beta_3\gamma$. All the points on the titration curves contained the same percentage of ethanol and glycerol. Under these poised conditions, it is not possible to obtain a meaningful measure of the dissociation constant for ε binding. The concentration dependence for ε binding does, however, afford a qualitative measure of the relative affinity of ε for the different γ constructs.

The $\alpha_3\beta_3\gamma$ complex which was assembled with the recombinant wild-type γ subunit exhibited a concentration-dependent response to ε like that of the native $\alpha_3\beta_3\gamma$ complex, both assemblies being fully inhibited at the higher ε concentrations (Figure 11) (Sokolov et al., 1999). It was consistently observed that a two to three-fold higher concentration of ε was required for 50% inhibition of the reduced $\alpha_3\beta_3\gamma^{WT}$ enzyme (closed circles) compared to the oxidized $\alpha_3\beta_3\gamma^{WT}$ enzyme (squares). This indicated that reducing the disulfide bond resulted in a decreased affinity for ε binding which is consistent with the results of earlier studies (Soteropoulos et al., 1992). The pattern of inhibition of the $\alpha_3\beta_3\gamma^{C199A,C205A}$ mutant

Figure 10. ***Epsilon titration of reconstituted $\alpha_3\beta_3\gamma$ complexes containing recombinant γ subunits with mutations in the dithiol domain.*** Mutant γ constructs were assembled with $\alpha_3\beta_3$ and purified by anion exchange chromatography. Samples were incubated for 30 min at room temperature either in the presence of 100 μM $CuCl_2$ (thiol oxidizing conditions) or 10 mM DTT (thiol reducing conditions). Two parts of incubation buffer containing 10 μg samples of each $\alpha_3\beta_3\gamma$ assembly, were mixed with one part of ε subunit isolation buffer (Richter and McCarty, 1987) containing the indicated amounts of the ε subunit, and incubated for 10 min at room temperature. At the end of the incubation, 0.5 ml of double strength calcium-dependent ATPase assay mixture, pre-warmed to 37°C, was added to initiate the assay. Squares, oxidized $\alpha_3\beta_3\gamma^{WT}$; filled circles, reduced $\alpha_3\beta_3\gamma^{WT}$; diamonds, oxidized $\alpha_3\beta_3\gamma^{C199A,C205A}$; open circles, oxidized $\alpha_3\beta_3\gamma^{\Delta 197-205}$; triangles, reduced $\alpha_3\beta_3\gamma^{\Delta 197\text{-}205}$. Curves were fitted using SigmaPlot 8.0 (Synstat Software Inc., California).

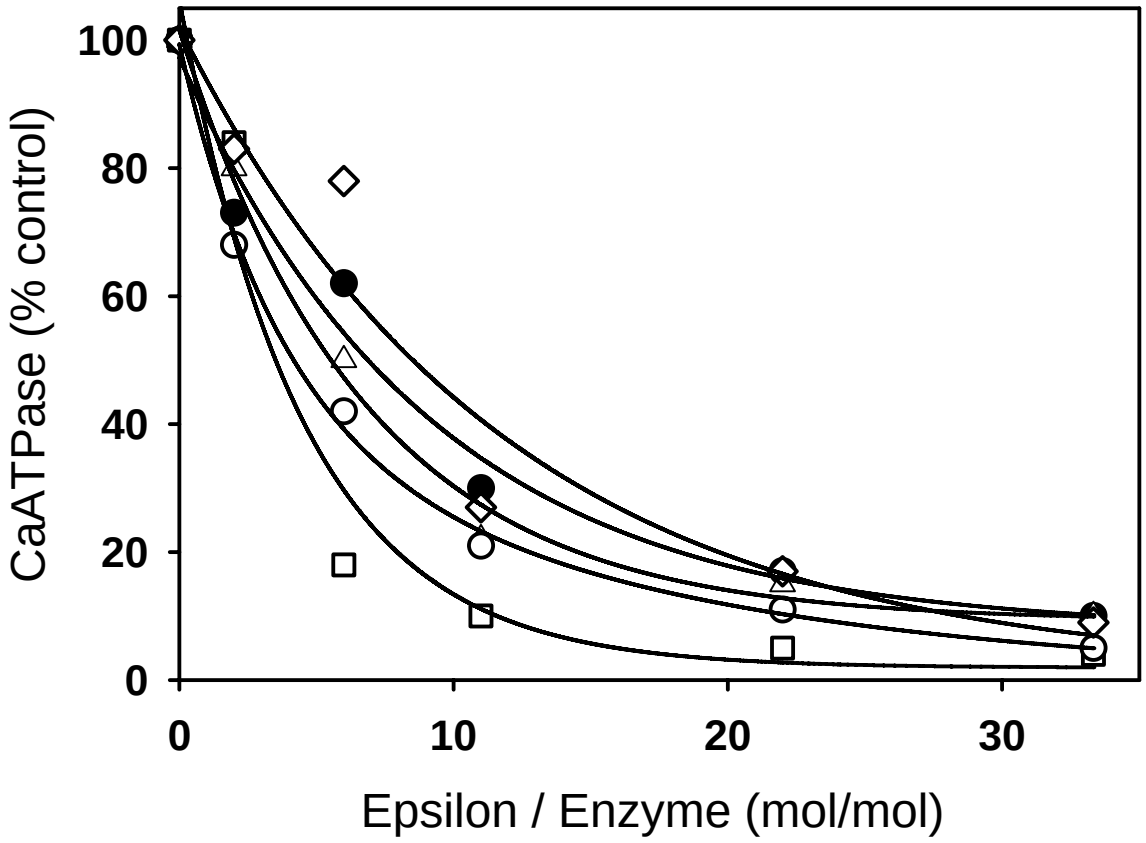
CaATPase (% control)
100
80
60
40
20
0
0
10
20
30
Epsilon / Enzyme (mol/mol)

Figure 11. ***Epsilon titration of reconstituted $\alpha_3\beta_3\gamma$ complexes containing recombinant γ subunits with deletions within the dithiol domain.*** Purified assemblies were pre-treated with 100 μM $CuCl_2$ to promote disulfide formation, reconstituted with the ε subunit and calcium-dependent ATPase activity measured as described in the legend to Figure 10. Filled squares, native $\alpha_3\beta_3\gamma$; open circles, $\alpha_3\beta_3\gamma^{\Delta 224\text{-}240}$; open triangles, $\alpha_3\beta_3\gamma^{\Delta 197\text{-}240}$; filled diamonds, $\alpha_3\beta_3\gamma^{N}+\gamma^{C}$.

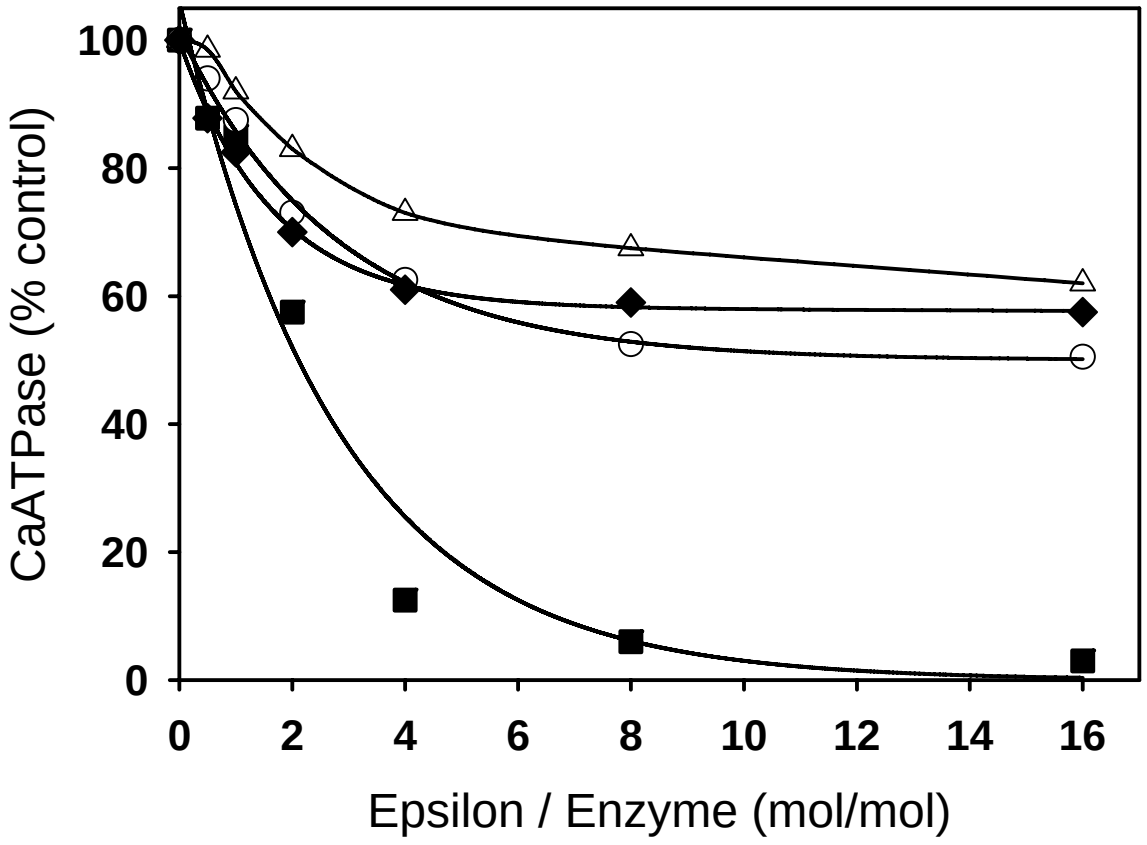
CaATPase (% control)
100
80
60
40
20
0
0
2
4
6
8
10
12
14
16
Epsilon / Enzyme (mol/mol)

closely resembled that of the reduced $\alpha_3\beta_3\gamma^{WT}$ enzyme, an expected consequence of blocking formation of the disulfide bond. Similarly, the pattern of ε inhibition of the $\alpha_3\beta_3\gamma^{\Delta 197\text{-}205}$ assembly in which the disulfide bond has been deleted resembled that of the reduced $\alpha_3\beta_3\gamma^{WT}$ assembly.

Figure 11 compares the sensitivities to added ε subunit of the enzyme assemblies containing the larger γ deletions and the combined N- and C-terminal fragments of the γ subunit. All of the mutant $\alpha_3\beta_3\gamma$ assemblies, including the enzyme assembled with the two separate γ fragments ($\alpha_3\beta_3\gamma^{N}+\gamma^{C}$), were maximally inhibited by ε to approximately 40%, significantly less than the *wild-type* which approached 100% inhibition. Therefore, the ε subunit still binds, even following deletion of the entire regulatory segment. Neither the concentration dependence on ε nor the extent of inhibition changed in response to addition of $CuCl_2$ or DTT (not shown) indicating that the mutants were insensitive to thiol oxidizing non-reducing conditions. This was true also of the $\gamma^{\Delta 224\text{-}240}$ mutant which still contained the disulfide bond but lacked the N-terminal flanking region, consistent with the lack of response of the ATPase activity of this mutant to DTT (Table 3).

3. Deletions within the extra loop on the γ subunit.

The γ model predicts a close interaction between the dithiol domain and the extra loop when the dithiol domain is in the closed conformation. This interaction is proposed to result in inhibition of catalytic function. To examine this aspect of the structure, several mutant γ subunits were prepared in which fragments of the putative loop structure were deleted as summarized in Table 1. The mutant γ subunit in which the entire loop between

Table 4. Effects of oxidizing/reducing conditions on ATPase activites of γ extra loop mutants.

Assembly[1]	ATPase Activity (μmole per min per mg protein)		Red/Ox[2]
	Mg^{2+}	Ca^{2+}	
$\alpha_3\beta_3\gamma^{WT}$	34.8 ± 3.7	19.8 ± 0.3	1.6
$\alpha_3\beta_3\gamma^{\Delta 65\text{-}68}$	62.9 ± 2.0	37.6 ± 0.1	1.3
$\alpha_3\beta_3\gamma^{\Delta 65\text{-}73}$	49.7 ± 3.2	32.8 ± 0.4	1.1
$\alpha_3\beta_3\gamma^{\Delta 68\text{-}73}$	56.69 ±1.0	42.3 ± 0.2	1.0
$\alpha_3\beta_3\gamma^{\Delta 74\text{-}78}$	10.2 ± 1.3	11.7 ± 0.6	1.2

[1]Core CF_1 assembled with the wild type γ subunit or with the indicated γ deletion mutants were purified, pre-treated with 100 μM $CuCl_2$ for 30 min and assayed as described in the *Experimental Procedures*.

[2]Ratio of CaATPase activity of the reduced assembly to that of the oxidized assembly. The enzyme assembly was pre-treated with either 10 mM dithiothreitol or 100 μM $CuCl_2$ prior to assay. Errors are expressed as standard deviations with n=4.

residues 65 and 78 was deleted failed to assemble with the α and β subunits. This suggests that the mutation affected folding and/or assembly of the complex. Each of the smaller deletion mutants, however, assembled to give normal yields of purified complexes with subunit stoichiometries qualitatively equivalent to that of the wild type complex (not shown). The catalytic activities of the mutant assemblies at saturating substrate concentrations, together with the effects of oxidizing and reducing conditions on the activities, are shown in Table 4. All but the $\gamma^{\Delta 74\text{-}78}$ mutant assembly exhibited CaATPase and MgATPase activities similar to those of the wild type construct. The activity of the $\gamma^{\Delta 74\text{-}78}$ mutant was significantly lower than those of the other assemblies indicating that removing these residues impairs catalytic function. All four mutants showed decreased responses to dithiol oxidation compared to the wild type assembly. The effect was most pronounced in the $\gamma^{\Delta 65\text{-}73}$ and $\gamma^{\Delta 68\text{-}73}$ mutants in which the response to oxidation was essentially eliminated.

4. Epsilon binding to γ loop deletion mutants.

In the experiment described in Figure 12, assembled enzyme complexes containing the γ loop deletion mutants were treated with $CuCl_2$ to oxidize the γ disulfide then titrated with purified ε subunit (Figure 11). All four mutants showed a markedly decreased inhibitory response to ε compared to that of the wild type construct. Note that the extent of inhibition by ε of the assembly containing the wild-type γ subunit was less than that shown in a similar experiment in Figures 10 and 11. This difference is due to variability in the inhibitory properties of the recombinant ε subunit from one preparation to another. However, the relative effect of the ε subunit on the different γ mutants was constant, showing ~40% of the

Figure 12. ***Epsilon titration of reconstituted $\alpha_3\beta_3\gamma$ complexes containing recombinant γ subunits with deletions in the extra loop.*** Purified assemblies were pre-treated with 100 μM $CuCl_2$ to promote disulfide formation, reconstituted with the ε subunit and calcium-dependent ATPase activity measured as described in the legend to Figure 10. Filled circles, $\alpha_3\beta_3\gamma$ assembly containing the recombinant wild type γ subunit, filled triangles, $\alpha_3\beta_3\gamma^{\Delta 65\text{-}68}$; open triangles, $\alpha_3\beta_3\gamma^{\Delta 65\text{-}73}$; filled squares, $\alpha_3\beta_3\gamma^{\Delta 68\text{-}73}$; open circles, $\alpha_3\beta_3\gamma^{\Delta 74\text{-}78}$.

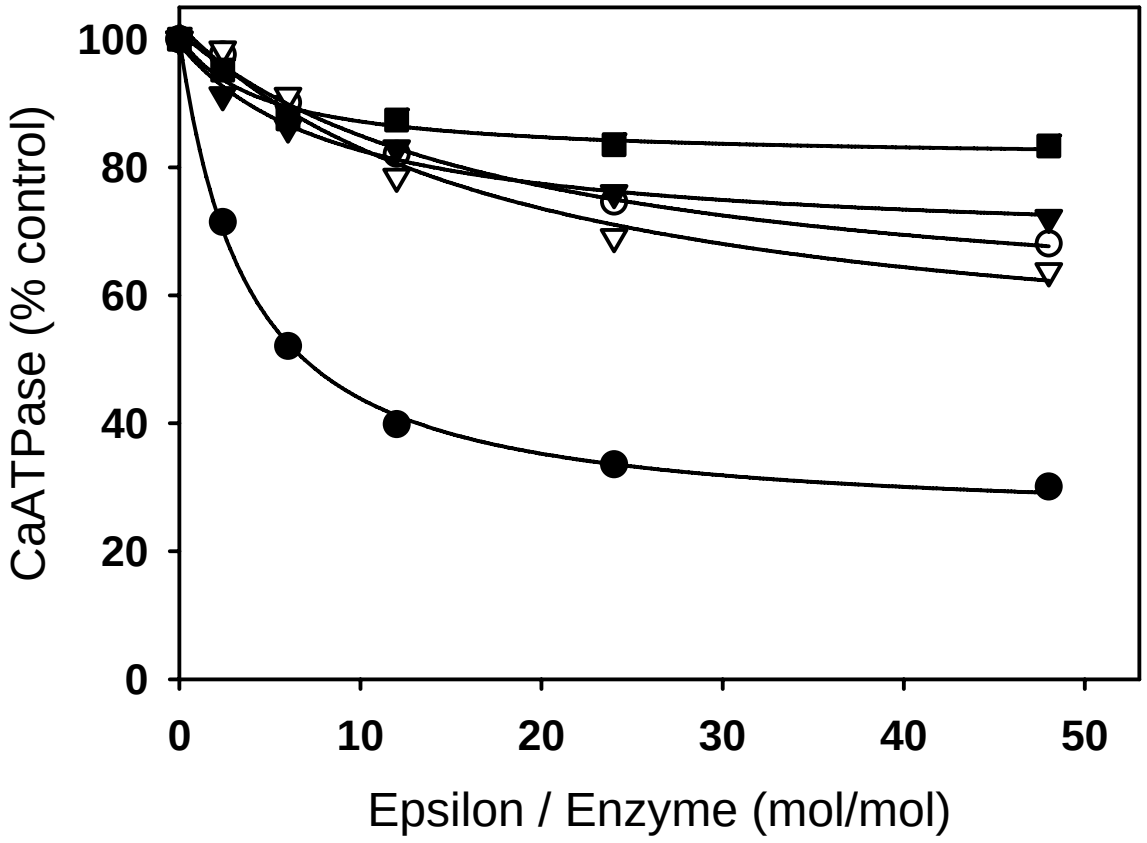
CaATPase (% control)
100
80
60
40
20
0
0
10
20
30
40
50
Epsilon / Enzyme (mol/mol)

maximum inhibition seen in the wild-type assembly. This was essentially the same result as that obtained for the $\gamma^{\Delta 224\text{-}240}$ and $\gamma^{\Delta 197\text{-}240}$ mutants (Figure 11).

D. Discussion

1. Structural requirements for dithiol regulation.

Deletions in the regulatory dithiol-containing domain of γ (residues 197 to 140) resulted in γ subunits that retained catalytic function. This result was expected from sequence alignments that indicate that the bulk of the regulatory domain is an evolutionary add-on, present only in photosynthetic organisms and, therefore, not essential for catalytic function. Deletion of the nine residues surrounding the two disulfide-forming cysteines (197-205), or substituting the disulfide-forming cysteines (199,205) with alanines, had the obvious effect of rendering the catalytic activity of the enzyme insensitive to conditions that promote disulfide oxidation or reduction. Interestingly, removing residues 224 to 240, which flank the dithiol-containing segment on the C-terminal side, had the same effect, indicating that the conformation of the entire regulatory domain may be important for regulation. This result is consistent with the modeled structure of the CF_1 γ subunit which indicated that residues 224-240 closely associate with the central domain of γ when the disulfide is formed, resulting in inhibition of catalysis (Richter et al., 2005). Removing these residues should significantly reduce the interaction and thus the inhibitory response.

An active F_1 enzyme was also assembled using the independently folded N- and C-terminal γ fragments. This assembly mimicked the $\gamma^{\Delta 197\text{-}205}$ mutant except that the fragments were not covalently linked. The activity of this assembly was insensitive to oxidizing/reducing agents since the disulfide-forming thiols were missing from the fragments.

It was shown previously that exposure of CF_1 to a small amount of trypsin resulted in cleavage of the γ subunit at Lys204 and Lys 219 with release of the intervening 15 amino acid fragment (Hightower and McCarty, 1996; Moroney and McCarty, 1982; Schumann et al., 1985). At the same time about twenty residues were cleaved from the N-terminus of the α subunit and the δ and ε subunits were cleaved to different extents (Moroney and McCarty, 1982). Following cleavage, CF_1 lost its latency and became fully activated. Activation correlated with α and γ cleavage making it difficult to determine if only one or both subunits were involved (Hightower and McCarty, 1996; Moroney and McCarty, 1982). The results obtained with the assembled γ fragments confirm the observation that cleavage of γ within the region of the dithiol results in permanent activation of the enzyme.

Mutations within the extra loop segment of the γ subunit were predicted to interfere with the response of enzyme catalysis to thiol oxidation or reduction since the loop was predicted to interact closely with the regulatory domain upon formation of the γ disulfide (Richter et al., 2005). Indeed, all of the loop mutants exhibited a reduced response to disulfide oxidizing conditions as indicated in Table 4. The effect was most pronounced in the $\alpha_3\beta_3\gamma^{\Delta 68\text{-}73}$ mutant suggesting the importance of residues 68 to 73 for disulfide regulation. The mutant in which the entire loop, residues 65 to 78, was deleted failed to reconstitute a stable enzyme complex. The mutant in which residues 74-78 were deleted reconstituted poorly (i.e. with very low yields) and showed reduced activity compared to the wild type assembly. Since this assembly remained intact during purification by ion exchange and gel filtration chromatography, the reduced activity did not appear to be the result of a decreased stability of the assembly. Comparison of the amino acid sequences of the spinach chloroplast, *E.coli* and bovine mitochondrial F_1 γ subunits indicated that loop residues 65 to 75 are naturally missing from the bovine mitochondrial enzyme but not residues 76 to 78.

These latter residues are immediately adjacent to one of the most highly conserved regions of the γ subunit, comprised of residues 79 to 100, and therefore may play an important role in maintaining structure within the central domain of the γ subunit.

2. Structural requirements for epsilon inhibition.

Deletion of all of the γ regulatory domain, or of the C-terminal segment comprised of residues 224-240, reduced by 50 to 60% the maximum extent of inhibition by ε. In contrast, deleting the nine residues containing the γ dithiols, or substituting the dithiol cysteines with alanines, while eliminating the oxidation/reduction response, did not change the maximum extent of inhibition by ε. Similarly, deletion of residues 65-78 within the extra loop also reduced the the maximum extent of ε inhibition by 50 to 70% with a concomitant decrease in the response of enzyme turnover to oxidation/reduction of the disulfide. One possible explanation for this result is that residues 224-240 and 65-78 together contribute to the inhibitory response of ε binding by forming part of the ε binding site. Indeed, a direct binding interaction between the ε subunit and the regulatory domain of the γ subunit of CF_1 has been proposed previously (Hightower and McCarty, 1996) based largely on two observations; first that removal of ε from CF_1 significantly increases the exposure of the γ dithiols to reducing agents while the surrounding region of γ becomes hypersensitive to trypsin (Richter et al., 1985), and secondly, that reduction of the γ disulfide increases the apparent dissociation constant for the ε subunit by more than 20-fold (Soteropoulos et al., 1992). In addition, fluorescence mapping studies (Johnson and McCarty, 2002; Richter et al., 1985) have placed two amino acid residues on the ε subunit, the single cysteine residue at position 6 and tryptophan at position 57, within 20 Å of the γ dithiols. The possibility that ε

binds in the immediate vicinity of the regulatory domain is strengthened by the observation that tryptic cleavage of γ close to the dithiol results in loss of ε inhibition (Hightower and McCarty, 1996; Richter et al., 1985), as well as by the apparent reduced inhibitory efficacy of ε in the F_1 assembled with the γ^N and γ^C fragments as shown in this study (Figure 11). These latter observations indicate that the regulatory domain must be intact both for optimal ε inhibition and for modulation of activity by dithiol oxidation/reduction.

The three-dimensional structures of the bovine heart MF_1 and EcF_1 ε subunits have been determined (Figure 4) (Menz et al., 2001; Rodgers and Wilce, 2000; Wilkens and Capaldi, 1998) and shown to consist of two domains, an N-terminal β-barrel domain and a C-terminal helix-turn-helix domain. In the solved structure of an EcF_1 γε complex (Fig. 12, left), the β-barrel domain interacts closely with one end of the twisted helical pair formed by the N- and C-termini of the γ subunit where it may also interact with the ring of c subunits in the F_O segment. The C-terminal domain of ε is comprised of a helix-turn-helix motif that wraps around the central domain of the γ subunit. The extreme C-terminal tip of ε extends down towards the center of the $\alpha_3\beta_3$ hexamer, possibly interacting directly with the α and β subunits (Cipriano et al., 2002; Xiong et al., 1998). The structure is dynamic, as indicated by cross-linking studies that show that the C-terminal arm of ε undergoes a significant conformational change in response to occupancy of catalytic sites with different nucleotides (Capaldi and Schulenberg, 2000; Suzuki et al., 2003).

A number of studies with CF_1 have indicated that the ε subunit is likely to exist in conformations similar to those of the EcF_1 enzyme. Cleavage of residues from the C-terminus of CF_1 ε resulted in loss of the inhibitory action of ε but had little or no effect on its ability to couple proton transport to ATP synthesis (Nowak and McCarty, 2004; Nowak et al.,

2002; Shi et al., 2001). In contrast, mutations within the β-barrel domain resulted in loss of coupling (Cruz et al., 1995). These observations indicated that the C-terminal arm of ε is responsible for the inhibitory action of ε and is consistent with similar observations with the bacterial enzyme (Cipriano and Dunn, 2006; Hara et al., 2001). We therefore propose that the inhibitory action of CF_1 ε results from a direct binding interaction between the C-terminal arm of ε and the central domain of the γ subunit, in particular, residues within the regulatory domain and the extra loop segment as indicated by these studies. Alternative interpretations are possible, for example mutations within the regulatory domain and extra loop may induce conformational changes that influence activity and ε binding at a distance without involving a direct interaction between these structural elements. Cross-linking studies are currently in progress to identify the site(s) of interaction between the C-terminal arm of ε and the γ subunit in CF_1.

Studies with thermophilic bacteria have indicated that the C-terminus of the ε subunit may be in an even more extreme position than that shown in EcF_1, being fully extended with the C-terminal tip extending well into the $\alpha_3\beta_3$ hexamer (Keis et al., 2006; Suzuki et al., 2003). In addition, Hisabori et al. (Hisabori et al., 1998) assembled an $\alpha_3\beta_3\gamma$ complex using recombinant α and β subunits from the thermophylic bacterium PS3 and the recombinant spinach chloroplast γ subunit. The hybrid enzyme exhibited the expected response to the oxidation state of the γ dithiol although the catalytic activity was very low (1-2% of that obtained with the native CF_1 assembly). However, the hybrid enzyme containing the reduced γ, or γ with the dithiol removed, bound ε with a significantly higher affinity, the opposite effect to that observed in CF_1 and in the $\alpha_3\beta_3\gamma$ assembly obtained in this study using the *wild-type* γ subunit. Finally, the hybrid thermophilic enzyme containing a mutant chloroplast γ

Figure 13. ***Comparison of partial structures of F_1 γ subunits from E.coli and chloroplasts.*** Similar perspectives of the γ subunits from *E.coli* (Menz et al., 2001) (PDB accession code:#1PSO) and the chloroplast homology model (Richter et al., 2005) F_1 are shown. The EcF_1 ε subunit, comprised of an N-terminal β-barrel and a C-terminal helix-turn-helix, is shown in grey. The twisted helical domain formed by the N- and C-termini of γ is shown in blue; the central domain in green; the extra loop in cyan. The residues corresponding to the extra loop (also cyan) are rotated towards the back of the central domain in the EcF_1 structure. The dithiol-forming cysteines γC199 and γC205, as well as cysteine 89, are shown spacefilled in yellow. Cysteine 89 of γ becomes solvent-exposed upon formation of a light-induced membrane potential in the CF_1F_O complex associated with thylakoid membranes (Moroney et al., 1984).

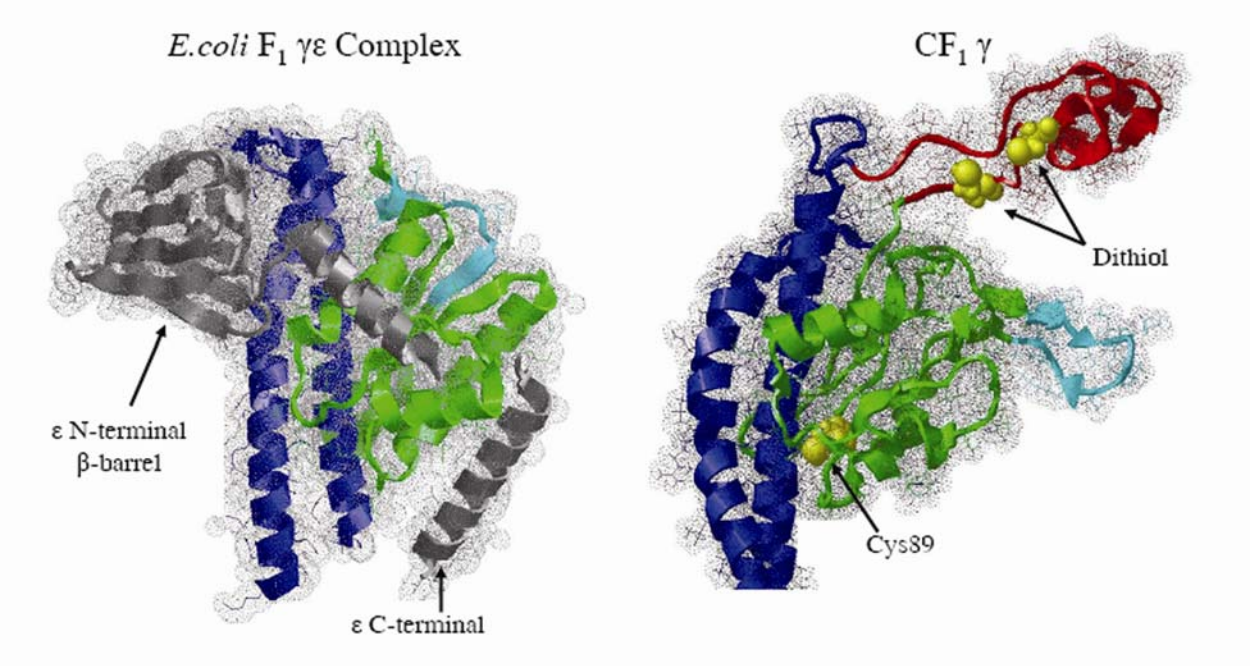
E.coli F_1 γε Complex
ε N-terminal
β-barrel
ε C-terminal
CF_1 γ
Dithiol
Cys89

subunit with the entire section between 194 and 230 deleted was not inhibited by the ε subunit, in contrast to the results of this study in which a similar mutant retained partial sensitivity to ε binding. These differences indicate that the conformation assumed by the γ subunit in the thermophilic bacteria/chloroplast hybrid may not be physiologically relevant, or that a slightly different conformation of γ in the thermophilic bacteria exists for increased stability.

In marked contrast to the EcF_1 γε complex as shown in Figure 13, the C-terminal arm of the bovine MF_1 δ subunit (equivalent to the EcF_1 and CF_1 ε subunits) is rotated approximately 180^o (Figure 4) such that it abuts the β-barrel domain of ε and does not interact directly with the γ subunit or with the $\alpha_3\beta_3$ hexamer (Menz et al., 2001). One possible explanation for the difference is that the two structures represent two different conformational states of the ε subunit that occur during the catalytic cycle or as part of an activation/inactivation process. These observations led to the idea that the ε subunit may act as a ratchet, oscillating between the two conformational states as part of a mechanism designed to prevent or reduce the rate of ATP hydrolysis by the enzyme (Tsunoda et al., 2001). Interestingly, the MF_1 contains an additional small subunit of ~8 KDa that has been designated as the ε subunit but which does not have a counterpart in the other F_1 enzymes. This subunit also binds to the γ subunit, occupying a position adjacent to the δ subunit where it may block a conformational change in which the C-terminal arm of the δ subunit moves to a position similar to that seen in the EcF_1 εγ structure (Rodgers and Wilce, 2000). Thus, if a similar ratcheting mechanism were to operate in the mitochondrial enzyme, it would necessarily involve large structural rearrangements within/among the small subunits. Moreover, since MF_1 lacks most of the residues that form the extra loop which is present in

both EcF_1 and CF_1 (colored cyan in Figure 13) and which was shown here to be required for the normal inhibitory action of ε in CF_1 raises the possibility that the MF_1 δ subunit may regulate catalysis in a manner different to that observed in the EcF_1 and CF_1 ε subunits. The lack of a demonstrated inhibition of the MF_1 δ subunit as well as the presence of a unique inhibitory subunit (IF_1) associated with the mitochondrial enzyme, which inhibits ATP hydrolysis in a manner similar to the ε subunits of EcF_1 and CF_1 (Jackson and Harris, 1988), would tend to reinforce this possibility.

3. Light-driven activation of CF_1; a potential mechanism.

The ε subunit of CF_1 undergoes a significant conformational change in response to formation of a light-driven membrane potential. This change was first detected using a polyclonal antibody against the intact ε subunit (Richter and McCarty, 1987) and later using an antibody specific for the C-terminal arm of ε (Cruz et al., 1995). In both cases, epitopes on ε were only recognized following imposition of the membrane potential. The existence of a light-driven change in the conformation of the C-terminal arm of ε is further supported by the observation that the apparent pK_a of εLys109, located in the small loop connecting the two helical elements of the C-terminal arm of ε, changes upon light-activation of CF_1 (Komatsu-Takaki, 1992). Moreover, formation of a light-induced membrane potential exposed the γ subunit to trypsin at the same sites that became exposed in soluble CF_1 when ε was removed (Richter et al., 1985; Schumann et al., 1985), again suggesting the dissociation of the C-terminal arm of ε from the central domain of γ upon light activation.

Light-driven conformational changes also occur in the γ subunit. Cysteine 89 of CF_1 γ, shown in yellow and space-filled in Figure 13 (right side), is sandwiched between the

twisted helical element and the central domain of γ. This residue is normally buried within the structure but becomes solvent-exposed upon forming a light-driven membrane potential (Moroney et al., 1984). Movement of γC89 from a buried to an exposed environment suggests a relative movement between the central domain and the twisted helical element of γ. It has been suggested that such a movement is essential, either for activation or for catalytic turnover, or both, and that it is impeded by oxidizing the γ dithiol (Richter, 2004; Richter et al., 2005). The results described in this study indicate that the CF_1 ε subunit binds in a similar manner to that of the EcF_1 ε, with the β-barrel domain of ε binding to the twisted helical element of γ and the helical C-terminal domain of ε binding to the central domain of the γ subunit. By binding to the central domain of γ, the C-terminal arm of ε would likely stabilize the closed, inhibited conformation of the γ regulatory domain (Richter et al., 2005). On the membrane, formation of a membrane potential would, by an interaction with the subunit III ring and the β-barrel domain of ε, induce a partial rotation of the ε subunit leading to release of the C-terminal arm of ε from its tight binding interaction, thus exposing the γ disulfide to the medium, favoring reduction and activation. This possible mechanism remains speculative and is the subject of ongoing studies in this laboratory.

In conclusion, the results of this study have identified structural elements within the γ subunit of CF_1 that are important for the regulatory interplay between this subunit and the inhibitory ε subunit. They also establish a testable mechanism for activation of the latent ATPase activity of the enzyme; a process that must be tightly regulated to prevent the futile depletion of ATP pools during dark periods when chloroplast electron transport is inactive.

Chapter 3. Interdomain cross-linking of the γ subunit affects catalysis

A. Introduction

The primary structural features of ATP synthases are highly conserved from one organism to another. The $\alpha_3\beta_3$ hexamer, comprised of alternating α and β subunits, contains six nucleotide binding sites located at each of the six α/β subunit interfaces. Three of these nucleotide binding sites are thought to be catalytic, located primarily on the β subunits, and three are thought to be regulatory, located primarily on the α subunits. The three catalytic sites exist in three distinct conformations as a result of asymmetric interactions between each α/β pair and the γ subunit (Abrahams et al., 1994; Gao et al., 1995). The rotation of the γ subunit within the $\alpha_3\beta_3$ hexamer is driven by nucleotide binding to the catalytic sites resulting in the γ subunit making, breaking, and reforming interactions with each α/β pair (Tucker et al., 2004). The three conformational states adopted by the nucleotide binding sites as observed in the MF_1 structure are similar to those suggested in the binding change mechanism of catalysis (Boyer, 1993; Boyer, 1997).

The presence of the γ subunit is necessary for the formation of the three asymmetric conformations of the β subunits (Gao et al., 1995). Crystallographic studies have shown that in the absence of the γ subunit the structures of the three β subunits are identical in the rat liver MF_1, EcF_1, and CF_1 (Shirakihara et al., 1997). While the $\alpha_3\beta_3$ hexamer is capable of a low level of ATPase activity, the presence of the γ subunit and the ability to form three asymmetrical conformations of the β subunits are required for high levels of cooperative catalysis (Dunn and Futai, 1980; Gao et al., 1995). Previous mutagenesis studies have indicated that residues involved in the β-γ subunit interactions not only play a role in the catalytic functions of the enzyme, but are also necessary for energy coupling during ATP

synthesis. The β-γ subunit interactions play an important role in providing overall stability to the F_1 complex (Nakamoto et al., 1995; Nakamoto et al., 1993; Tucker et al., 2001).

The β subunits contain at least three different contact or catch regions that interact with different segments of the N- and C-terminal helical elements of the γ subunit (Abrahams et al., 1994). One of these catch regions is made up of a conserved helical loop containing C-terminal β subunit residues, β^{394}DELSEED^{400} (using CF_1 numbering) that interacts with the N-terminal helix of the γ subunit in the vicinity of M23 (Figure 14). When a nucleotide fills the catalytic site, the β subunit undergoes a structural change sandwiching the bound nucleotide between C- and N-terminal domains of the β subunit. During catalysis the DELSEED region of the β subunits moves in close proximity to or farther away from the γ subunit depending on the nucleotide occupancy of the β subunit. This subunit contact implicates the DELSEED region of the β subunit in playing a crucial role in rotational catalysis (Ketchum and Nakamoto, 1998). Another contact region between the C-terminal residues of the γ subunit involves anionic loop structures on the α and β subunits. In the MF_1 enzyme, the two main residues responsible for this interaction are γR256 and γQ257 (corresponding to γR304 and γQ305 in CF_1 in Figure 14), which form hydrogen bonds with residues located on an anionic loop on the β_E subunit that does not have any nucleotide bound (Figure 14).

While the β-γ subunit interactions have been studied extensively, little information is known about the conformational changes that occur within the γ subunit during rotational catalysis. High resolution crystal structures have been obtained for the mitochondrial F_1 γ subunit and part of the *E.coli* F_1 γ subunit. The structure of the chloroplast γ subunit has yet to be solved. The γ subunits consist of a long twisted helical domain connected by a central, more globular, domain. The CF_1 γ subunit is different from that of other species in that it

Figure 14. **β-*γ subunit interactions in CF$_1$*.** The homology model of the CF_1 showing the γ subunit (grey) and the β subunits (blue). A) Side view of a single β subunit and the γ subunit showing the DELSEED loop (red) and the anionic loop region on β (green). The residues on the γ subunit shown are γM23 (pink) and residues γR302-Q305 (yellow); B) Depiction showing all three β subunits and the different interaction with the γ subunit based on nucleotide occupancy.

A

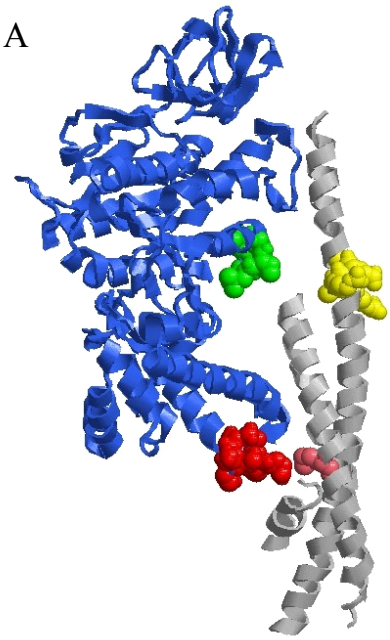

B

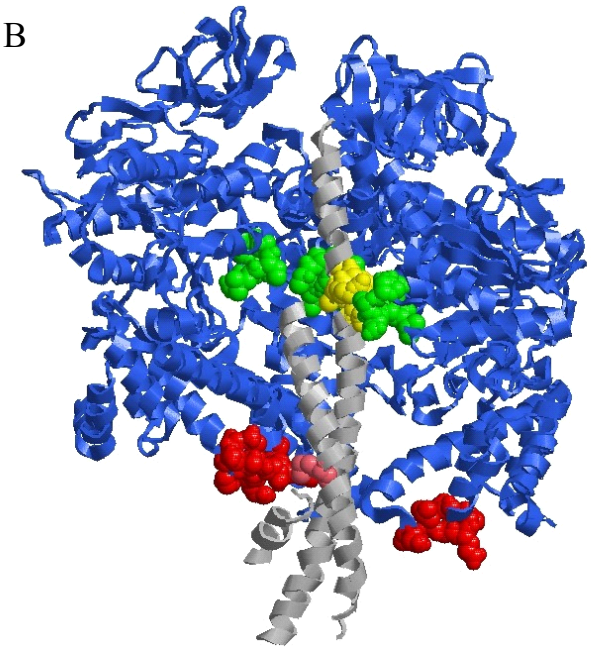

also contains a regulatory dithiol region consisting of ~40 amino acids (Richter et al., 2005). This unique domain partially regulates ATP synthesis and hydrolysis, and yet is located over 60 Å away from the catalytic sites on the β subunits. The oxidation and reduction of the critically placed dithiol is thought to modulate essential conformational changes within the γ subunit (Richter et al., 2005), however the exact mechanism of regulation is still unknown.

The recently published homology model of the CF_1 γ subunit, described in the preceding chapter, has provided some insight into the potential structure of the regulatory domain (Samra et al., 2006) as well as potential inter-domain movements that may be required for catalysis. The homology model shows the organization of the central domain of the γ subunit adjacent to the C-terminal α helix and the proposed location of a cysteine in the central domain, γC89. γC89 is known as the "light site" cysteine since it can be labeled with a thiol reactive maleimide probe only when bound to the CF_0 segment in the presence of a light-induced transmembrane potential (Moroney et al., 1980). Previous experiments have further shown that labeling γC89 with thiol reactive maleimide probes strongly inhibits the ATP synthesis and hydrolysis activities of CF_1 (Moroney et al., 1980; Nalin et al., 1983). Additional experiments demonstrated that exposing membrane bound CF_1 to bifunctional maleimides during proton driven ATP synthesis resulted in cross-linking between γC89 and γC322 (located on the distal tip of the C-terminal α helix). The formation of this cross-link resulted in inhibition of ATP hydrolysis and synthesis (Moroney and McCarty, 1979).

The original MF_1 crystal structure indicated the presence of only two bound nucleotides as was predicted by the "binding change" mechanism (Abrahams et al., 1994). Interestingly, a higher resolution MF_1 crystal structure was obtained with all three catalytic sites occupied with MgATP analogs (Menz et al., 2001). The Menz MF_1 crystal structure indicated that MgADP-fluoroaluminate was bound at two of the catalytic sites, while the β_E

site contained an ADP and a sulfate ion. The β_E site containing ADP appears to be in a half-open conformation, whereas normally the catalytic sites are observed in either a closed (nucleotide bound) or open (empty) conformation. This half-open catalytic site is thought to be an intermediate state that temporarily occurs during catalysis before nucleotide release (ADP+Pi). The crystal structure, with three nucleotides bound, also showed a difference in the structural arrangement in the γ subunit. Superimposing the Abrahams γ subunit on the Menz γ subunit structure showed the N- and C-terminal helices were more twisted in the Menz structure. Further comparisons of the β_E structures indicated that steric effects would dictate that some amount of γ subunit rotation was necessary to accommodate the half-open conformation. The Menz crystal structure indicated that there may potentially be much more internal elasticity between the N- and C-terminal helices and the central domain of the γ subunit than previously thought. In the chloroplast enzyme, it is possible that formation of the regulatory disulfide bond on the γ subunit partially impairs the formation of the half-open β_E conformation, by inhibiting necessary conformational changes between the γ subunit twisted helices, resulting in the partial loss of catalytic activity (Richter et al., 2005). However, since γC89 becomes exposed in the presence of a membrane potential, a partial rotation of the N- and C-terminal helices relative to the central domain may be the conformation change that is blocked by formation of the regulatory disulfide bond (Richter et al., 2005).

To examine the role of inter-domain conformational changes within the γ subunit of CF_1 during catalysis, we prepared γ subunit mutants containing pairs of cysteines in select locations to potentially cross-link the N- and C-terminal α helices together, to cross-link the C-terminal α helix to the central domain, and to cross-link the two loop regions within the central domain. The cross-linking of the different portions of the γ subunit is expected to

identify if inter-helical conformational changes or conformational changes between the central domain and the C-terminal helix are necessary for catalytic activity. The mutant γ subunits were assembled into a hybrid photosynthetic F_1 complex containing the α and β subunits from *Rhodospirillum rubrum* F_1 (RrF_1) described in previous studies (Du and Gromet-Elhanan, 1999; Du et al., 2001; Tucker et al., 2004). These hybrid enzymes have similar but distinct catalytic properties to the RF_1 and CF_1 enzymes (Du and Gromet-Elhanan, 1999; Tucker et al., 2001). The γ subunit cysteine mutants were also assembled with $\alpha_3\beta_3$ hexamers isolated from native CF_1, resulting in a functional homogeneous enzyme (Gao et al., 1995).

Fluorescence labeling experiments and non-reducing SDS-PAGE of the assembled mutants indicated that several of the introduced cysteinyl pairs formed dithiols that were readily reducible. All of the γ subunit cysteine pair mutations exhibited normal CaATPase activities in both the hybrid and native enzyme systems, independent of the redox state of the introduced dithiol, indicating that large scale movements between the respective domains are not required for catalytic turnover. Pairs of cysteinyl residues designed to cross-link the N- and C- terminal helices together led to a loss of activation by oxyanions without a loss of basal CaATPase and MgATPase activities. The results provide evidence for the involvement of a "catch" formed between the twisted helical domain of the γ subunit and the DELSEED loop region on the β subunit in a critical enzyme activation process.

B. Experimental Procedures

1. Materials

Intact CF_1 and CF_1 lacking δ and ε subunits were isolated from spinach as described elsewhere (McCarty and Racker, 1968; Richter et al., 1985). Purified CF_1 was stored as an ammonium sulfate precipitate at 4°C and desalted prior to use. Native ε and δ subunits were isolated from CF_1 and stored for short periods (1-3 days) at 4°C or for longer periods at -20°C in a buffer containing 20% ethanol (V/V) and 30% glycerol (V/V) (Richter et al., 1984; Richter et al., 1985; Younis et al., 1977). DEAE cellulose, antibiotics (ampicillin, tetracycline, and chloramphenicol), Sephadex G-50 resin, and Ni-NTA resin were purchased from Sigma-Aldrich. Hydroxyapatite HTP gel was from BioRad. Tryptone and yeast extract were obtained from DIFCO. ATP (grade II) was purchased from Midwest Scientific and urea (ultra pure) was purchased from ICN Biomedicals Inc. Dialysis tubing (8,000 M.W. cut-off) was obtained from Biodesign Inc. (New York). All other chemicals were of the highest quality reagent grade available.

2. Production of γ subunit mutants

Mutant CF_1 γ subunits were constructed by enzymatic amplification of the expression plasmid pET8c-gamma.BB1 (Sokolov et al., 1999). This plasmid contained the wild-type γ subunit gene with all four native cysteines mutated to alanines, resulting in a "Cysless" γ subunit. The following primers were obtained from Integrated DNA Technologies (Iowa): A89C/F, 5'-pGTG GTC TTT GCG GCG GGT TTA AT-3', A89/R, 5'-pGTC GCC GGT AAC CAC CAT CAA CGC-3', N143C/F, 5'-pTTC GAC GGA ACA TGT CTA CCA ACC GCC-3', N143C/R, 5'-pGTA CCT GTC GAC GGG AAT CTC AGG-3', L30C/F, 5'-pGTC GCC GCC GCT TGT GTC CGC-3', L30C/R, 5'-pGAG CTT CAT TGC TTC GGT GAT CTT CTG-3', V31C/F, 5'-pGCC GCC GCT AAA TGT CGC CGT GCG-3', V31C/R, 5'-pGAC GAG CTT CAT TGC TTC GGT GAT-3', A276C/F, 5'-pGCT AGT GAA CTT TGT GCG

AGG ATG ACT-3', A276C/R, 5'-pAAG TGA TTC TTG TAA AGC CCT CAA AAT-3', R278C/F, 5'-pAGT GAA CTT GCT GCG TGT ATG ACT GCT-3', R278C/R, 5'-pAGC AAG TGA TTC TTG TAA AGC CCT CAA-3'. PCR reactions, plasmid DNA purification, and recombinant plasmid ligation were carried out as described elsewhere (Tucker et al., 2001). The resulting plasmid was transformed into competent *E.coli* XL1-blue cells (Novagen). The entire sequence of each mutant gene was confirmed by the Iowa State DNA Sequencing Facility. Sequenced plasmids were then transformed into the expression host *E.coli* BL21(DE3)/pLysS (Novagen), and the mutant γ subunits were expressed in insoluble inclusion bodies as described earlier (Gao et al., 1995). The following mutant γ subunits were expressed: $\gamma^{A89C,N143C}$, $\gamma^{A89C,A276C}$, $\gamma^{A89C,R278C}$, $\gamma^{K30C,A276C}$, $\gamma^{K30C,R278C}$, $\gamma^{V31C,A276C}$, and $\gamma^{V31C,R278C}$.

3. Assembly and purification of hybrid $\alpha_3\beta_3\gamma$ complexes

Inclusion bodies from the three core subunits ($RrF_1\alpha_{6xhis}$, $RrF_1\beta$, and $CF_1\gamma^{mutant}$) were solubilized in 8 M urea, diluted in refolding buffer, and assembled as previously described (He et al., 2007). Following an overnight dialysis, the assembled protein complexes were purified by DEAE anion exchange chromatography (Gao et al., 1995). Further purification was achieved with size-exclusion chromatography using a Superdex 200 (Pharmacia) column and a Biorad Biologic HR fast performance chromatography system running at a flow rate of 0.5 mL/min. The recombinant protein samples were eluted in 50 mM Tricine-NaOH (pH. 7.8) and 50 mM NaCl. 20% Glycerol ATP was added to the eluted protein samples with final concentrations of 20% (v/v) and 1 mM, respectively, before storage at -80°C.

4. Assembly of γ subunit mutants within the CF_1 $\alpha_3\beta_3$ hexamer

Assembly and purification of recombinant $\alpha_3\beta_3\gamma$ complexes – Mutant CF_1 γ subunits were solubilized in 8M urea and folded as described earlier (He et al., 2007). The native chloroplast $\alpha_3\beta_3$ hexamers were purified from CF_1 by hydroxylapetite chromatography (Gao et al., 1995). Individually folded γ subunits containing the cysteine mutations were reconstituted with $\alpha_3\beta_3$ hexamers and purified by DEAE anion exchange chromatography (Gao et al., 1995).

Reconstitution of $\alpha_3\beta_3\gamma$ assemblies with thylakoid membranes deficient in CF_1 – Spinach chloroplast thylakoids were treated with NaBr to generate thylakoid membranes lacking CF_1 (Cruz et al., 1995; Cruz et al., 1997). Purified reconstituted $\alpha_3\beta_3\gamma$ assemblies were incubated with the ε-δ at saturating molar ratios (15 μg δ–ε per 10 μg $\alpha_3\beta_3\gamma$) for 1 hr at room temperature in 40 mM Tris-HCl (pH 8.0). The assembled complex was filtered through a Sephadex G-50 centrifuge column to remove unbound ε and δ subunits. Assembled enzyme complexes (~100 μg) were reconstituted with CF_1-deficient thylakoid membranes (equivalent to 20 μg of chlorophyll) in a buffer containing 20 mM Tricine-NaOH (pH 8.0), 1 mM $MgCl_2$, and 0.2 mg/ml bovine serum albumin in a final volume of 0.5 ml on ice for 10 min (Andreo et al., 1982; Patrie and McCarty, 1984).

5. ATP synthesis by γ subunit mutants

Proton permeability measurements – Reconstituted thylakoid membranes equivalent to 20 μg of chlorophyll were assayed for pH gradient formation, as shown in Figure 15, using 9-amino-6-chloro-2-methoxyacridine (ACMA) fluorescence quenching in an assay buffer of 1 ml total volume. The assay buffer contained 40 mM Tricine – NaOH (pH 8.0), 50 mM NaCl, 50 μM phenazine methosulfate, 2 μM ACMA, and 2.5 mM ascorbate (pH 6.8). ACMA (excitation at 410 nm and emission at 450 nm) fluorescence quenching was measured

Figure 15. ***Measurement of pH gradient.*** The thylakoid particles were purified and CF_1 stripped off the membrane. CF_1 wild-type and mutant protein assemblies were reconstituted with the membrane described in the *Experimental Procedures* section. The electron transport chain is indicated in yellow. The unprotonated ACMA dye can penetrate the membrane freely whereas the protonated dye cannot and is retained within the thylakoid lumen space. The ACMA fluorescence is reduced upon protonation.

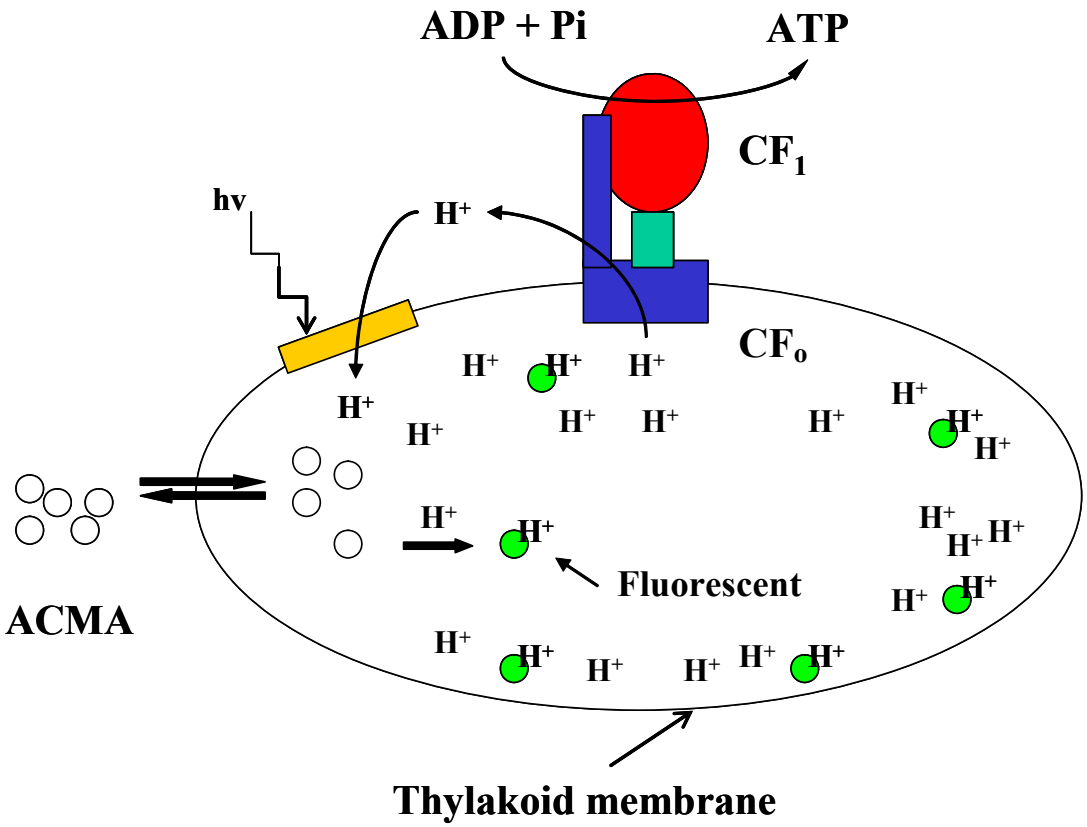
ADP + Pi
ATP
CF1
hv
H+
CFo
ACMA
Fluorescent
Thylakoid membrane

as described previously (Cruz et al., 1995). Fluorescence quenching was reported as percentage of the ratio of ΔF/F of mutant assemblies relative to wild type CF_1, where ΔF was the difference in fluorescence and F the steady state fluorescence (Evron and McCarty, 2000).

ATP synthesis measurements – ATP synthesis was measured in 1 ml of assay mixture containing 50 mM Tricine – NaOH (pH 8.0), 50 mM NaCl, 5 mM $MgCl_2$, 0.05 mM PMS, 2 mM potassium phosphate (pH 7.0), 1 mM ADP (ATP - free), and reconstituted thylakoid membranes equivalent to 20 μg of chlorophyll. The reaction was carried out under a light intensity of 2.5×10^6 ergs/cm^2/s for 2 min at 22ºC (Andreo et al., 1982). Trichloroacetic acid was added to the reaction after the light was switched off, to a final concentration of 0.5% (v/v) and the mixture was centrifuged at 30,000 ×g for 5 min at room temperature. The resulting supernatant was assayed for ATP concentration instantly using a Sirius II luminometer in which 100 μl of the supernatant solution was mixed in a Sarstedt tube with 100 μl of assay buffer, containing 25 mM Tris-acetate (pH 7.75), 2 mM EDTA, 50 mM DTT, 0.02 mM D-luciferin, 1.5 mg/ml BSA, 20 mM magnesium acetate, and 0.3 μg/ml luciferase. The luminescence was measured by integrating the signal for 5 sec after injection. The same reaction mix was used to determine concentrations of ATP standards (10^{-11} M to 10^{-5} M in 10 – fold increments) dissolved in 25 mM Tris-acetate (pH 7.75).

6. Fluorescence accessibility studies of γ subunit mutants

Labeling of unfolded γ subunit mutants - Isolated inclusion bodies for each cysteine pair mutation were solubilized in 8 M urea and 50 mM Tricine (pH 8.0) for 20 min at 4°C. Approximately 1 mg of each solubilized mutant was labeled using the following procedure. First they were treated with 100 μM $CuCl_2$ for 30 min, and another 1 mg sample of each was reduced in 25 mM DTT for 30 min. The samples were passed through Sephadex G-50

centrifuge columns, equilibrated with 8 M urea 50 mM Tricine (pH 8.0), to remove any remaining DTT or $CuCl_2$. Reduced samples were passed through an additional Sephadex G-50 column to ensure all DTT was removed. Approximately 100 µg of each inclusion body sample was incubated with 30 µM fluorescein maleimide for 30 min. To each sample 100 µM DTT was added to quench any unreacted probe.

Labeling hybrid $\alpha_3\beta_3\gamma$ complexes - Approximately 120 µg of each $\alpha_3\beta_3\gamma$ complex was labeled as described for the γ inclusion bodies, minus the 8M urea treatment. Each labeled $\alpha_3\beta_3\gamma$ sample was precipitated with 40% (v/v) trichloroacetic acid and centrifuged at 10,000 x g for 20 min. The residual protein pellets were dissolved in SDS mix, minus DTT.

Labeling unfolded hybrid $\alpha_3\beta_3\gamma$ complexes – Assembled protein complexes were unfolded by incubation incubated in 8 M urea, 50 mM Tricine (pH 8.0), and 1 mM ATP, for 1 hr. Approximately 90 µg of each unfolded complex was labeled as described above.

Gel electrophoresis – Gel electrophoresis was performed under non-reducing conditions using pre-cast NuPage@ (Invitrogen, San Diego) gels (4-20% acrylamide gradient) with each lane containing approximately 7.5-10 µg of protein.

7. Other procedures

ATPase activities were determined by measuring phosphate release (Taussky and Shorr, 1953) for 5 minutes at 37°C. The assay mixture for calcium-dependent ATPase activity contained 50 mM Tris-HCl (pH 8.0), 5 mM ATP and 5 mM $CaCl_2$. That for magnesium-dependent ATPase activity contained 40 mM Tricine-NaOH (pH 8), 4 mM ATP, 2 mM $MgCl_2$ and 50 mM Na_2SO_3 (Hu et al., 1993). Protein concentrations were determined by the Bradford method (Bradford, 1976).

C. Results

1. Cysteine mutations in the γ subunit

To examine possible inter-domain motions within the γ subunit that occur during rotational catalysis, several pairs of adjacent residues were mutated to cysteines in an attempt to directly cross-link the N- and C-terminal α helices to each other as well as the C-terminal α helix to the central domain. The 6 residues mutated to cysteines, as described in the *Experimental Procedures*, where chosen based on predicted adjacent positions in the α helices, and the central domain in the recently published homology model of the chloroplast gamma subunit (Richter, 2004). The predicted positions of these residues are shown in Figure 16.

A recombinant "Cys-less" gamma subunit, with the four native cysteinyl residues (γC89, γC199, γC205, and γC322) mutated to alanines, was used as a template to construct the mutant γ subunits. Gamma subunits containing cysteinyl pair mutations were created to cross-link the different γ subunit regions together (Table 5). Since the positioning of the mutant cysteines residues in these experiments are based on a hypothetical model of the γ subunit, several cysteinyl pairs were constructed placing the pairs in nearby positions in the event that the N-and C-terminal α helices of the γ subunit homology structure are slightly different than those in the native γ subunit structure. The mutants $\gamma^{A89C,A276C}$ and $\gamma^{A89C,R278C}$ (Figure 16A and 16B) were designed to attempt to cross link the N-terminal α helix (residues A276 and R278) with the central domain of the γ subunit (A89). The mutant $\gamma^{A89C,N143C}$ (Figure 16G) was created to attempt to cross-link two adjacent loop regions of the central domain of the γ subunit. The mutants $\gamma^{A89C,R278C}$, $\gamma^{K30C,A276C}$, $\gamma^{K30C,R278C}$,

Table 5. Gamma subunit cysteinyl-pair mutations indicating proposed locations of cross-links

Mutation	Location on γ subunit		Cysteine Pairs	Linkage
γ^{A89C}	Central Domain		$\gamma^{A89C, A276C}$	Central domain and C-term helix
γ^{K30C}	N-terminal helix		$\gamma^{A89C, R278C}$	Central domain and C-term helix
γ^{V31C}	N-terminal helix		$\gamma^{A89C, N143C}$	Loops of central domain
γ^{A276C}	C-terminal helix		$\gamma^{K30C, A276C}$	N- and C-terminal helices
γ^{R278C}	C-terminal helix		$\gamma^{V31C, A276C}$	N- and C-terminal helices
γ^{N143C}	Central Domain		$\gamma^{K30C, R278C}$	N- and C-terminal helices
			$\gamma^{V31C, R278C}$	N- and C-terminal helices

Figure 16. ***Placement of putative cross-linking dithiols.*** The homology model of the γ subunit of the chloroplast ATP synthase is shown in grey. The residues mutated to cysteines in this study are space filled: γK30 (red), γV31 (cyan), γC89 (yellow), γA276 (green), γR278 (purple), and γN143 (pink). The dithiol pairs A) $\gamma^{A89C\ (yellow),A276C\ (green)}$ and B) $\gamma^{A89C\ (yellow),R278C\ (purple)}$ were designed to cross-link the C-terminal helix to the central domain of the γ subunit; the dithiol pairs C) $\gamma^{K30C\ (red),A276C\ (green)}$, D) $\gamma^{V31C\ (cyan),A276C\ (green)}$, E) $\gamma^{K30C\ (red),R278C\ (purple)}$, and F) $\gamma^{V31C\ (cyan),R278C\ (purple)}$ were designed to cross-link the N- and C-terminal helices of the γ subunit; the dithiol pair G) $\gamma^{A89C\ (yellow),N143C\ (pink)}$ was designed to cross-link two loops of the central domain of the γ subunit. All the introduced cysteines are indicated in H.

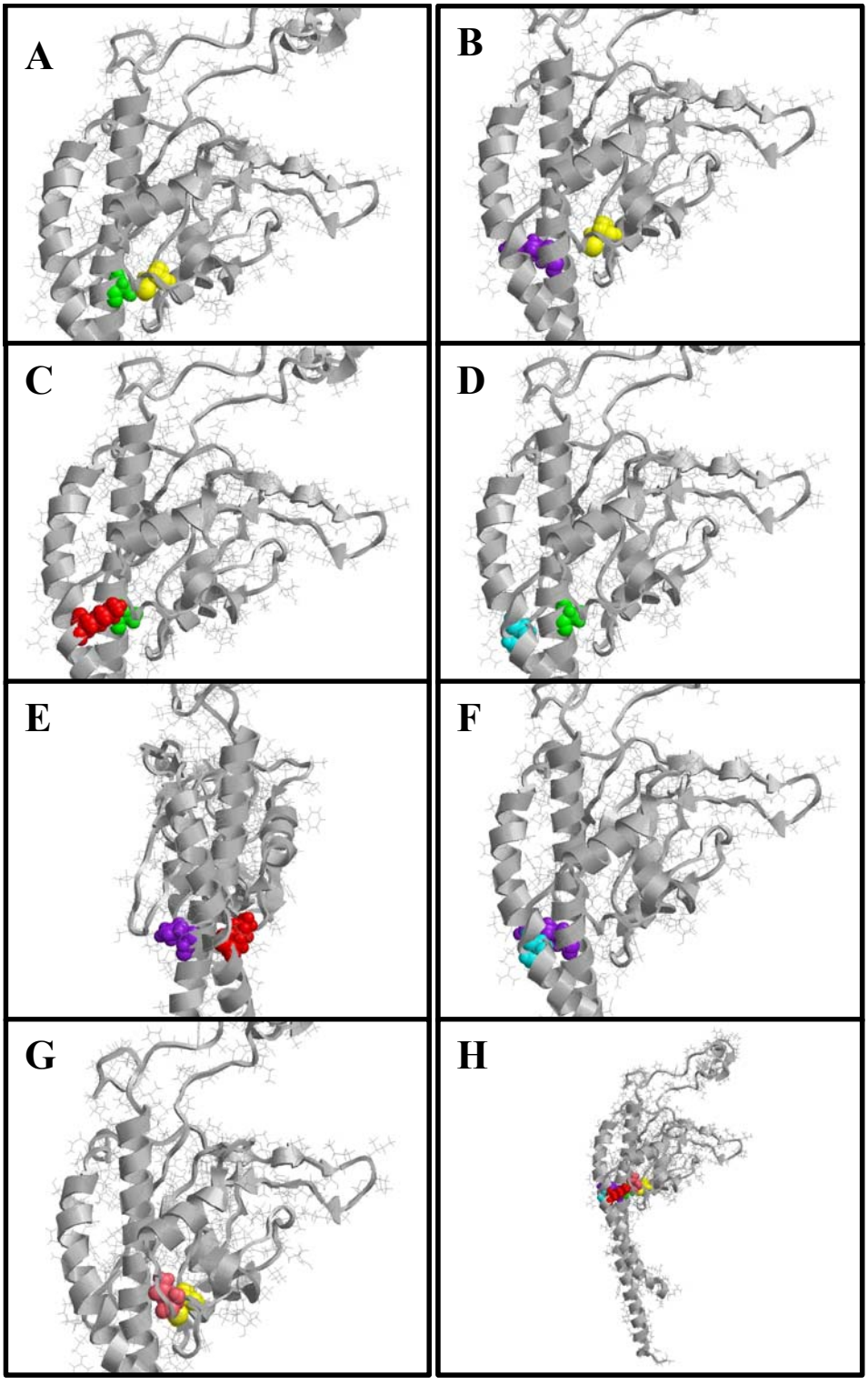
A
B
C
D
E
F
G
H

$\gamma^{V31C,A276C}$, and $\gamma^{V31C,R278C}$ (Figure 16B, 16C, 16E, 16D, and 16F) were created to cross-link the N- and C-terminal α helices in a region where the helices twist together and are in close proximity. Formation of disulfide bonds between the introduced cysteinyl pairs was expected to prevent or limit relative inter-domain motion of the γ subunit, thereby exploring the requirement for such motion in the catalytic process.

2. Catalytic activities of mutant γ subunits in hybrid enzymes

Both the wild type and mutant chloroplast γ subunits were assembled with recombinant α and β subunits from *R. rubrum* F_1 to form functional hybrid enzymes as described in the *Experimental Procedures*. The assembly conditions and the wild-type catalytic activities have been well characterized (Du and Gromet-Elhanan, 1999; Tucker et al., 2001). The purified hybrid enzyme assemblies exhibit both CaATPase and MgATPase activities and are capable of CaATP-dependent and MgATP-dependent γ subunit rotation (Tucker et al., 2004). The Ca^{2+}- and Mg^{2+}-dependent ATPase activities of the purified hybrid mutant assemblies were compared to those of the wild type hybrid enzyme as shown in Tables 6 through 8. The assemblies were exposed to conditions that were expected to either promote disulfide bond formation (100 μM $CuCl_2$, 1 hr at RT) or promote disulfide bond reduction (25 mM DTT, 1 hr at RT). The enzyme containing the wild type γ subunit, possessing only the two regulatory disulfide-forming thiols, was, as expected, significantly activated (~52%) under reducing conditions (Table 6). Since the mutants are deficient in the regulatory thiols they should be maximally activated (Samra et al., 2006) and any change observed following exposure to oxidizing or reducing conditions should be due to forming and breaking an inter-domain cross-link between the two introduced cysteinyl residues.

Table 6. CaATPase activities of mutant γ subunits assembled with the hybrid (α_R and β_R) subunits

Hybrid protein[1]	Linkage	Ca^{2+}ATPase Activity (μmole per min per mg protein)	
		Oxidized[2]	Reduced[2]
$\alpha_3\beta_{3'}\gamma^{WT}$	N/A	31.5 ± 4.0	47.8 ± 2.1
$\alpha_3\beta_{3'}\gamma^{K30C, A276C}$	N- & C-term helices	42.1 ± 5.1	45.6 ± 0.6
$\alpha_3\beta_{3'}\gamma^{V31C, A276C}$	N- & C-term helices	42.1 ± 2.1	44.7 ± 1.5
$\alpha_3\beta_{3'}\gamma^{K30C, R278C}$	N- & C-term helices	42.1 ± 3.6	46.3 ± 2.9
$\alpha_3\beta_{3'}\gamma^{V31C, R278C}$	N- & C-term helices	37.5 ± 5.2	37.0 ± 2.3
$\alpha_3\beta_{3'}\gamma^{A89C, A276C}$	C-term helix & central domain	55.3 ± 2.8	57.8 ± 1.1
$\alpha_3\beta_{3'}\gamma^{A89C, R278C}$	C-term helix & central domain	53.7 ± 4.2	57.9 ± 1.1
$\alpha_3\beta_{3'}\gamma^{A89C, N143C}$	Loop regions of central domain	37.9 ± 1.1	41.3 ± 3.3

[1]Hybrid F_1 assemblies were purified and assayed as described in the *Experimental* section.
[2]The enzyme assembly was pre-treated with either 25 mM DTT (reduced) or 100 μM $CuCl_2$ (oxidized) prior to assay. Errors are expressed as standard deviations with n = 4.

The CaATPase activities of all of the mutants were within 20% of the activity of the reduced wild type enzyme and did not respond significantly to thiol oxidizing conditions (Table 6). The MgATPase activities of the mutants (Table 7) varied between 29 and 80% of the activity of the wild type assembly, however, as with the CaATPase activities, they did not respond to oxidizing or reducing conditions. In all but two cases, the oxyanion (sulfite)-stimulated MgATPase activity (Table 8) was within 20% of that of the wild type enzyme. The exceptions were the assemblies containing the $\gamma^{K30C,A276C}$ mutant and the $\gamma^{V31C,A276C}$ mutant. The MgATPase activity of the $\gamma^{K30C,A276C}$ mutant was reduced by 62%. The $\gamma^{V31C,A276C}$ mutant showed no statistically significant stimulation by sulfite. As with the CaATPase and MgATPase activities, the sulfite-stimulated MgATPase activities were insensitive to oxidizing conditions. This indicated either that the thiol pairs failed to form cross-linking disulfide bridges or that catalysis was not altered significantly upon formation of cross-links.

3. Accessibility of introduced cysteine residues to fluorescent probes.

As a first step to determine whether or not the introduced cysteine residues in the hybrid enzyme assemblies form cross-linking disulfide bridges, the mutant γ subunits were solubilized from inclusion bodies into 8 M urea, exposed to either oxidizing or reducing conditions, desalted on Sephadex G-50 then exposed to fluoresceinyl maleimide. The treated γ subunits were subjected to electrophoresis on polyacrylamide gels in the presence of SDS and visualized first by examining their fluorescence under long wavelength ultraviolet light followed by staining with Coomassie blue. The results are shown in Figure 17. Following treatment under reducing conditions, all of the γ subunits, with the exception of the Cys-less γ

Table 7. MgATPase activities of mutant γ subunits assembled with the hybrid (α_R and β_R) subunits

Hybrid protein[1]	Linkage	Mg^{2+}ATPase Minus Sulfite Activity (μmole per min per mg protein)	
		Oxidized[2]	Reduced[2]
$\alpha_3\beta_{3'}\gamma^{WT}$	N/A	8.3 ± 0.2	14.0 ± 0.9
$\alpha_3\beta_{3'}\gamma^{K30C, A276C}$	N- & C-term helices	3.9 ± 0.8	4.1 ± 1.1
$\alpha_3\beta_{3'}\gamma^{V31C, A276C}$	N- & C-term helices	4.3 ± 1.0	3.9 ± 1.7
$\alpha_3\beta_{3'}\gamma^{K30C, R278C}$	N- & C-term helices	7.2 ± 0.9	8.3 ± 1.6
$\alpha_3\beta_{3'}\gamma^{V31C, R278C}$	N- & C-term helices	6.1 ± 1.2	5.8 ± 0.9
$\alpha_3\beta_{3'}\gamma^{A89C, A276C}$	C-term helix & central domain	9.5 ± 0.3	10.1 ± 0.1
$\alpha_3\beta_{3'}\gamma^{A89C, R278C}$	C-term helix & central domain	8.4 ± 2.2	9.1 ± 0.5
$\alpha_3\beta_{3'}\gamma^{A89C, N143C}$	Loop regions of central domain	9.5 ± 2.1	11.2 ± 2.3

[1]Hybrid F_1 assemblies were purified and assayed as described in the *Experimental* section.
[2]The enzyme assembly was pre-treated with either 25 mM DTT (reduced) or 100 μM $CuCl_2$ (oxidized) prior to assay. Errors are expressed as standard deviations with n = 4.

Table 8. MgATPase activities of mutant γ subunits assembled with the with the hybrid (α_R and β_R) subunits

Hybrid protein[1]	Linkage	Mg^{2+}ATPase Plus Sulfite Activity (μmole per min per mg protein)	
		Oxidized[2]	Reduced[2]
$\alpha_3\beta_{3'}\gamma^{WT}$	N/A	21.3 ± 1.5	39.5 ± 3.8
$\alpha_3\beta_{3'}\gamma^{K30C, A276C}$	N- & C-term helices	14.9 ± 1.0	15.1 ± 0.9
$\alpha_3\beta_{3'}\gamma^{V31C, A276C}$	N- & C-term helices	4.24 ± 2.5	3.8 ± 3.0
$\alpha_3\beta_{3'}\gamma^{K30C, R278C}$	N- & C-term helices	36.5 ± 1.0	38.2 ± 2.6
$\alpha_3\beta_{3'}\gamma^{V31C, R278C}$	N- & C-term helices	32.3 ± 1.7	31.4 ± 2.0
$\alpha_3\beta_{3'}\gamma^{A89C, A276C}$	C-term helix & central domain	41.6 ± 3.5	42.8 ± 1.2
$\alpha_3\beta_{3'}\gamma^{A89C, R278C}$	C-term helix & central domain	44.8 ± 1.9	43.7 ± 2.2
$\alpha_3\beta_{3'}\gamma^{A89C, N143C}$	Loop regions of central domain	35.4 ± 1.4	37.6 ± 0.9

[1]Hybrid F_1 assemblies were purified and assayed as described in the *Experimental* section.
[2]The enzyme assembly was pre-treated with either 25 mM DTT (reduced) or 100 μM $CuCl_2$ (oxidized) prior to assay. Errors are expressed as standard deviations with n = 4.

Figure 17. ***SDS-PAGE of ures-solubilized, fluorescein-labeled γ mutations.*** Inclusion bodies containing the mutant γ subunits were solubilized in urea and labeled with fluorescein maleimide under oxidizing and reducing conditions as described in the *Experimental Methods*. The upper portion of the figure shows the gel stained with Coomassie brilliant blue, while the lower portion is the same gel indicates the relative fluorescence of the labeled protein. Lane 1, γ^{WT} (oxid); Lane 2, γ^{WT} (red); Lane 3, $\gamma^{Cysless}$ (oxid); Lane 4, $\gamma^{Cysless}$ (red); Lane 5, $\gamma^{K30C,A276C}$ (oxid); Lane 6, $\gamma^{K30C,A276C}$ (red); Lane 7, $\gamma^{V31C,A276C}$ (oxid); Lane 8, $\gamma^{V31C,A276C}$ (red); Lane 9, $\gamma^{A89C,N143C}$ (oxid); Lane 10, $\gamma^{A89C,N143C}$ (red); Lane 11, γ^{WT} (oxid); Lane 12, γ^{WT} (red); Lane 13, $\gamma^{A89C,A276C}$ (oxid); Lane 14, $\gamma^{A89C,A276C}$ (red); Lane 15, $\gamma^{A89C,R278C}$ (oxid); and Lane 16, $\gamma^{A89C,R278C}$ (red); Lane 17, $\gamma^{K30C,R278C}$ (oxid); Lane 18, $\gamma^{K30C,R278C}$ (red); Lane 19, $\gamma^{V31C,R278C}$ (oxid); Lane 20, $\gamma^{V31C,R278C}$ (red).

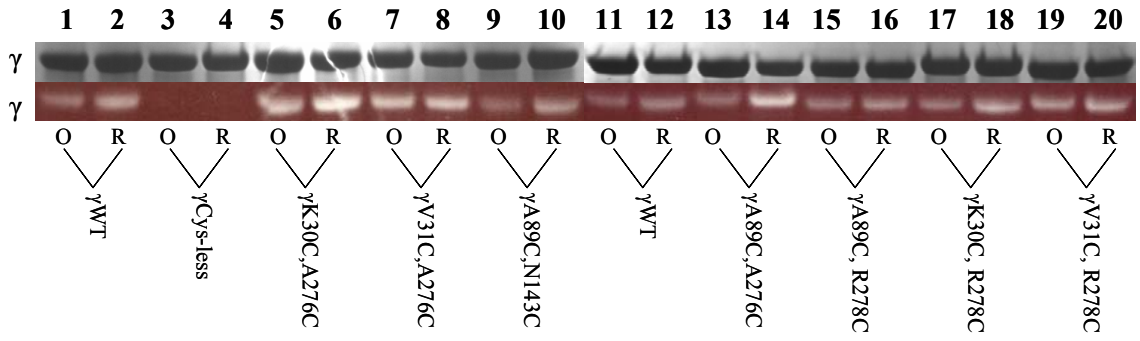
1 2 3 4 5 6 7 8 9 10 11 12 13 14 15 16 17 18 19 20
γ
γ
O R O R O R O R O R O R O R O R O R O R
γWT
γCys-less
γK30C,A276C
γV31C,A276C
γA89C,N143C
γWT
γA89C,A276C
γA89C, R278C
γK30C, R278C
γV31C, R278C

subunit control (lanes 3 and 4), were labeled with the fluorescent maleimide indicating that exposed cysteine residues were present. Since the labeling was performed in the presence of urea, which is expected to maintain the γ polypeptides in an unfolded state, a significant amount of disulfide bond formation was not expected. However, with a few of the mutants, most notably the $\gamma^{A89C,\ A276C}$ (lanes 13 and 14) and $\gamma^{K30C,\ R278C}$ (lanes 17 and 18) mutants, there was a significant decrease in labeling upon exposure to oxidizing conditions indicating that some cross-linking had occurred. The results confirmed the presence of the introduced cysteine residues in the mutant γ subunits and also demonstrated the specificity with which the introduced cysteinyl residues can be targeted with the fluorescent probe.

As a second step, the mutant γ subunits were folded and assembled into hybrid $\alpha_3\beta_3\gamma$ complexes which were purified by anion exchange and size exclusion chromatography then exposed to oxidizing/reducing conditions. The assemblies were desalted as before then exposed to fluoresceinyl maleimide. The results are shown in Figure 18 which compares the relative fluorescence and Coomassie blue-staining of the α, β, and γ subunit bands. The α subunit is labeled in this experiment due to the presence of two solvent-accessible cysteine residues on this subunit in contrast to the β subunit which lacks accessible cysteine residues. Lanes 1 and 2 show the wild type γ subunit control assembly in which the nascent disulfide is essentially completely oxidized and therefore inaccessible to the fluorescent probe, whereas upon reduction it becomes accessible and is strongly labeled. Clear differences were also observed between the extent of labeling following disulfide oxidation versus reduction with four of the seven mutant assemblies, those containing $\gamma^{K30C,A276C}$, $\gamma^{V31C,A276C}$, $\gamma^{A89C,N143C}$, and $\gamma^{A89C,A276C}$. Two of the other three mutants, $\gamma^{V31C,R278C}$ and $\gamma^{K30C,R278C}$, were labeled to a lesser extent indicating a lower solvent accessibility. These

Figure 18. ***SDS-PAGE of hybrid enzyme assemblies containing fluorescein-labeled γ subunit cysteines residues.*** Purified hybrid enzymes containing the mutant gamma subunits were labeled with fluorescein maleimide under oxidizing and reducing conditions as described in the *Experimental Methods*. The upper portion of the figure shows the gel stained with Coomassie brilliant blue, while the lower portion is the same gel indicating relative fluorescence of the labeled protein. Lane 1, $\alpha_3\beta_3\gamma^{WT}$ (oxid); Lane 2, $\alpha_3\beta_3\gamma^{WT}$ (red); Lane 3, $\alpha_3\beta_3\gamma^{K30C,A276C}$ (oxid); Lane 4, $\alpha_3\beta_3\gamma^{K30C,A276C}$ (red); Lane 5, $\alpha_3\beta_3\gamma^{V31C,A276C}$ (oxid); Lane 6, $\alpha_3\beta_3\gamma^{V31C,A276C}$ (red); Lane 7, $\alpha_3\beta_3\gamma^{V31C,R278C}$ (oxid); Lane 8, $\alpha_3\beta_3\gamma^{V31C,R278C}$ (red); Lane 9, $\alpha_3\beta_3\gamma^{K30C,R278C}$ (oxid); Lane 10, $\alpha_3\beta_3\gamma^{K30C,R278C}$ (red); Lane 11, $\alpha_3\beta_3\gamma^{A89C,N143C}$ (oxid); Lane 12, $\alpha_3\beta_3\gamma^{A89C,N143C}$ (red); Lane 13, $\alpha_3\beta_3\gamma^{A89C,A276C}$ (oxid); Lane 14, $\alpha_3\beta_3\gamma^{A89C,\ A276C}$ (red); Lane 15, $\alpha_3\beta_3\gamma^{A89C,\ R278C}$ (oxid); Lane 16, $\alpha_3\beta_3\gamma^{A89C,\ R278C}$ (red).

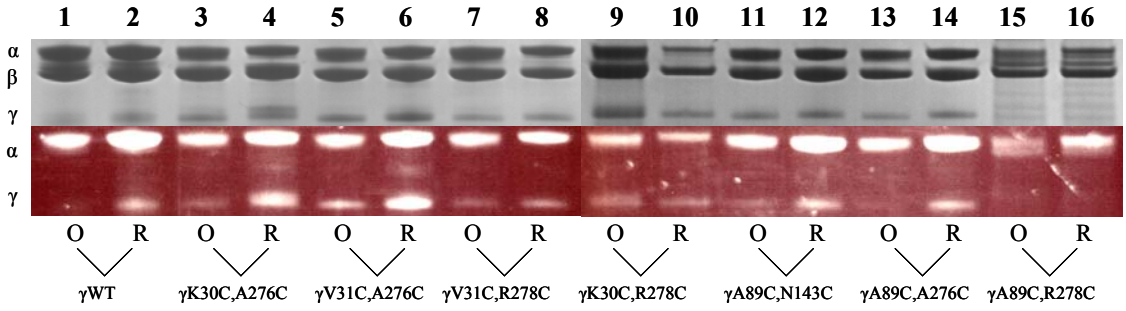
1 2 3 4 5 6 7 8 9 10 11 12 13 14 15 16
α
β
γ
α
γ
O R O R O R O R O R O R O R O R
γWT
γK30C,A276C
γV31C,A276C
γV31C,R278C
γK30C,R278C
γA89C,N143C
γA89C,A276C
γA89C,R278C

two mutants also showed a less marked difference between oxidizing and reducing conditions. The $\gamma^{A89C,R278C}$ mutant was partially proteolysed during the experiment so the result is inconclusive for this mutant.

In the control experiment shown in Figure 19, the purified wild type and mutant hybrid assemblies were treated in the same manner as in Figure 18 except that urea was added to a final concentration of 6 M prior to exposure to oxidizing or reducing conditions. The assemblies were then exposed to fluoresceine maleimide. Under these conditions the enzyme assembly is expected to disassociate and the α and β subunits will denature. The γ subunit, however, is more resistant to denaturation and is expected to maintain its tertiary structure even in the presence of SDS (Richter et al., 1984). This is confirmed from the observation that, unlike the unfolded subunit shown in Figure 16, in each of the mutants in this experiment the γ subunit retained sufficient structure to form disulfide bonds under oxidizing conditions (Figure 19).

Accompanying formation of the nascent regulatory disulfide bond in the γ subunit is a small shift (increase) in the mobility of the γ subunit during SDS gel electrophoresis (Ketcham et al., 1984). The shift can be seen most clearly in Figure 19 (lanes 1 and 2) for the wild type control. Only the reduced form (the band with the lower mobility, lane 2) can be labeled with the fluorescent probe. Similar mobility shifts were observed for the mutant assemblies following oxidation or reduction although the extent of resolution of the bands is different for different gels. In Figure 19, lanes 1 through 8 are from one gel and demonstrate clear resolution of the two bands. Lanes 9 through 16 are from a different gel with which the two bands failed to resolve. When the two bands did resolve, the extent of fluorescence labeling appeared to correspond nicely with the amount of the non-cross-linked γ band present. In lanes 1 through 8, a qualitative measure of the extent of disulfide bond formation

Figure 19. ***SDS-PAGE of hybrid enzyme assemblies containing fluorescein-labeled mutant γ subunits denatured in 8 M Urea.*** Purified hybrid enzymes containing the mutant gamma subunits were labeled with fluorescein maleimide under oxidizing and reducing conditions following denaturation in 8 M urea as described in the *Experimental Methods*. The upper portion of the figure shows the gel stained with Coomassie brilliant blue, while the lower portion is the same gel indicating relative fluorescence of the labeled protein. Lane 1, $\alpha_3\beta_3\gamma^{WT}$ (oxid); Lane 2, $\alpha_3\beta_3\gamma^{WT}$ (red); Lane 3, $\alpha_3\beta_3\gamma^{K30C,A276C}$ (oxid); Lane 4, $\alpha_3\beta_3\gamma^{K30C,A276C}$ (red); Lane 5, $\alpha_3\beta_3\gamma^{V31C,A276C}$ (oxid); Lane 6, $\alpha_3\beta_3\gamma^{V31C,A276C}$ (red); Lane 7, $\alpha_3\beta_3\gamma^{V31C,R278C}$ (oxid); Lane 8, $\alpha_3\beta_3\gamma^{V31C\ R278C}$ (red); Lane 9, $\alpha_3\beta_3\gamma^{K30C,R278C}$ (oxid); Lane 10, $\alpha_3\beta_3\gamma^{K30C,R278C}$ (red); Lane 11, $\alpha_3\beta_3\gamma^{A89C,N143C}$ (oxid); Lane 12, $\alpha_3\beta_3\gamma^{A89C,N143C}$ (red); Lane 13, $\alpha_3\beta_3\gamma^{A89C,A276C}$ (oxid); Lane 14, $\alpha_3\beta_3\gamma^{A89C,A276C}$ (red); Lane 15, $\alpha_3\beta_3\gamma^{A89C,R278C}$ (oxid); Lane 16, $\alpha_3\beta_3\gamma^{A89C,R278C}$ (red)..

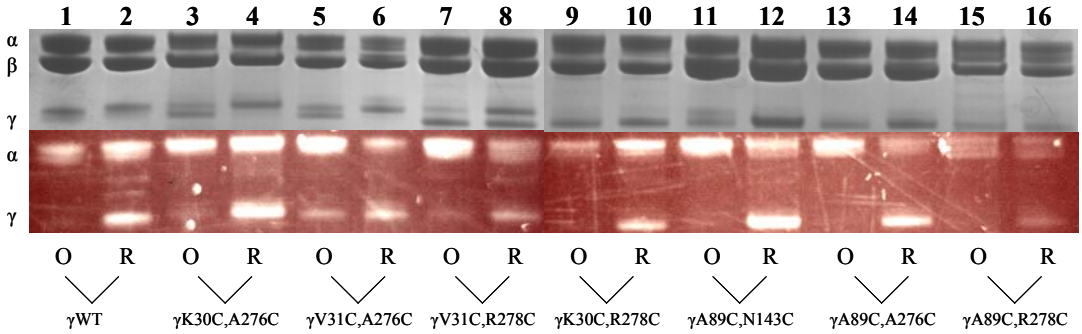
1 2 3 4 5 6 7 8 9 10 11 12 13 14 15 16
α
β
γ
α
γ
O R O R O R O R O R O R O R O R
γWT
γK30C,A276C
γV31C,A276C
γV31C,R278C
γK30C,R278C
γA89C,N143C
γA89C,A276C
γA89C,R278C

could also be obtained by comparing the Coomassie blue staining density of the two bands. For example, with the mutant assembly shown in lanes 3 and 4, more than 50% of the γ subunit is cross-linked under oxidizing conditions and essentially none under reducing conditions.

In all but the $\gamma^{K30C,R278C}$ assembly, the introduced pairs of cysteine residues became cross-linked to each other with >50% efficiency under oxidizing conditions. The $\gamma^{A89C,R278C}$ assembly shown in lanes 15 and 16 in Figures 18 and 19 was most likely partially proteolysed, indicated by the multiple protein bands on the gel, so the results are inconclusive. The $\gamma^{K30C,R278C}$ and $\gamma^{V31C,R278C}$ mutants (Figure 18 lanes 7, 8, 9, and 10) did not show a significant increase in fluorescence labeling following exposure to reducing conditions suggesting that the thiols are poorly accessible to DTT.

4. Catalytic activities of γ subunit cysteine mutants in native chloroplast enzyme assemblies

The two mutants, $\gamma^{V31C,A276C}$ and $\gamma^{K30C,A276C}$, that exhibited a complete or partial loss of sulfite-stimulated MgATPase activity in the hybrid enzyme system, were assembled with the native chloroplast $\alpha_3\beta_3$ hexamer $\gamma^{V31C,R278C}$ as described previously (Gao et al., 1995; Sokolov et al., 1999). This was done in order to examine the effects of the introduced cysteinyl pairs on proton-coupled activities (see section 6). The $\gamma^{V31C,R278C}$ mutant and wildtype γ were also assembled as controls. The ATP hydrolysis activities of the assemblies are summarized in Tables 9, 10, and 11. The three mutant enzymes had CaATPase activities comparable to that of the wild type enzyme (Table 9). The MgATPase activities for the $\alpha_3\beta_3\gamma^{K30C,A276C}$ and $\alpha_3\beta_3\gamma^{V31C,A276C}$ mutants were similar to that of the wildtype enzyme

Table 9. CaATPase activities of mutant γ subunits assembled with the CF_1 $\alpha_3\beta_3$ hexamer

Protein preparation[1]	Linkage	Ca^{2+}ATPase Activity (μmole per min per mg protein)	
		Oxidized[2]	Reduced[2]
$\alpha_3\beta_{3'}\gamma^{WT}$	N/A	15.8 ± 3.0	25.4 ± 1.1
$\alpha_3\beta_{3'}\gamma^{V31C, A276C}$	N- & C-term helices	21.3 ± 0.6	21.0 ± 0.7
$\alpha_3\beta_{3'}\gamma^{K30C, A276C}$	N- & C-term helices	20.4 ± 3.7	22.5 ± 3.1
$\alpha_3\beta_{3'}\gamma^{V31C, R278C}$	N- & C-term helices	24.7 ± 1.1	25.6 ± 3.3

[1]Core F_1 assemblies were purified and assayed as described in the *Experimental* section.
[2]The enzyme assembly was pre-treated with either 25 mM DTT (reduced) or 100 μM $CuCl_2$ (oxidized) prior to assay. Errors are expressed as standard deviations with n = 4.

Table 10. MgATPase activities of mutant γ subunits assembled with the CF_1 $\alpha_3\beta_3$ hexamer

Protein preparation[1]	Linkage	Mg^{2+} ATPase Minus Sulfite Activity (μmole per min per mg protein)	
		Oxidized[2]	Reduced[2]
$\alpha_3\beta_{3'}\gamma^{WT}$	N/A	2.3 ± 1.0	3.2 ± 1.0
$\alpha_3\beta_{3'}\gamma^{V31C, A276C}$	N- & C-term helices	2.0 ± 1.6	1.7 ± 1.9
$\alpha_3\beta_{3'}\gamma^{K30C, A276C}$	N- & C-term helices	2.8 ± 1.1	2.2 ± 1.2
$\alpha_3\beta_{3'}\gamma^{V31C, R278C}$	N- & C-term helices	2.3 ± 0.8	2.1 ± 0.3

[1]Core F_1 assemblies were purified and assayed as described in the *Experimental* section.
[2]The enzyme assembly was pre-treated with either 25 mM DTT (reduced) or 100 μM $CuCl_2$ (oxidized) prior to assay. Errors are expressed as standard deviations with n = 4.

Table 11. MgATPase activities of mutant γ subunits assembled with the CF_1 $\alpha_3\beta_3$ hexamer

Protein preparation[1]	Linkage	Mg^{2+} ATPase Plus Sulfite Activity (μmole per min per mg protein)	
		Oxidized[2]	Reduced[2]
$\alpha_3\beta_{3'}\gamma^{WT}$	N/A	32.6 ± 1.2	45.8 ± 0.9
$\alpha_3\beta_{3'}\gamma^{V31C, A276C}$	N- & C-term helices	15.7 ± 4.0	16.7 ± 4.2
$\alpha_3\beta_{3'}\gamma^{K30C, A276C}$	N- & C-term helices	34.1 ± 1.5	36.2 ± 3.8
$\alpha_3\beta_{3'}\gamma^{V31C, R278C}$	N- & C-term helices	41.2 ± 1.2	41.9 ± 1.9

[1]Core F_1 assemblies were purified and assayed as described in the *Experimental* section.
[2]The enzyme assembly was pre-treated with either 25 mM DTT (reduced) or 100 μM $CuCl_2$ (oxidized) prior to assay. Errors are expressed as standard deviations with n = 4.

(Table 10). As shown in Table 11, the reduced $\alpha_3\beta_3\gamma^{K30C,A276C}$ mutant showed a ~25% decrease of sulfite stimulated MgATPase activity and the reduced $\alpha_3\beta_3\gamma^{V31C,A276C}$ showed an ~65% decrease in sulfite stimulated MgATPase activity compared to the wild type enzyme. Thus the extent of loss of sulfite-stimulation was less than that observed with the hybrid enzyme (Table 8).

5. Binding of the inhibitory ε subunit to mutant γ assemblies

To assess the role of the introduced cysteine mutations in mediating ATPase inhibition by the ε subunit, the three cysteinyl pair mutants that were assembled with the native chloroplast α and β subunits were titrated with purified recombinant ε subunit. The titration data is shown in Figure 19. The experimental conditions needed for ε reconstitution require diluting the ε preparations from the ethanol/glycerol mixture in which they were isolated and stored approximately 1 part with 2 parts of the assay buffer such that the final concentrations of ethanol (~7%) and glycerol (~10%) can maintain ε solubility while allowing ε to rebind to the $\alpha_3\beta_3\gamma$ assembly. The native CF_1 was reduced for 30 mins with 25 mM DTT, to reduce the regulatory disulfide, which is not present in the three cysteinyl pair mutants, and the three mutant enzymes were oxidized for 1 hr with 100 μM $CuCl_2$ to induce disulfide bond formation prior to addition of the ε subunit. Figure 20 indicates that the three mutant enzymes were all inhibited by the ε subunit to a similar extent as the wild type chloroplast enzyme, suggesting that the formation of internal cross-links did not significantly affect the response of the enzyme to ε binding.

6. Effects of cysteine mutations on ATP synthesis

Figure 20. ***Epsilon titration of reconstituted CF_1 $\alpha_3\beta_3\gamma$ complexes containing mutant γ subunits with cysteines mutations.*** Mutant γ constructs were assembled with chloroplast $\alpha_3\beta_3$ and purified by anion exchange chromatography (Gao et al., 1995). Samples were incubated for 30 min at room temperature in the presence of 100 μM $CuCl_2$ in the case of the mutants and 25 mM DTT for the wild type enzyme. Two parts of incubation buffer containing 10 μg samples of each $\alpha_3\beta_3\gamma$ assembly were mixed with one part of ε subunit isolation buffer (Richter and McCarty, 1987) containing the indicated amounts of the ε subunit, and incubated for 10 min at room temperature. At the end of the incubation, 0.5 ml of double strength calcium-dependent ATPase assay mixture, pre-warmed to 37°C, was added to initiate the assay. Filled circles, reduced $\alpha_3\beta_3\gamma^{WT}$; Filled squares, $\alpha_3\beta_3\gamma^{K30C,\ A276C}$; Open circles, $\alpha_3\beta_3\gamma^{V31C,\ A276C}$; Filled triangles, $\alpha_3\beta_3\gamma^{V31C,\ R278C}$.

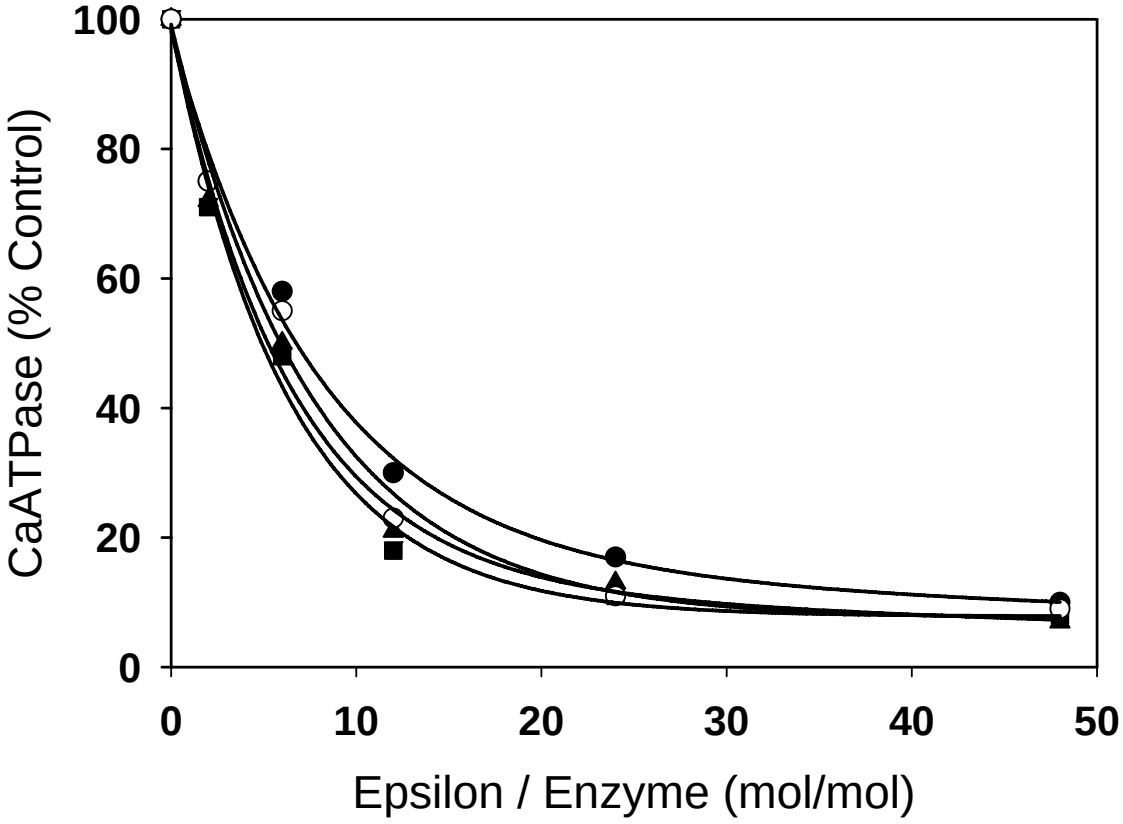
100
80
60
40
20
0
CaATPase (% Control)
0
10
20
30
40
50
Epsilon / Enzyme (mol/mol)

To examine the effects of mutations at positions γK30, γV31, and γA276 on ATP synthesis, the native chloroplast enzymes $\alpha_3\beta_3\gamma^{K30C,\ A276C}$, $\alpha_3\beta_3\gamma^{V31C,\ A276C}$, and $\alpha_3\beta_3\gamma^{V31C,\ R278C}$ were complexed with the δ and ε subunits and reconstituted with CF_1-deficient thylakoid membranes. Neither the δ nor the ε subunit is necessary for binding of CF_1 to the membrane, but both are required for optimal coupling of the light-induced proton gradient to ATP synthesis (Richter et al., 1984). In the absence of CF_1, protons flow freely through CF_O and the thylakoid membranes are unable to maintain an effective proton gradient. Addition of CF_1 blocks the free flow of protons across the membrane, restoring the ability to form and maintain a proton gradient (Richter et al., 1984).

The ability of the F_1 assemblies containing the mutant γ subunits to block the free flow of protons across the membrane was examined using ACMA fluorescence. CF_1 assembled using the recombinant wild type γ subunit showed a maximum ACMA quenching of about 40% (Figure 21B). Similar extents of quenching were observed with the $\gamma^{V31C,R278C}$ and $\gamma^{K30C,A276C}$ mutants; however, the extent of ACMA quenching was reduced to about 20% with the $\gamma^{V31C,A276C}$ mutant indicating that this double mutation had significantly impaired the activity of the enzyme to block the flow of protons across the membrane. When ATP synthesis was measured using the luciferin/luciferase couple, the $\alpha_3\beta_3\gamma^{V31C,R278C}$ enzyme showed wild-type levels of ATP synthesis, but the $\alpha_3\beta_3\gamma^{K30C,A276C}$ showed a ~20% decrease in ATP synthesis compared to the wild type enzyme (Table 12). The $\alpha_3\beta_3\gamma^{V31C,A276C}$ showed a ~65% reduction of ATP synthesis compared to the wild-type enzyme. While all the mutant enzymes were proton-leaky, this does not explain the significant loss of ATP synthesis activity in the $\alpha_3\beta_3\gamma^{V31C,\ A276C}$ mutant (Table 12). To exhibit formation of a

Table 12. Proton gradient formation and ATP synthesis by mutant γ subunits assembled with the CF_1 $\alpha_3\beta_3$ hexamer

Protein preparation	Linkage	Relative ΔF/F (%)[1]	ATP Synthesized (μmol P_i /h/mg chlorophyll)
$\alpha_3\beta_3\gamma^{WT}$	N/A	60	66.02 ± 3.37
$\alpha_3\beta_3\gamma^{K30C, A276C}$	N- & C-term helices	40	53.48 ± 1.34
$\alpha_3\beta_3\gamma^{V31C, A276C}$	N- & C-term helices	40	22.69 ± 5.01
$\alpha_3\beta_3\gamma^{V31C, R278C}$	N- & C-term helices	50	57.20 ± 2.14

[1] ACMA quenching and ATP synthesis by purified F_1 assemblies were determined as described in the *Experimental Methods*. Errors are expressed as standard deviations with n = 4.

Figure 21. ***Comparison of proton gradient formation by thylakoid membranes with reconstituted CF_1 $\alpha_3\beta_3\gamma$ complexes containing mutant γ subunits with cysteines mutations.*** Proton gradient formation in thylakoid membrane preparations reconstituted with: A) No CF1; B) $\alpha_3\beta_3\gamma^{WT}$; C) $\alpha_3\beta_3\gamma^{V31C,R278C}$; D) $\alpha_3\beta_3\gamma^{K30C,A276C}$; and E) $\alpha_3\beta_3\gamma^{V31C,A276}$. The traces were determined by measuring ACMA fluorescence quenching as described in the Experimental Methods. The up arrows indicate when the light is turned on and the down arrows indicate when the light is turned off.

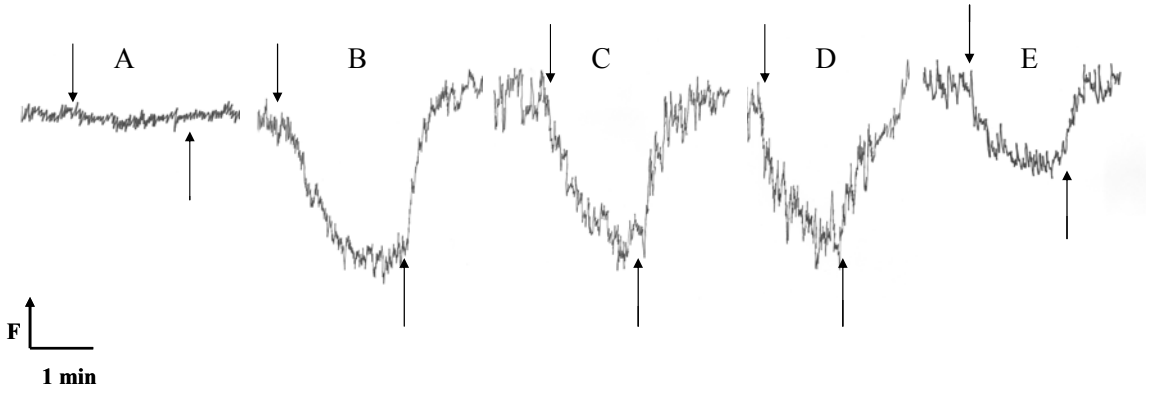
A
B
C
D
E
F
1 min

significant light-induced proton gradient across the thylakoid membranes, more that 95% of the F_0 channels in the membranes must be blocked by F_1 assemblies. Therefore, the small differences in the effect of ACMA quenching do not represent major differences in the amount of F_1 bound. These results, combined with the assay data from the native and hybrid systems, clearly indicate that the $\gamma^{V31C,A276C}$ mutation has detrimental effects on magnesium dependent catalytic functions of the chloroplast ATP synthase.

D. Discussion

The extent of fluorescence labeling of the γ mutants under oxidizing and reducing conditions indicated that we were clearly able to cross-link the N-terminal α-helix to the central domain ($\gamma^{A89C,A276C}$), cross-link adjacent loops in the central domain ($\gamma^{A89C,N143C}$) and cross-link the N- and C-terminal α-helices ($\gamma^{K30C,A276C}$ and $\gamma^{V31C,\ A276C}$). The mutants $\gamma^{V31C,R278C}$ and $\gamma^{K30C,R278C}$ both designed to crosslink the N- and C-terminal α-helices, while able to form a dithiol, resulted in a smaller amount of fluorescent labeling than the other cysteinyl pairs. The reduced labeling of these two mutants may indicate that γR278 is less accessible to thiol reactive probes than the cysteine introduced at other positions in the γ subunit. Unfortunately, the $\gamma^{A89C,R278C}$ protein assembly was degraded to such a large extent that the amount of dithiol formation, cross-linking the N-terminal helix to the central domain, was undetermined.

The absence of any effect on activity by cross-links formed in the $\gamma^{A89C,N143C}$, $\gamma^{A89C,A276C}$, and the $\gamma^{A89C,R278C}$ enzymes suggest that movement of the central domain relative to the C-terminal α helix of the gamma subunit is not essential for ATPase activity.

However, further studies on the effects of these mutations during ATP synthesis are ongoing. It is possible that the cross-links formed by these mutations will have an effect on ATP synthesis, especially since previous data (Moroney et al., 1984; Nalin et al., 1983) indicated that structural changes involving γCys89 occur during ATP synthesis but not during ATP hydrolysis. Cross-linking the $\gamma^{V31C,R278C}$ and $\gamma^{K30C,R278C}$ thiols had little effect on ATPase activity, regardless of the redox state of the introduced thiols.

The three mutants that were examined for ATP synthesis effects, $\alpha_3\beta_3\gamma^{K30C,A276C}$, $\alpha_3\beta_3\gamma^{V31C,A276C}$, and $\alpha_3\beta_3\gamma^{V31C,R278C}$ were fully inhibited by the binding of the ε subunit. The results presented in Chapter 2 indicate that ε subunit binds to the N- and C-terminal helices and across the central domain of the γ subunit as in the EcF_1. The lack of any effect of these mutations on ε subunit inhibition indicate that the cysteines in these three mutants do not alter the structure of the γ subunit to an extent where ε inhibition would be effected.

The $\gamma^{V31C,A276C}$ and $\gamma^{K30C,A276C}$ mutants in this study showed the unexpected effect of reducing or abolishing the sulfite stimulated MgATPase activity as well as impairing ATP synthesis. These effects appear to be independent of the redox state of the introduced cysteines, indicating that the presence of the cysteinyl mutations introduce some type of conformational change in the γ subunit, interfering with a critical step in the oxyanion activation and proton coupling processes.

The region of contact between the N- and C-terminal helices in the vicinity of γK30/V31 and γA276 is close to one of the major points of contact described between the γ subunit and the α and β subunits in MF_1 (Abrahams et al., 1994). One important interaction identified in the MF_1 crystal structure is that of γM23 and βE381. βE381 resides within the DELSEED loop region on the β subunit, a region that is highly conserved and known to be

necessary for efficient catalytic turnover. Mutational studies of βE381 indicate that it plays a role in effectively communicating coupling information from the γ subunit to the catalytic site on the β subunit (Ketchum et al., 1998). Replacement of all five acidic residues in the DELSEED region did not prevent γ subunit rotation, however, it reduced MgATPase activity to ~40% that of wild type (Hara et al., 2000). Recent experiments have confirmed that the DELSEED region is not absolutely required for generating γ subunit rotational torque (Hara et al., 2000). It is, therefore, more likely that the $\beta^{DELSEED}$-γ interaction plays a role in activating or optimizing catalytic turnover rather than in the stepwise rotational-torque generating process.

It has been suggested that the interaction between βE381 and γM23 is directly involved in energy coupling during ATP synthesis (Al-Shawi et al., 1997). Mutating γM23 to a lysine residue in the EcF_1 reduced the rate of MgATP hydrolysis, as well as reducing the amounts of ATP-dependent proton pumping and ATP synthesis (Nakamoto et al., 1995). An additional mutation, γQ269R, restored normal activity to the γM23K mutant. Actin filament rotation assays of the γM23K mutant in TF_1 showed that the mutation did not prevent γ rotation during ATP hydrolysis, suggesting again that the interaction does not play a critical role in rotational catalysis (Hara et al., 2000). The crystal structure indicates that γQ269 (Q255 in MF_1) takes part in hydrogen bonding to one of the adjacent β subunits (Abrahams et al., 1994); however, experiments have shown that the γQ269-β interaction is not critical for ATP synthesis or hydrolysis. Mutations of γQ269 to arginine, lysine, glycine and leucine in the EcF_1, significantly reduced MgATPase and ATP synthesis activities (Nakamoto et al., 1995).

An interaction between the C-terminal helix of the γ subunit and the $\alpha_3\beta_3$ hexamer as indicated in the MF_1 crystal structure, involves γR254 (γR304 in CF_1) and γQ255 (γQ305 in

CF_1) (Abrahams et al., 1994). Recent studies in this laboratory have indicated that three residues on the N-terminal tip of the CF_1 γ subunit (γR304, γQ305, and γR302) are not essential for rotational catalysis, but that the catch formed by the interaction between these residues and anionic loops on the α and β subunits plays a critical role in the process of oxyanion activation (He et al., 2007). Residue γQ305 in the CF_1 is analogous to residue γQ269 in the EcF_1, the mutation responsible for restoring hydrolysis activity to the γM23K mutation. The γQ305A mutation assembled into the hybrid enzyme had normal CaATPase and MgATPase activities, but showed a complete loss of sulfite-stimulated MgATPase activity in this study, very similar to the results of the $\gamma^{V31C,\ A276C}$ assembled in the hybrid system (He et al., 2007). The loss of oxyanion activation in the γQ305A mutant was suggested to result from disruption of an interaction between γQ305 and the anionic loop on the β_E, The disruption of this contact results in a loss of communication of the activation effect obtained by the binding of ATP into an adjacent non-catalytic site (Figure 14) (He et al., 2007).

1. A Model for Oxyanion Stimulation

At least part of the stimulatory effect of oxyanions likely results from a destabilization of MgADP bound in a non-catalytic site, allowing it to be exchanged with MgATP. The presence of sulfite has been previously shown to increase the exchange of MgADP bound to CF_1 (Hu, N. and Richter, M.L. unpublished results). Data collected by He et al. (2007) suggested that the β_E-γQ305 interaction is responsible for communicating the binding of MgATP to a non-catalytic site, loosening the tightly bound MgADP in the adjacent catalytic site.

The $\gamma^{V31C, A276C}$ mutant did not exhibit any changes in catalytic activity in response to the oxidation state of the introduced thiols. The fluorescence accessibility study clearly shows that the two cysteines in this mutant can form a disulfide. Interestingly, by introducing these two cysteines in close proximity to one another where the N- and C-terminal helices of the γ intertwine, some component of catalysis is impaired that only effects oxyanion stimulated MgATPase activity and ATP synthesis, and yet does not effect the CaATP activity. The results observed with the $\gamma^{V31C,A276C}$ mutation is are comparable to the results obtained from the γQ305A mutation, which also resulted in a loss of oxyanion stimulation and a marked decrease in ATP synthesis. The γM23K mutation in EcF_1, known to interfere with a hydrogen bond between γM23 and βQ381 located in the DELSEED loop, also exhibited a loss of MgATPase and impaired synthesis. The loss of activity in the γM23K can be restored by a γQ269R (γQ305 in CF_1), demonstrating the importance of the β-γ interactions during Mg-dependent catalysis.

The results of this current study suggest that interactions between the βDELSEED loop and the γ subunit helices results in conformational changes in the DELSEED loop that aids in the release of nucleotide from the catalytic site. Thus the βQ381-γM23 interaction is also involved in signaling conformational rearrangement in the nucleotide binding site, aiding in the release of the tightly bound nucleotide. The complete loss of oxyanion stimulation in the $\gamma^{V31C,A276C}$ mutant, and the partial loss of oxyanion stimulation in the $\gamma^{K30C,A276C}$ mutant, is due to the presence of the introduced cysteine residues imparting some small conformational change in the intertwined helices of the γ that interferes with the contact between the γ subunit twisted helical pair and the DELSEED loop region of the β subunits. During catalysis in the presence of Mg^{2+}, the Mg^{2+} traps the bound ADP into a tightly bound

conformation, which can only be relieved by the presence of oxyanions. During Mg^{2+} dependent ATP synthesis, the proton-motive force overcomes the inhibition of the enzyme observed from the tightly bound ADP. The activation by oxyanions on MgATPase activity, by aiding in the release of the tightly bound ADP, mimics the activation of the proton-motive force during ATP synthesis. When the interaction between γ and the DELSEED loop on β is disrupted by the cysteine mutations, the loss of communication through the γ subunit to the nucleotide binding sites eliminates the activation effects normally observed by the presence of oxyanions. Ca^{2+} ions do not induce the tight inhibitory conformation that occurs in the presence of Mg^{2+}. This would explain the presence of normal CaATPase activities by the γ subunit cysteine mutants, but the complete or partial loss of oxyanion stimulation during MgATP hydrolysis.

In the native chloroplast enzyme system, the $\gamma^{V31C,A276C}$ and $\gamma^{K30C,A276C}$ mutants did partially exhibit sulfite-induced oxyanion stimulation of MgATPase activity. The rates of ATP synthesis were also impaired, by 67% in the case of the $\gamma^{V31C,A276C}$ mutant. Again this mimicked the results of the γQ305A mutant assembled in the chloroplast enzyme, suggesting the partial loss of oxyanion stimulation occurs by a similar mechanism to that in the exhibited by the mutants in the hybrid system. In the native chloroplast enzymes containing the $\gamma^{V31C,A276C}$ and $\gamma^{K30C,A276C}$ mutants, the percentage loss of ATP synthesis activity is comparable to the percentage loss of sulfite stimulated MgATPase activity relative to the wild type enzyme activities. This is expected since oxyanion stimulation is replaced by the transmembrane proton gradient when the F_1 is membrane bound and coupled to the F_0 (Du and Boyer, 1990; Murataliev and Boyer, 1994). In addition, ATP synthesis by F_1 is also a

Mg-dependent process, explaining why the $\gamma^{V31C,A276C}$ and $\gamma^{K30C,A276C}$ mutants had a similar effect on ATP synthesis.

The observation that oxyanions partially stimulated MgATPase activity in the $\gamma^{V31C,A276C}$ and $\gamma^{K30C,A276C}$ mutants assembled with the native chloroplast α and β subunits but not at all with the hybrid enzyme assembly is most likely due to slight differences in the γ-β subunit interactions in the different enzyme systems. The basal MgATPase rates of CF_1 are very low (k_{cat} ~16) in the absence of oxyanions. In CF_1, ADP binds very tighty to two nucleotide binding sites, one catalytic and one non-catalytic (Malyan, 2006). The tight binding of two ADPs results in a mostly inhibited CF_1 enzyme and low basal MgATPase activites. However, in the hybrid enzyme system, the MgATPase activity is already partially activated (k_{cat} ~130) in the absence of oxyanions, resulting in a much higher level of sulfite stimulation than observed in CF_1. Since the hybrid enzymes exhibit a much higher MgATPase activity they are less susceptible to Mg^{2+} inhibition and less reliant on oxyanion stimulation. The differences the initial MgATPase rates explains the observation that the $\gamma^{V31C,A276C}$ and $\gamma^{K30C,A276C}$ mutants in the chloroplast enzyme exhibited some oxyanion stimulated MgATPase activities, whereas the same mutants in the hybrid enzyme system showed little or no oxyanion stimulation. It is, therefore, reasonable to assume that activation of ATP hydrolysis activity in CF_1 requires MgATP to fill non-catalytic sites, suggesting that optimal turnover requires replacing the tightly bound MgADP located in the non-catalytic site.

In summary, the results of this study have shown that cross-links can be formed between introduced cysteines in the N- and C-terminal helices of the γ subunit, the N-terminal helix and the central domain, and two loops of the central domain. However, cross-linking

the different regions of the γ subunit together had little effect on ATP hydrolysis or synthesis. Notably, the cysteine residue substitutions $\gamma^{V31C,\ A276C}$ and $\gamma^{K30C,\ A276C}$ significantly reduced oxyanion-stimulated MgATPase activity and ATP synthesis activity while maintaining normal CaATPase activity. The $\gamma^{V31C,A276C}$ mutation showed a complete loss of oxyanion-stimulated MgATPase activity in the hybrid enzyme system, and a partial loss of oxyanion-stimulated MgATPase activity in the chloroplast enzyme system. This mutation also reduced ATP synthesis by nearly 70%. The results point to specific interactions between residues on the N- and C-terminal twisted helices of the γ subunit and the DELSEED loop on β subunits that, while not necessary for generating rotational torque during the binding change process, are required for activation of Mg-dependent synthesis and hydrolysis by oxyanions. The results are consistent with a model in which the conformational state of one of the three β subunits, identified in the crystal structure of MF_1, represents a state that is specifically required for activating the enzyme in the presence of Mg^{2+} ions. This conformational state is not, as previously proposed (Menz et al., 2001), representative of a torque-generating step in the catalytic cycle.

Chapter 4. Single Molecule Dynamics of the Regulatory Domain of the Chloroplast ATP synthase γ subunit

A. Introduction

One of the most prominent features of single-molecule approaches to chemical biology is the ability to visualize molecular motion as well as the chemical activities of individual molecules or macromolecular complexes. While large strides have been made in the ability to solve high resolution structures using NMR and X-ray crystallography, these techniques provide little information about the dynamic inter- and intramolecular processes that lead to function. Recent ultrafast spectroscopy techniques allow observation of molecular motions on the femtosecond time scale (Fierz et al., 2007). Experiments on these time scales are usually conducted using large samples of molecules, thus requiring simultaneous motions among all the molecules for accurate measurements. These types of measurements are also normally conducted using short burst measurements, on the picosecond time scale, in order to catch the sample of molecules in similar states. Collecting these data over long time periods results in a loss of correlation of the data because the motions of the molecules in a large sample lose synchrony with each over time. A majority of biological processes and enzymatic reactions occur on the millisecond to second time scale; however, even at these time scales most of the molecules in a large sample are not well synchronized. The largest advantage of single-molecule experiments is the elimination of the problem of sample synchronization, allowing detailed dynamics information to be collected in real time and at a higher level of accuracy.

Many of the types of molecular motions measured using single-molecule techniques are similar to those visualized in molecular dynamics (MD) simulations. The use of

molecular dynamics simulations has significantly aided in the understanding of macromolecular structure and function (Karplus, 2002). One of the limitations of molecular dynamics is that the time scale available to conduct simulations is limited to picoseconds to nanoseconds (Duan and Kollman, 1998), making accurate representations of certain processes difficult since a large majority of biological processes occur at the millisecond time scale or longer. While critics of molecular dynamics simulations have argued that the time scale limits the amount of data that can be obtained through simulations, recent advances in computing technology and methodologies have allowed molecular processes to be modeled at the 100 nanosecond time scale (Kasson et al., 2006). Even with these advances is it is still well known that many biological processes occur beyond the time scale capabilities of molecular dynamics simulations, these include conformational changes induced by ligand binding or conformational changes induced by chemical reactions. Observing processes at these slower time scales require the use of single-molecule experiments.

There is a large amount of information that can be collected using single molecule experiments, ranging from simple fluorescence amplitude shifts to anisotropic changes and fluorescence resonance energy transfer (FRET) experiments. In order to collect accurate single molecule spectroscopy data, there are several main criteria that must be considered. First, one has to ensure that only one molecule is in resonance with the excitation source and that no fluorescent contaminants (free probe, multiple probes on one molecule, probe aggregates) are present in the sample. Second, a large signal to noise ratio should be obtained over the largest period of time possible. Maximization of fluorescence signal can be obtained by using fluorophores with a high quantum yield and by increasing the amount of power output from the excitation source. Typically, a minimum signal to noise ratio of 3:1 is required before accurate data can be collected.

Some of the most exciting single molecule experiments have involved studies of the rotational dynamics of the ATP synthase. Initial experiments by Noji provided a basis for future single molecule experiments with direct evidence of rotation of the γ subunit, via an attached fluorescent actin filament, within the $\alpha_3\beta_3$ hexamer (Noji et al., 1997). Later that year Yasuda observed that the actin filaments rotated in distinct 120° steps which correlate to the catalytic function of the enzyme, in this case ATP-dependent hydrolysis (Yasuda et al., 1997).

These initial single molecule experiments a decade ago have led to far more advanced experimental protocols in recent years to observe rotational catalysis of ATP synthase. Single molecule experiments have further resolved the 120° steps into an 80-90° substep, driven by ATP binding and a 30-40° substep driven by the release of products from hydrolysis (Yasuda et al., 2001). Recent experiments use gold beads attached to the γ subunit to monitor rotational kinetics, as well a magnetic tweezers to artificially drive and pause the rotation of the γ subunit during catalysis (Hirono-Hara et al., 2005). In another approach, timescales of catalytic rotation were monitored by attaching a gold nanorod to the γ subunit. A change in intensity of the scattered light was observed as the nanorod rotated (Spetzler et al., 2006). It is worth noting that all of these techniques require the attachment of large fluorescent or magnetic appendages to the γ subunit. It is, however, not clear how the attachment of these tracking devices affects catalytic function of the enzyme.

A majority of the single molecule fluorescence experiments used to study the ATP synthase have been performed using the EcF_1 enzyme. Tucker et al., (2004) was the first to perform ATPase activity-driven actin filament rotation experiments using the chloroplast γ subunit assembled into a hybrid enzyme system. The chloroplast γ subunit is unique among the ATP synthases in that it contains a regulatory domain comprised of approximately 40

amino acids (residues 196-242) that is largely absent in γ subunits from other organisms. This regulatory domain is highly conserved in higher plants and contains two cysteines (γC199 and γC205) which, when oxidized, result in partial inactivation of the enzyme. This regulatory dithiol is hypothesized to have evolved to provide a molecular switch via its reversible oxidation and reduction. While no high resolutions structures currently exist for the chloroplast γ subunit, recently a homology model of the chloroplast γ subunit was published providing insight into the possible structure of the regulatory domain (Richter et al., 2005). The homology model was created based on its sequence and putative structural homology to the bacterial and mitochondrial γ subunits, of which high resolution structures have been solved. The model was described in detail in Chapter 2.

Molecular dynamics simulations (Figure 22) of the regulatory domain within the homology model have shown that it is possible for the domain to adopt a wide range of conformations. The simulations indicate that the two loop regions of the regulatory domain can adopt many different conformations ranging between 0 and 10Å apart. Over 10,000 simulated structures were generated, but the two in which the cysteines were closest together and farthest apart shown in Figure 6. These two structures are hypothesized to mimic the reduced (open) and oxidized (closed) forms of the regulatory domain. The model thus predicts the conformational states available to the enzyme during inhibition and activation. The model further predicts that inter-domain interactions within the γ subunit may be responsible for catalytic regulation (Richter et al., 2005).

In this study, single-molecule fluorescence experiments were used to examine the dynamic behavior of the regulatory domain of the γ subunit. This was approached by attaching single dye molecules to either of the disulfide bridge-forming thiols on the γ subunit

Figure 22. ***Predicted Range of Motion Between The Regulatory Domain and Extra Loop Region of the CF_1 γ Subunit.*** This figure is a representation of the predicted movements between the center of mass of the regulatory domain and the extra loop. The simulation predicts a maximum range of motion of up to 20Å between the center of the regulatory domain and the extra loop. The large range of motion is predicted to correspond to the oxidized and reduced state of the regulatory disulfide, as shown in Figure 5. (Simulation performed by Andrew J. Giessel)

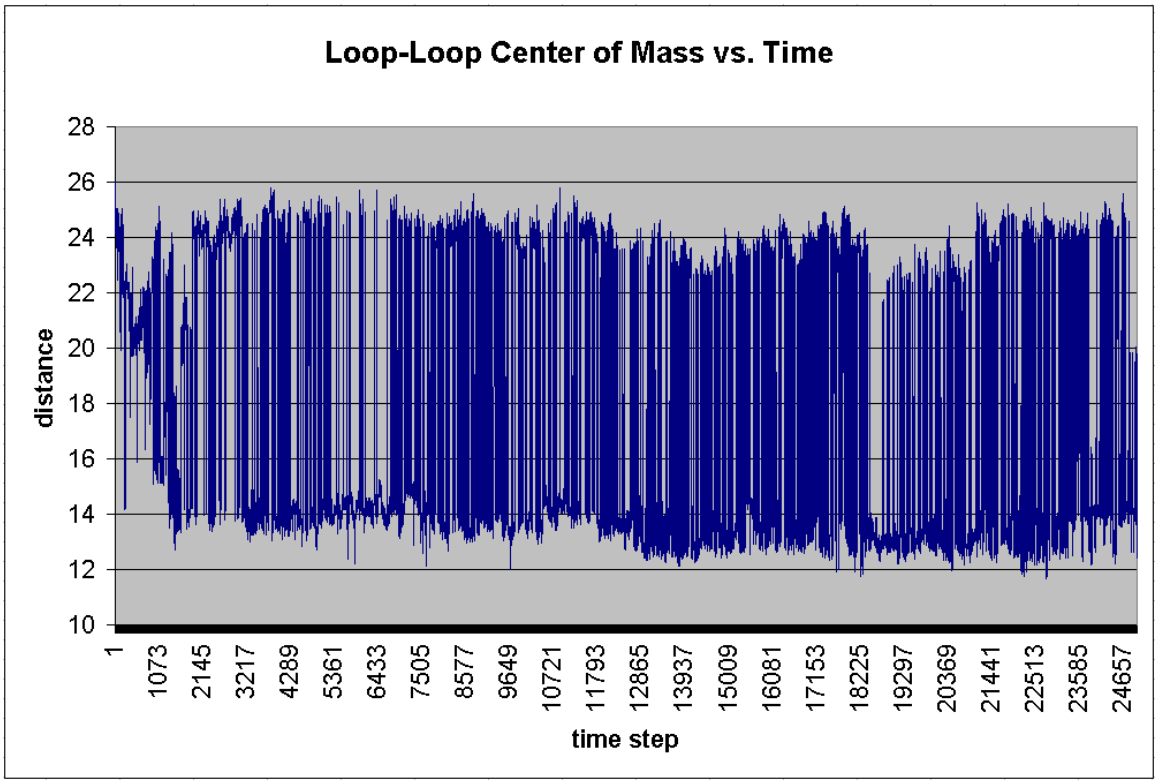
Loop-Loop Center of Mass vs. Time
distance
28
26
24
22
20
18
16
14
12
10
1
1073
2145
3217
4289
5361
6433
7505
8577
9649
10721
11793
12865
13937
15009
16081
17153
18225
19297
20369
21441
22513
23585
24657
time step

with the expectation that changes in the polarization or the fluorescence amplitude of the dye will occur during the catalytic cycle and/or in response to the binding of the inhibitory ε subunit. γC199/C205 was labeled with a thiol reactive probe, tetramethylrhodamine (TMR), in both the hybrid enzyme system and the native CF_1 enzyme. Several immobilization strategies were explored to attach the labeled F_1 molecules to the surface of glass slides for collection of fluorescence data. An additional CF_1 sample was labeled with TMR at γC322, a cysteine located at the C-terminal α helix of the γ subunit, to provide a control. Fluorescence trajectories were collected from the labeled enzymes under different catalytic conditions and time constants were generated using an autocorrelation function.

B. Experimental Procedures

1. Materials

Intact CF_1 and CF_1 lacking δ and ε subunits were isolated from spinach as described elsewhere (McCarty and Racker, 1968; Richter et al., 1985). Purified CF_1 was stored as an ammonium sulfate precipitate at 4°C and desalted prior to use. Native ε and δ subunits were isolated from CF_1 and stored for short periods (1-3 days) at 4°C or for longer periods at -20°C in a buffer containing 20% ethanol (v/v) and 30% glycerol (v/v) (Richter et al., 1984; Richter et al., 1985; Younis et al., 1977). DEAE cellulose, antibiotics (ampicillin, tetracycline, and chloramphenicol), Sephadex G-50 resin, and Ni-NTA resin were purchased from Sigma-Aldrich. Hydroxyapatite HTP gel was from BioRad. Tryptone and yeast extract were obtained from DIFCO. ATP (grade II) was purchased from Midwest Scientific and urea (ultra pure) was purchased from ICN Biomedicals Inc. Dialysis tubing (8,000 M.W. cut-off) was obtained from Biodesign Inc. (New York). Fluorescent probes were obtained from

Molecular Probes (Invitrogen). Glass coverslips and silicone grease were obtained from Fisher Scientific. All other chemicals were of the highest quality reagent grade available.

2. Assembly and purification of hybrid $\alpha_3\beta_3\gamma$ complex

Inclusion bodies from the three core subunits ($RrF_1\alpha_{6Xhis}$, $RrF_1\beta$, and $CF_1\gamma^{C89A,\ C322A}$) were solubilized in 8 M urea, diluted in refolding buffer, and assembled as previously described (He et al., 2007). The assembled protein complexes were purified after overnight dialysis by DEAE anion exchange chromatography (Gao et al., 1995) and further purification was performed by Ni-NTA chromatography (He et al., 2007). Additional purification was achieved by size-exclusion chromatography using a Superdex 200 (Pharmacia) column attached to a Biorad Biologic HR fast performance chromatography system running at a flow rate of 0.5mL/min. The recombinant protein samples were eluted in 50 mM Tricine-NaOH (pH. 7.8) and 50 mM NaCl. 20% (v/v) glycerol and 1 mM ATP were added to the eluted protein samples before storage at -80°C.

3. Labeling of γC199/C205 on the hybrid enzyme assembly

500 µg of assembled $\alpha^{6xHis}{}_3\beta_3\gamma^{C89A,\ C322A}$ hybrid enzyme was incubated for 30 min in 100 µM $CuCl_2$ to oxidize the regulatory disulfide. A further incubation of the enzyme with 5 mM N-ethylmaleimide (NEM) for 30 min was used to block any exposed cysteines, primarily on the *R. rubrum* α subunits. A 10 min incubation with 25 mM DTT was followed by two consecutive passages through a Sephadex G-50 centrifuge column equilibrated with 25 mM Tris-HCl, pH 8.0 and 1 mM ATP. The enzyme was incubated with 20 µM tetramehtylrhodamine-5-maleimide (TMR) for 30 mins. After labeling, 1 mM DTT was added to quench any unreacted TMR, followed again by two consecutive passages through a

Sephadex G-50 centrifuge column equilibrated with 25 mM Tris-HCl, pH 8.0 and 1 mM ATP. 20% (v/v) glycerol and 1 mM ATP was added to the eluted protein samples before storage at -80°C.

4. Assembly of the flow cell and hybrid protein surface attachment

Construction of the flow cells and adherence of the $\alpha^{x6His}{}_3\beta_3\gamma^{C89A,\ C322A}$ hybrid enzyme were carried out initially as previously described (Noji et al., 1997). Flow cells were assembled by placing two pieces of greased parafilm between two acid washed coverslips. This flow cell has a central chamber that has a volume of 20-30 µL. A series of buffers were injected into the flow cell to allow attachment of the $\alpha^{x6His}{}_3\beta_3\gamma^{C89A,\ C322A}$ to the surface of the glass coverslip: 1) 50 µL of Buffer A (10 mM Hepes-NaOH, pH 7.2, 25 mM KCl, 5 mM $MgCl_2$) with 0.8 µM HRP-Ni^{2+}NTA was incubated in the flow cell for 5 min; 2) 50 µL of Buffer B (Buffer A with 10 mg/ml BSA) with 3 nM of the TMR labeled hybrid enzyme complex for 5 min incubation. Each one of these treatments was followed by washing the flow cell chamber with ~100 µL of Buffer B. Prior to placement on the microscope, the flow cell was then injected with a buffer containing 50 mM Tricine-NaOH (pH 8.0), 4 mM ATP, 216 µg/ml glucose oxidase, 36 µg/ml catalase, 25 mM glucose, 10 mg/ml BSA , and either 4 mM $CaCl_2$ for CaATPase conditions or 2 mM $MgCl_2$ for MgATPase conditions (Tucker et al., 2004).

5. Collection of single-molecule fluorescence trajectories

Fluorescently labeled protein samples were excited using a focused intensity of ~1 mW/cm^2 from a circularly polarized 542.2 nm HeNe laser (Research Electro-optics, Colorado). The excitation laser beam was passed through a filter (D543/10X, Chroma,

Illinois) and through the epi-illumination port of an inverted microscope, from where it is further reflected by a dichroic mirror (Q555LP, Chroma, Illinois) onto a 100x, 1.3 numerical aperture objective lens (Nikon Superfluor, New York). The objective lens collected fluorescence, which is further transmitted through the dichroic mirror and an emission filter (SPCM-AQR-14, Perkin-Elmer Optoelectronics, Canada). A representative figure of the experimental setup is shown in Figure 23. Signals relayed from the photodiodes were processed by a PCI-6052E card (National Instruments, Texas) for the creation of fluorescence scans. This card also controlled a nanopositioning scanning stage onto which the slides were mounted. Fluorescence trajectories were collected with a 500 μs per channel bin width. Analysis of obtained fluorescence trajectories was performed using software designed in the Dept. of Chemistry at the University of Kansas by members of the Johnson research group. Fluorescence trajectories were binned by a factor of four, resulting in fluorescence data points every 2 ms. Autocorrelation analysis was performed using Origin v7.5 (Origin Lab Corp., Massachusetts).

6. Labeling of CF_1 γC199/C205 and γC322 with TMR

Labeling of CF_1 γC205 with TMR was accomplished using essentially the same method described in Chapter 3 for labeling γC205 in the hybrid enzyme. In order to label γC322 with TMR, 1 mg of isolated CF_1 enzyme was incubated for 30 min in 100 μM $CuCl_2$ to oxidize the cysteines of the regulatory disulfide. The oxidized enzyme was then incubated with 20 μM tetramehtylrhodamine-5-maleimide (TMR) for 30 min. After labeling, 1 mM DTT were added to quench any unreacted TMR, followed by two consecutive passages through a Sephadex G-50 centrifuge column equilibrated with 25 mM Tris-HCl, pH 8.0 and 1 mM ATP. 20% (v/v) glycerol and 1 mM ATP was added to the eluted protein samples

Figure 23. ***Representation of the Single-Molecule Experimental Setup.*** In the single-molecule spectroscopy experiment, laser light enters the fluorescence microscope from the rear, is further reflected by a dichroic mirror through an objective lens onto the sample. The fluorescence is detected by single-photon counting modules capable of collecting photon counts at small time scales. The sample rests on a XY Piezo scanner, allowing for precise positioning and scanning of the sample of molecules.

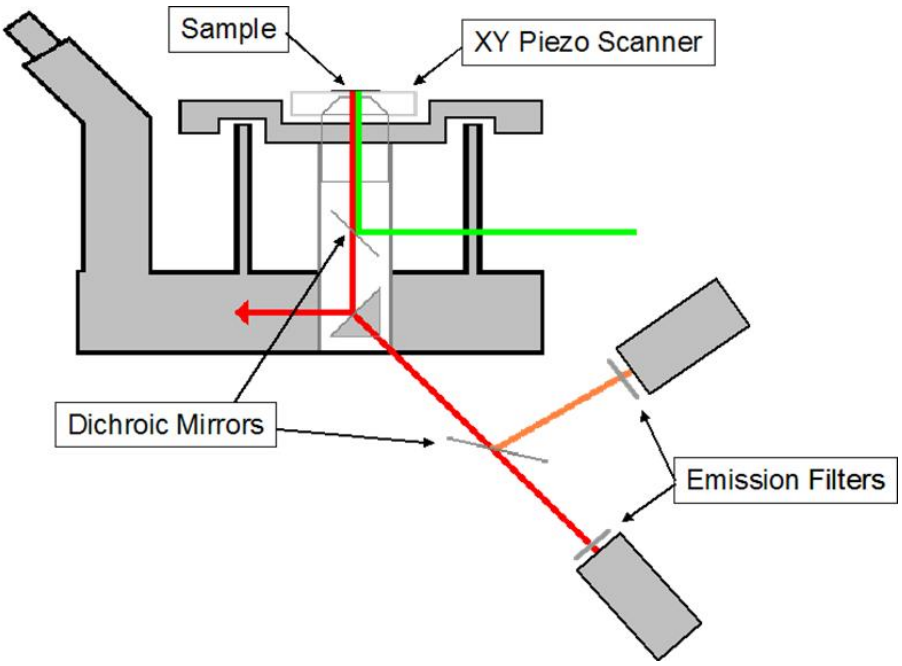
Sample
XY Piezo Scanner
Dichroic Mirrors
Emission Filters

before storage at -80°C. Labeling was confirmed by gel electrophoresis using pre-cast NuPage@ (Invitrogen, San Diego) gels (4-20% acrylamide gradient) with each lane containing approximately 7.5 μg of labeled proteins as shown in Figure 26. The stoichiometry of probe labeling was determined by using the extinction coefficient of 95,000 $M^{-1}cm^{-1}$ for TMR.

7. Labeled CF_1 protein immobilization

Labeled CF_1 was diluted in CaATP buffer containing 50 mM Tricine-NaOH (pH 8.0), 4 mM $CaCl_2$, and 4 mM ATP, to an approximate concentration of 1 nM. One protein sample with γC205 labeled with TMR was incubated with 50mM Adenylylimidodiphosphate (AMP-PNP) and 2 mM $MgCl_2$ for 90 mins, desalted twice through a Sephadex G-50 centrifuge column, and diluted in the CaATP buffer as necessary. 10 μL of labeled CF_1 in the CaATP buffer was added to 30 μL of gel solution comprised of a ~2.2% low gelling temperature agarose (Sigma-Aldrich, Type VIIA) and CaATP buffer. The gel solution was kept at 30°C until mixed with labeled protein at room temperature. The labeled CF_1 in the gel solution was placed on a clean 25 mm x 25 mm coverslip and allowed to solidify for ~5 min before mounting on the inverted microscope. Another clean 22 mm x 22 mm is placed on top of the solidified gel to keep the water in the gel from evaporating during collection of the single-molecule fluorescence trajectories.

8. Other procedures

ATPase activities were determined by measuring phosphate release (Taussky and Shorr, 1953) for 5 minutes at 37°C. The assay mixture for calcium-dependent ATPase activity contained 50 mM Tris-HCl (pH 8.0), 5 mM ATP and 5 mM $CaCl_2$. That for

magnesium-dependent ATPase activity contained 40 mM Tricine-NaOH (pH 8), 4 mM ATP, 2 mM $MgCl_2$ and 50 mM Na_2SO_3 (Hu et al., 1993). Protein concentrations were determined by the Bradford method (Bradford, 1976).

C. Results

1. Analysis of hybrid enzyme fluorescence trajectories

We have hypothesized that the dithiol containing regulatory domain of the γ subunit opens and closes as a function of catalytic as a function of catalytic turnover. The main goal of these studies was to detect and monitor in real time this conformational change as a function of catalytic turnover. We attached environmentally sensitive fluorescent rhodamine dye (TMR) to the $\gamma^{C199/C205}$ pair following disulfide reduction with DTT and removal of excess DTT by gel filtration. The enzyme assembly chosen initially for these experiments was the hybrid system used previously to observe rotation of a fluorescent actin filament (Tucker et. al, 2004). With this system, the enzyme assembly was immobilized on the surface of a Ni-NTA-coated glass coverlip by poly-Histidine tags genetically engineered into the N-terminal domains of the α subunits (Noji et al., 1997). The $\gamma^{C89A,C322A}$ mutant used for these studies was designed to remove the two cysteines not comprising the regulatory disulfide bond (γC89 and γC322), in order to minimize any potential labeling with TMR at a site other than the $\gamma^{C199/C205}$ pair. Under the conditions used, only one of the two cysteines residues of the $\gamma^{C199/C205}$ pair, on average, were labeled with TMR (Snyder et al., 1985). Single molecule trajectories were collected using the labeled protein sample in three different buffer conditions: 1) CaATP buffer, 2) MgATP buffer, and 3) Ca^{2+} buffer minus ATP. The

specific activities of the labeled protein were obtained after dilution in these buffers, to accurately represent the environment in the flow cell during data collection (Table 13). Both protein samples in the MgATP and CaATP buffer exhibited wild-type ATPase activities, while the calcium buffer minus ATP sample showed negligible ATPase activity.

The protein samples were injected into the flow-cells as described in the *Experimental Procedures* section. Prior to data collection, the microscope objective is focused on the interior surface (bottom) of the flow cell. The surface of the flow-cell was scanned using a 10 micron x 10 micron grid in order to find isolated molecules. Once an isolated molecule is detected, the shutter to the laser is closed and the computer relocated the scanner such the objective was directly under the selected molecule. Collection of fluorescence counts begins several seconds before the shutter is opened. Fluorescence trajectories for between 150 and 200 molecules from each protein sample were collected over a period of several days until approximately 100 significant trajectories were obtained. Significant trajectories are defined as those having a signal to noise ratio of at least 3:1 during continuous illumination, as well as exhibiting a single-step photobleaching event of the probe as indicated. Samples of trajectories are shown in Figure 24. In order to increase the apparent lifetime of the TMR, an oxygen scavenging system was present in the final buffer injected into each flow cell; however, the collected data indicated that the apparent lifetimes of the TMR were not affected by the presence or absence of the oxygen scavenging system.

Each individual fluorescence trajectory was analyzed using an autocorrelation function that is incorporated into data analysis software created by the Johnson lab. Autocorrelation functions are a commonly used mathematical function to detect patterns or ordered processes in seemingly random signals. As its name suggests, autocorrelation functions determine the degree to which a signal correlates to itself verses background noise.

Table 13. Catalytic activities for RrF_1 protein samples labeled with TMR at γC199/C205

Conditions	ATPase Activity (μmole per min per mg protein)
CaATP[1]	**24.8 ± 0.76**
MgATP[2]	**2.5 ± 0.98**
Ca^{2+}[3]	**0.29 ± 0.11**

[1] Assayed using CaATP buffer as described in the *Experimental Methods*. [2] Assayed using MgATP buffer as described in the *Experimental Methods*. [3] Assayed using CaATP buffer minus ATP as described in the *Experimental Methods*. Errors are expressed as standard deviations with n = 3.

Figure 24. ***Sample trajectories of hybrid protein assemblies in CaATPase buffer.*** Shown are sample fluorescence trajectories. A) Collection of a single molecule trajectory that potentially is labeled with two dye molecules showing a two-step photobleaching. B) A trajectory exhibiting a fast photobleaching step. C) A normal trajectory that is suitabile for analysis. The downward arrows indicate when the shutter is opened and the upward arrows indicate photobleaching.

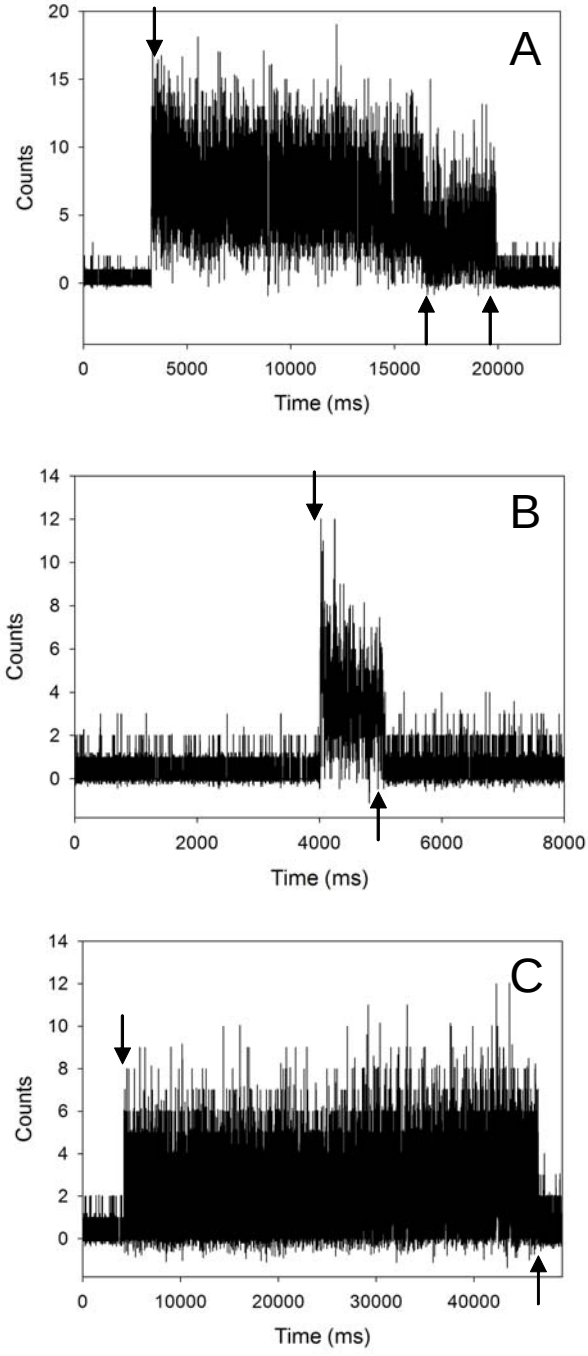
A
Counts
Time (ms)
B
Counts
Time (ms)
C
Counts
Time (ms)

In this instance, the autocorrelation function will identify ordered events that occur in the fluorescence amplitude changes exhibited by each TMR molecule upon illumination. The autocorrelation function also determines the periodic component of the event and the expected frequency of that component. Completely random events or fluorescence signals in this study will exhibit no autocorrelation. In other words, only periodic, non-random events can be autocorrelated.

The autocorrelation data from all the trajectories was averaged and plotted, and two-component exponential decay curves were fitted to each set of data as shown in Figure 25. The two components of each decay curve represent the time-scales of two different ordered events detected in the fluorescence signals from the TMR molecules. The autocorrelation time constants for the labeled hybrid enzymes are shown in Table 14. All three of the protein samples show both a long and a short time component. The short time component is very similar in all three protein samples, on the order of 3-5 ms. The long time components vary, from ~53 ms in the MgATP buffer, ~75 ms in the CaATP buffer, and ~82 in the CaATP buffer minus ATP. The % decay is the relative decay that occurs in a given time scale in relation to the total amount of fluorescence decay. The data in Table 14 indicate that for all the samples labeled at γC199/C205, ~70% of the decay from fluorescence fluctuations is from the fast time component, whereas ~30% of the decay from fluorescence fluctuations is from the longer time component. In the absence of ATP, the hydrolysis activity of the hybrid enzyme is slowed by approximately two orders of magnitude as shown in Table 13. The changes observed in both the fast and slow components, although statistically significant, were small (on the same magnitude) relative to the measured differences in catalytic rates of the enzyme assemblies under the different substrate conditions. This indicates that the environmental changes leading to the measured amplitude shifts in TMR fluorescence

Table 14. Autocorrelation Time Constants for RrF_1 protein assemblies labeled with TMR at γC199/C205

Buffer	Time Constant	Time (ms)	% Decay
MgATPase	**1**	**3.47 ± 0.36**	**72%**
	2	**52.77 ± 3.43**	**28%**
CaATPase	**1**	**4.11 ± 0.31**	**71%**
	2	**75.37 ± 2.09**	**29%**
-ATP[1]	**1**	**4.97 ± 0.08**	**73%**
	2	**81.84 ± 3.43**	**27%**

[1] Data collect in the presence of CaATPase buffer w/o ATP as described in the *Experimental Methods*. Errors are expressed as standard deviations with n = 3.

Figure 25. ***Autocorrelation Analysis of RrF_1 Hybrid Enzyme Single-Molecule Fluorescence Trajectories.*** Each autocorrelation decay curve represents analysis of trajectories recorded from approximately 100 single molecules. The autocorrelations were fitted to a two-component exponential decay curve. A) autocorrelation of $\alpha_3\beta_3\gamma$ assembly in the presence of MgATP buffer; B) autocorrelation of $\alpha_3\beta_3\gamma$ assembly in the presence of CaATP buffer; C) autocorrelation of $\alpha_3\beta_3\gamma$ assembly in the presence of Ca^{2+} minus ATP buffer.

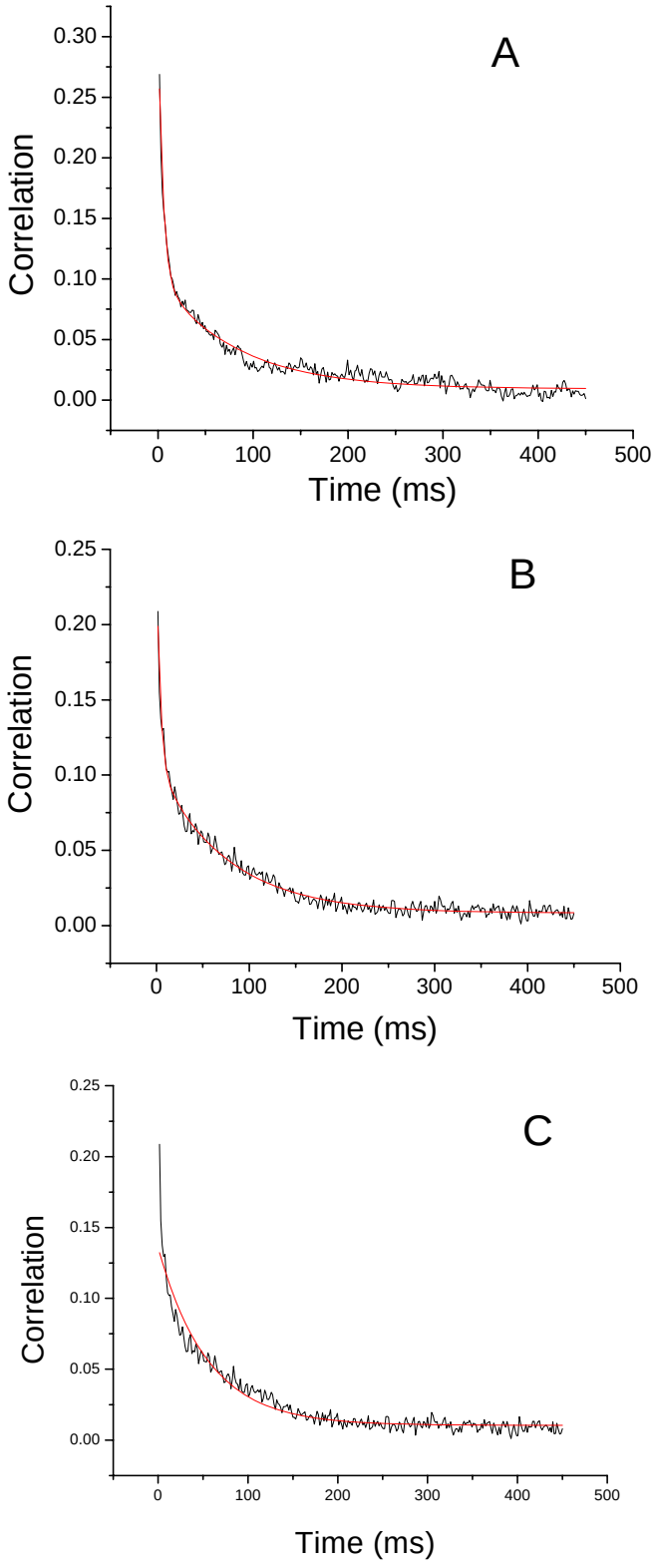
A
Correlation
0.30
0.25
0.20
0.15
0.10
0.05
0.00
0
100
200
300
400
500
Time (ms)
B
Correlation
0.25
0.20
0.15
0.10
0.05
0.00
0
100
200
300
400
500
Time (ms)
C
Correlation
0.25
0.20
0.15
0.10
0.05
0.00
0
100
200
300
400
500
Time (ms)

represent periodic domain movements that are not related to catalytic turnover. While the data is not definitive, the observed rates of shifts in fluorescence amplitude indicate that the regulatory domain is flexible as suggested by the model (Figure 6).

A significant problem with the experimental approach used in these studies is uncertainty in surface immobilization. During data collection, there were a large number of trajectories in which the fluorescence amplitude gradually decreased during collection, indicating that the molecule was slowly moving out of alignment with the laser. Indeed, initial surface scans indicated that some of the molecules drifted across the field of the laser scan. For this reason, alternative strategies of enzyme immobilization were investigated including antibody attachment and agarose gel grafting. The latter method has been successfully used by others to restrict protein motion on solid surfaces and proved useful in these studies (Slaughter et al., 2007). Since a poly-Histidine tag is not required using this method, the native chloroplast $\alpha_3\beta_3\gamma$ assembly was used instead of the hybrid enzyme

2. Analysis of CF_1 fluorescence trajectories

Samples of isolated CF_1, minus ε and δ subunits, were selectively labeled with TMR on γC199/C205 while another sample of CF_1 was labeled with TMR on γC322 (Figure 26). The protein was immobilized in a 1% low melting temperature agarose gel on glass coverslips. Initial surface scans of the CF_1 sample in Ca^{2+} buffer showed very little evidence of sample drifting (Figure 27). Single molecule trajectories were collected from five different protein samples: 1) $\alpha_3\beta_3\gamma$ labeled on γC199/C205 in CaATP buffer; 2) $\alpha_3\beta_3\gamma$ labeled on γC199/C205 with the inhibitory ε subunit bound in CaATP buffer; 3) $\alpha_3\beta_3\gamma$ labeled on γC199/C205 inhibited by AMP-PNP in CaATP buffer; 4) $\alpha_3\beta_3\gamma$ labeled on γC322 inhibited by AMP-PNP in CaATP buffer; and 5) $\alpha_3\beta_3\gamma$ labeled on γC322 in CaATP buffer. The

Figure 26. ***SDS-PAGE of CF_1 Labeled with TMR.*** Inclusion bodies of the mutant gamma subunits were solubilized in urea and labeled with fluoresceinyl maleimide under oxidizing and reducing conditions as described in the *Experimental Methods*. The upper portion of the figure shows the gel stained with Coomassie brilliant blue, the lower portion is the same gel indicating fluorescence of the labeled protein upon illumination with low-wavelength ultraviolet light. Lane 1, CF_1 labeled with TMR on γC199/C205; Lane 2, CF_1 blocked with NEM and labeled with TMR; Lane 3, CF_1 labeled with TMR on γC322.

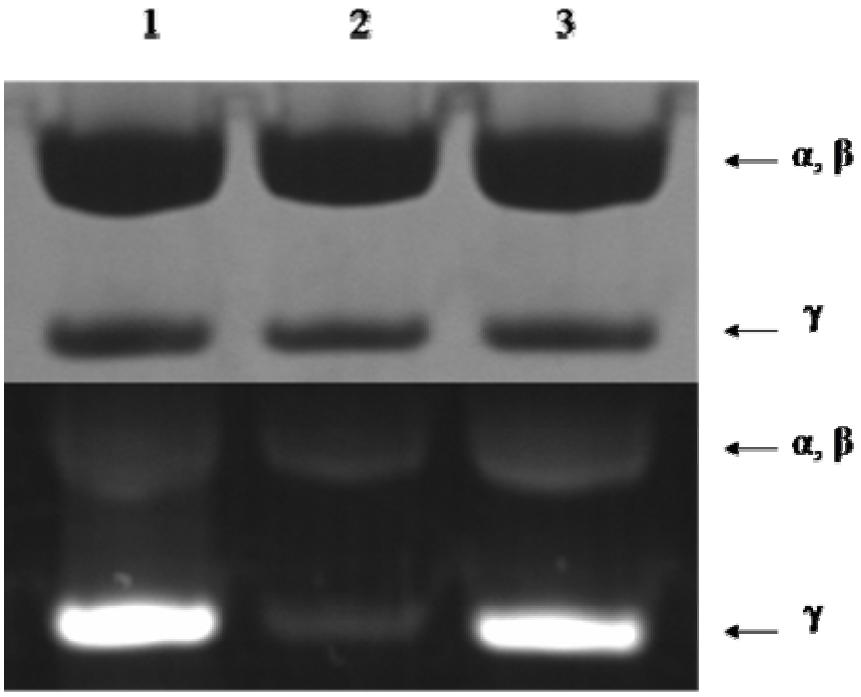
1
2
3
α, β
γ
α, β
γ

Figure 27. ***Initial Surface Scans of CF_1 Labeled on γC199/C205.*** 10 μm x 10 μm surface scans of labeled CF_1 immobilized on agarose. The white circles indicate single F_1 molecules embedded in the agarose. A) Normal surface scan with optimum protein concentrations for data collection (~ 1 nM); B) A surface scan with the very bright spots indicating protein aggregates or a single molecule with multiple fluorophores while the flat lines indicate mobile fluorescent items; C) Background surface scan indicating the lack of any molecules; D) A surface scan showing a very high protein concentration (~ 20 nm) not suitable for data collection since individual molecules cannot be resolved.

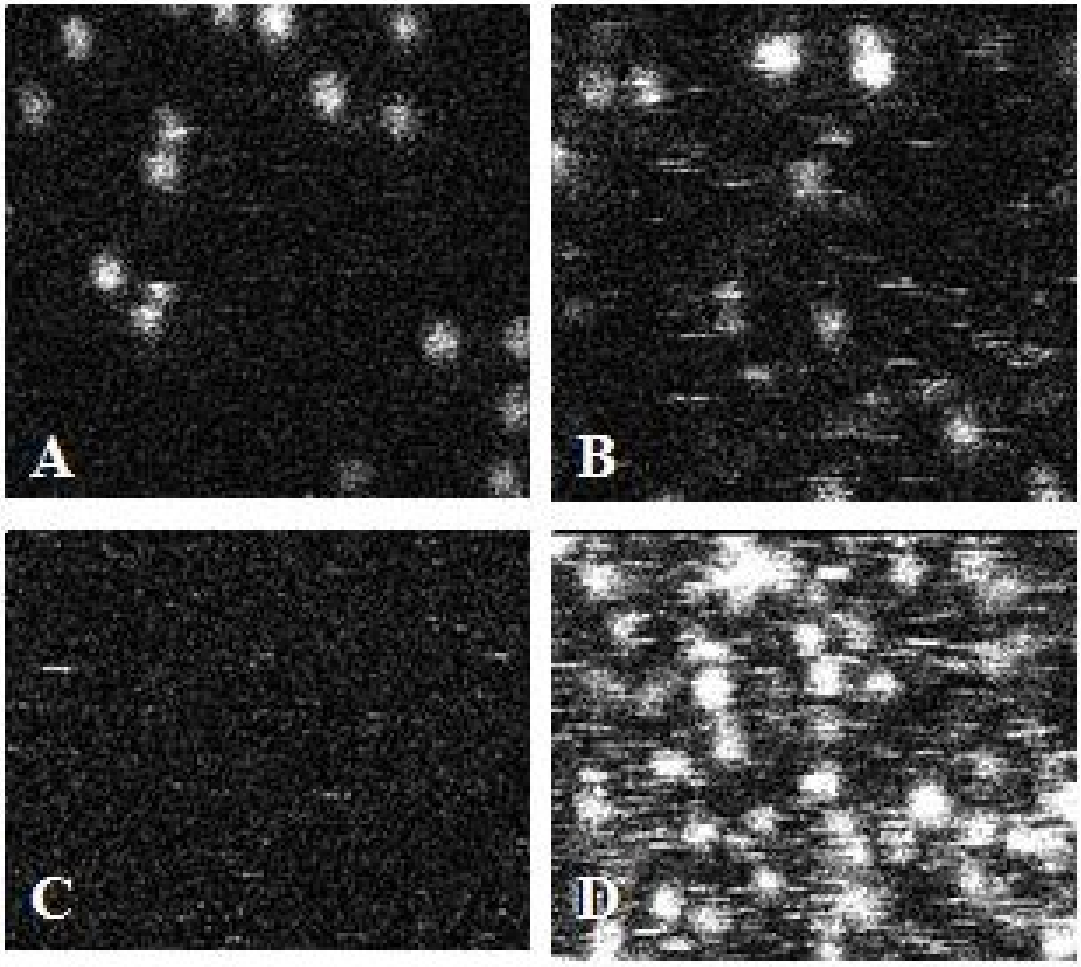
A
B
C
D

CaATP activities of the five labeled samples are shown in Table 15. The presence of AMP-PNP, a poorly-hydrolysable ATP analogue, strongly inhibits ATPase activity as shown in Table 15. The enzymes labeled at γC199/C205 or γC322 exhibited normal CaATPase activities. Single molecule trajectories were collected as described for the hybrid enzymes. Approximately 90 molecules were observed, autocorrelated and averaged under each condition. As in the previous experiments with the hybrid enzyme, periodic oscillations in the fluorescence amplitude of the rhodamine dye molecule attached to the γ dithiols in CF_1(-δε) were observed. The shifts were observed in the majority of samples examined and were well above background noise. The autocorrelation function was applied to data collected for several hundred molecules and the averaged results fit closely to a three-component exponential decay (Figure 28, Table 16). The amplitude of the third component, which was not evident in the experiments with the hybrid enzyme, comprised approximately 11% of the total signal.

Two significant effects were observed in these experiments. The first involved binding of the inhibitory ε subunit to the enzyme which led to a significant increase (11% to 30%) in the fraction of the decay that was attributed to the longest time component. Under the experimental conditions used, the ε subunit inhibited the catalytic activity of the enzyme by approximately 30%. These data are consistent with the expectation that ε binding reduces the rate of opening and closing of the regulatory region.

The second significant change was seen upon treatment of the enzyme with the poorly-hydrolysable ATP analogue AMP-PNP. AMP-PNP is known to bind to both catalytic and non-catalytic sites on CF_1, locking the enzyme into a fully inhibited conformation (Nalin and Cross, 1982). Remarkably, AMP-PNP reduced all three time constants by more than 50% without significantly affecting their relative amplitudes (Table 16). In the control

Table 15. Activities of Labeled CF_1 enzymes

Protein Sample	CaATPase Activity (μmole per min per mg protein)
$\alpha_3\beta_3\gamma^{*C199/C205}$	19.7 ± 1.67
$\alpha_3\beta_3\gamma^{*C199/C205}$ + ε	12.8 ± 1.11
$\alpha_3\beta_3\gamma^{*C199/C205}$ + AMP-PNP	1.8 ± 1.40
$\alpha_3\beta_3\gamma^{*C322}$	19.4 ± 1.99
$\alpha_3\beta_3\gamma^{*C322}$ + AMP-PNP	2.01 ± 0.89

*Denotes residue labeled with TMR. Errors are expressed as standard deviations with n = 3.

Table 16. Autocorrelation Time Constants for CF_1 enzymes

Protein Sample	Time Constant	Time (ms)	% Decay
$\alpha_3\beta_3\gamma_{*C199/C205}$	1	8.59 ± 2.12	57.7%
	2	124.03 ± 16.15	31.2%
	3	1792.84 ± 706.82	11.1%
$\alpha_3\beta_3\gamma_{*C199/C205}$ + ε	1	7.66 ± 2.27	47.7%
	2	117.28 ± 24.90	22.6%
	3	1266.38 ± 282.73	29.7%
$\alpha_3\beta_3\gamma_{*C199/C205}$ + AMP-PNP	1	3.81 ± 0.01	58.1%
	2	48.62 ± 8.33	27.3%
	3	731.44 ± 158.88	14.6%
$\alpha_3\beta_3\gamma_{*C322}$	1	9.0 ± 2.23	63.5%
	2	202.76 ± 42.1	33.4%
	3	3722.74 ± 810.65	3.1%
$\alpha_3\beta_3\gamma_{*C322}$ + AMP-PNP	1	12.4 ± 0.83	72.3%
	2	294.1 ± 30.89	24.1%
	3	4500 ± 980.12	3.6%

*Denotes residue labeled with TMR. Errors are expressed as standard deviations with n = 3.

Figure 28. ***Autocorrelation Analysis of CF_1 Single-Molecule Fluorescence Trajectories.*** Each autocorrelation decay curve represents analysis of trajectories recorded from approximately 90 single molecules. The autocorrelations were fit to a three-component exponential decay curve. All of the samples contained CaATP buffer as described in the *Experimental Procedures*: A) $\alpha_3\beta_3\gamma_{*C199/C205}$-labeled enzymes; B) $\alpha_3\beta_3\gamma_{*C199/C205}$-labeled + ε enzymes; C) $\alpha_3\beta_3\gamma_{*C322}$-labeled enzymes; D) $\alpha_3\beta_3\gamma_{*C199/C205}$-labeled + AMP-PNP enzymes.

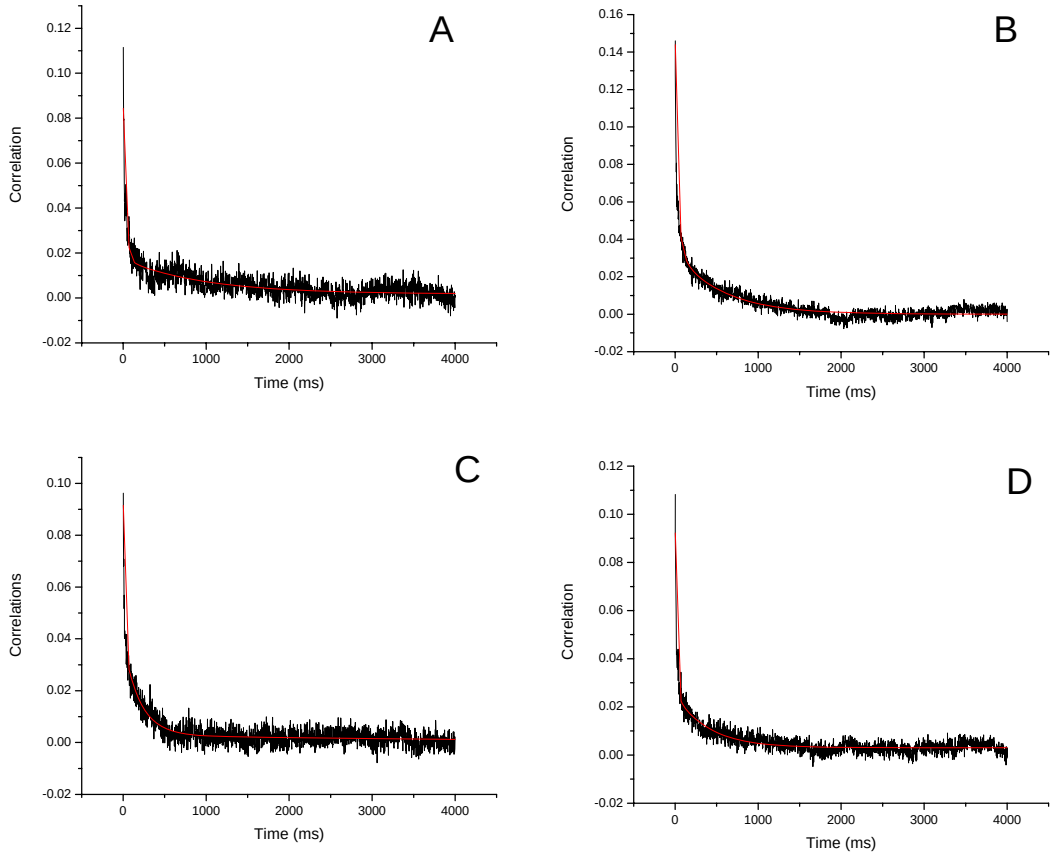
A
Correlation
Time (ms)
B
Correlation
Time (ms)
C
Correlations
Time (ms)
D
Correlation
Time (ms)

enzyme, in which the C-terminal γC322 was labeled instead of the disulfide sulfhydryls, amplitude shifts in fluorescence of the rhodamine dye were also observed (Figure 28, Table 16). The autocorrelation decay also indicated the contribution of three components. In this case, however, AMP-PNP had a very small and opposite effect to the dye on the γC199/C205 couple, causing increases of a few percent in all three time constants. The data clearly indicate that the amplitude shifts being measured when the dye molecules are placed at different positions within the enzyme represent different processes.

It should be pointed out that the relatively large standard deviations for the longer decay component reflect differences in the rate at which different molecules underwent photobleaching during the experiment. A significant number (>30%) of the surface-immobilized molecules photobleach within a few seconds after turning on the excitation light, thus minimizing the time available to measure the contribution of the longer autocorrelation decay component.

D. Discussion

The structural model of the CF_1 γ subunit, together with molecular dynamic simulations, have led to the hypothesis that a reversible opening and closing motion of the dithiol domain constrains other local domain motions within the γ subunit that modulate catalytic function. In an attempt to directly monitor the regulatory domain motion to a) detect the opening and closing movement, and b) to see if domain opening and closing occurs as a single event upon enzyme activation or if it occurs during each catalytic cycle, a fluorescent rhodamine dye was covalently attached to one of the two regulatory dithiols. The fluorescence of the rhodmine dye is sensitive to local changes in the environment such as changes in polarity and solvent accessibility. Therefore, we expected that the system could

report such changes as movement of the regulatory domain into/out of contact with the central domain of the γ subunit.

The agarose gel method of immobilizing enzyme molecules on the surfaces of glass coverslips proved to be the simplest method and provided highly reproducible measurements of dye behavior. Shifts in the fluorescence amplitude of the rhodamine dye when attached to the γC199/C205 pair on immobilized enzyme molecules were observed. The autocorrelation analysis of the data indicated that several (≥3) different environmental factors contributed to the observed amplitude shifts. While the amplitude shifts occur on a time scale that of the expected turnover rate of the enzyme (reaction time in the range of 2-20 msec), they did not appear to relate directly to catalytic turnover since they did not correlate with changes in enzyme activity. This was evident for both the hybrid and native enzymes.

Binding of the inhibitory ε subunit caused a statistically significant increase in the contribution of the longest time component in the autocorrelation decay. This is the expected consequence of binding the ε subunit to the enzyme which is hypothesized to stabilize the closed configuration of the regulatory domain (See the discussion in Chapter 2). This result implies that the observed shifts in fluorescence amplitude of the rhodamine dye are indeed sensing the opening and closing of the regulatory domain.

The observation that addition of AMP-PNP to the enzyme caused a large decrease in all three time constants is more difficult to explain. In the mitochondrial F_1, binding of AMP-PNP to catalytic and non-catalytic sites locks the enzyme into a rigid state – a prerequisite to obtaining a fixed, structurally asymmetric state of the enzyme in which inter-subunit interactions can be resolved (Menz et al., 2001). By analogy to the mitochondrial enzyme, one possible explanation for the reduced time constants observed with CF_1 in the presence of AMP-PNP is that the locked conformation induced by AMP-PNP binding results in a

conformational state in which the "closed" conformation of the regulatory domain on the γ subunit is partially destabilized. Thus, the frequency with which the domain oscillates between the open and closed conformations is increased. There is, however, insufficient information available to confirm or refute this interpretation.

To resolve the events that result in regulation by the dithiol domain, further experiments will employ a much more advanced and direct measurement of regulatory domain movement. Single-molecule fluorescence resonance energy transfer (FRET) is a powerful tool now regularly used to measure protein conformational changes (Johnson, 2006). Using FRET, a donor fluorophore is excited and, when in close proximity (<100Å) of an acceptor fluorophore, transfers energy by a non-radiative, dipole-dipole coupling mechanism to the acceptor fluorophore. In this case, increased fluorescence is observed for the acceptor and decreased fluorescence is measured for the donor fluorophore. A good donor-acceptor pair requires spectral overlap between the emission wavelength of the donor and the excitation wavelength of the acceptor. The characteristic transfer distance is known for the donor-receptor pair, thus allowing distances between residues to be measured. The distance at which energy transfer is 50% efficient (*i.e.* 50% of excited donors are deactivated by FRET) is defined by the Förster Radius (R_0). R_0 is dependent on the spectral properties of the donor and acceptor fluorophores (Richter et al., 1985).

For FRET studies, a cysteine will be introduced into the N-terminal α helix (in the region of residues 10-20) of the γ subunit so that it can be labeled with the donor thiol reactive probe. Another fluorophore, labeled at γC199/C205, will serve as the acceptor fluorophore. A common difficulty of single-molecule FRET is labeling a single protein or protein complex with two separate fluorophores at two different locations. However, using the labeling methods described in the *Experimental Procedures*, this problem is easily

avoidable when labeling the chloroplast γ subunit with thiol-reactive probes. These types of FRET experiments allow direct observation of domain motion in real-time. This technique should provide significant insight into domain motion of the regulatory domain of the chloroplast γ subunit during both catalytic and inhibited activities.

Chapter 5. Conclusion

The overall goal of the experiments described in this dissertation was to better understand the mechanism for the dithiol-dependent switch between inactive and active states within the photosynthetic F_1 enzyme. It was proposed that activation of the enzyme occurs when the C-terminal arm of the ε subunit moves away from the γ subunit, thus exposing the oxdizied disulfide and allowing it to be readily reduced, resulting in a fully activated enzyme. The exact mechanism through which inhibition by the formation of the regulatory disulfide occurs still remains unknown.

Structural analysis by preparation and characterization of deletion mutants of the regulatory domain of the γ subunit, as well as an extra loop region indicated by the homology model, have provided insight into structural changes that occur within different domains of the γ subunit in response to the redox state of the regulatory dithiol. Molecular dynamics simulations of the regulatory domain implied that when the regulatory dithiol is oxidized, the regulatory domain adopts a much more compact conformation than when the dithiol is reduced. Surprisingly, deletions within the extra loop region of the central domain of the γ subunit resulted in a loss of redox regulation. This indicates that conformational changes within the central domain may also play a role in the regulation process as it does in the *E.coli* F_1. The partial loss of ε inhibition by the extra loop deletions suggests that the C-terminal arm of the ε subunit binds across the central domain of the γ subunit. The deletion of the entire regulatory domain does not eliminate ε binding, indicating that a significant binding interaction occurs between the N-terminal β-barrel of ε and the intertwined helical elements of the γ subunit, again as shown in the *E.coli* F_1. The data suggest a model by which the ε subunit inhibits catalytic activity by a conformational change between the central

domain and the intertwined helical elements of the γ subunit that is necessary for optimal catalytic turnover.

The most remarkable feature of the regulatory domain is the ability to reduce the catalytic activity of the enzyme by ~ 50% when the regulatory disulfide is oxidized; however, the regulatory disulfide is located over 60 Å away from the catalytic sites on the enzyme. It is proposed that regulation of catalysis by the regulatory domain occurs by partially blocking an internal γ subunit movement between either the central domain and the N-terminal helices or the movement between the intertwined helices. To examine the role of interdomain movement within the γ subunit during catalysis, cysteine pairs were introduced to cross-link the N- and C-terminal intertwined helices as well as to cross-link the central domain to the C-terminal helix. Cross-linking experiments were conducted using hybrid enzyme assemblies containing each cysteinyl pair labeled with flouresceinyl malemide following exposure of the enzyme to either oxidizing or reducing conditions. The gel profiles indicated that several of the pairs of cysteines were capable of forming a cross-linking disulfide bond. ATP hydrolysis and synthesis assays, however, indicated that the redox state of the introduced cysteinyl pairs had no significant effect on activity; that is, none of the disulfide cross-links reduced catalytic function.

Two of the mutants exhibited a loss of oxyanion stimulated MgATPase activity as well as impairment of ATP synthesis, while exhibiting normal CaATPase activites. The results point to specific interactions between residues on the N- and C-terminal helices of the γ subunit and the DELSEED loop on β subunits that, while not necessary for generating rotational torque during the binding change process, are required for activation of Mg-dependent synthesis and hydrolysis by protons or oxyanions. The results are consistent with a model in which a catalytic site in one of the three β subunits adopts a state that is

specifically required for activating the enzyme in the presence of Mg^{2+} ions. This conformational state is not, as previously proposed, representative of a torque-generating step in the catalytic cycle. Experiments are currently underway to measure ATP synthesis and hydrolysis for the remaining four cysteinyl pair mutants that were not examined in this study. It is important to note that while this study has ruled out two specific interdomain motions within the γ subunit as being important for regulating catalysis, it has not ruled out all possible interdomain movements, nor has it ruled out more subtle interdomain movements that may take place even when segments of the γ subunit have been cross-linked together. Further experiments are being planned to explore the possibility that other segments of N- and C-terminal intertwined helices that may interact during catalysis.

Molecular dynamics simulations using the homology model of the γ subunit indicated the potential for a large scale structural rearrangement within the regulatory domain. In fact, the results of the simulations predicted a 10 Å movement between the extra loop region (residues 65-78) and the loop structure of the regulatory domain. Single-molecule experiments were undertaken to directly monitor conformational changes within the regulatory domain during rotational catalysis. Amplitude fluctuations of a rhodamine dye attached to one of the two cysteines located in the regulatory domain were monitored under conditions of normal CaATPase hydrolysis, with or without the ε subunit bound, and in the presence or absence of AMP-PNP. While the autocorrelation decay times generated for the various enzyme samples examined did indicate changes in the decay time constants in the enzyme samples inhibited with AMP-PNP, the data collected was difficult to interpret. Future experiments employing the use of single-molecule FRET are planned to more accurately map domain movements within the regulatory domain during catalysis.

One of the most exciting outcomes of this study is the indirect validation of the chloroplast γ subunit homology model. The molecular dynamics simulations accurately predicted that the extra loop domain played a role in the redox regulation of the enzyme, and that it may be necessary for the binding of the ε subunit. The inability of some of the cysteinyl pair mutations to form disulfides suggest that the location of these residues within the N-and C-terminal helices of the homology model were not precisely predicted. In addition, the location of some of the residues in the homology model, where the cysteine mutations were placed, are oriented on the helices in such a way that they are facing away from each other. The results indicate that there is some elasticity within the helices allowing them to adopt different orientations without loss of catalytic function. Docking simulations are planned to further explore the binding interactions of the ε subunit to the γ subunit homology model to gain further insight into the regulatory process. Ultimate resolution of the mechanism of regulation will, however, require the solution of the structure of the γ and ε subunits within the F_1 complex.

References

Abrahams, J. P., A. G. Leslie, R. Lutter and J. E. Walker (1994). Structure at 2.8 A resolution of F1-ATPase from bovine heart mitochondria. *Nature* **370**(6491): 621-8.

Al-Shawi, M. K., C. J. Ketchum and R. K. Nakamoto (1997). Energy coupling, turnover, and stability of the F0F1 ATP synthase are dependent on the energy of interaction between gamma and beta subunits. *J Biol Chem* **272**(4): 2300-6.

Andreo, C. S., W. J. Patrie and R. E. McCarty (1982). Effect of ATPase activation and the delta subunit of coupling factor 1 on reconstitution of photophosphorylation. *J Biol Chem* **257**(17): 9968-75.

Averboukh, L., S. A. Douglas, S. Zhao, K. Lowe, J. Maher and A. B. Pardee (1996). Better gel resolution and longer cDNAs increase the precision of differential display. *Biotechniques* **20**(5): 918-21.

Bianchet, M. A., J. Hullihen, P. L. Pedersen and L. M. Amzel (1998). The 2.8-A structure of rat liver F1-ATPase: configuration of a critical intermediate in ATP synthesis/hydrolysis. *Proc Natl Acad Sci U S A* **95**(19): 11065-70.

Boyer, P. D. (1993). The binding change mechanism for ATP synthase--some probabilities and possibilities. *Biochim Biophys Acta* **1140**(3): 215-50.

Boyer, P. D. (1997). The ATP synthase--a splendid molecular machine. *Annu Rev Biochem* **66**: 717-49.

Bradford, M. M. (1976). A rapid and sensitive method for the quantitation of microgram quantities of protein utilizing the principle of protein-dye binding. *Anal Biochem* **72**: 248-54.

Bragg, P. D. and C. Hou (1986). Chemical crosslinking of alpha subunits in the F1 adenosine triphosphatase of Escherichia coli. *Arch Biochem Biophys* **244**(1): 361-72.

Bragg, P. D. and C. Hou (1986). Effect of disulfide cross-linking between alpha and delta subunits on the properties of the F1 adenosine triphosphatase of Escherichia coli. *Biochim Biophys Acta* **851**(3): 385-94.

Capaldi, R. A. and B. Schulenberg (2000). The epsilon subunit of bacterial and chloroplast F(1)F(0) ATPases. Structure, arrangement, and role of the epsilon subunit in energy coupling within the complex. *Biochim Biophys Acta* **1458**(2-3): 263-9.

Cerione, R. A., R. E. McCarty and G. G. Hammes (1983). Spatial relationships between specific sites on reconstituted chloroplast proton adenosinetriphosphatase and the phospholipid vesicle surface. *Biochemistry* **22**(4): 769-76.

Chen, Z., I. Wu, M. L. Richter and P. Gegenheimer (1992). Over-expression and refolding of beta-subunit from the chloroplast ATP synthase. *FEBS Lett* **298**(1): 69-73.

Cipriano, D. J., Y. Bi and S. D. Dunn (2002). Genetic fusions of globular proteins to the epsilon subunit of the Escherichia coli ATP synthase: Implications for in vivo rotational catalysis and epsilon subunit function. *J Biol Chem* **277**(19): 16782-90.

Cipriano, D. J. and S. D. Dunn (2006). The role of the epsilon subunit in the Escherichia coli ATP synthase. The C-terminal domain is required for efficient energy coupling. *J Biol Chem* **281**(1): 501-7.

Cross, R. L. (2000). The rotary binding change mechanism of ATP synthases. *Biochim Biophys Acta* **1458**(2-3): 270-5.

Cruz, J. A., B. Harfe, C. A. Radkowski, M. S. Dann and R. E. McCarty (1995). Molecular dissection of the epsilon subunit of the chloroplast ATP synthase of spinach. *Plant Physiol* **109**(4): 1379-88.

Cruz, J. A., C. A. Radkowski and R. E. McCarty (1997). Functional Consequences of Deletions of the N Terminus of the [epsilon] Subunit of the Chloroplast ATP Synthase. *Plant Physiol* **113**(4): 1185-1192.

Digel, J. G., N. D. Moore and R. E. McCarty (1998). Influence of divalent cations on nucleotide exchange and ATPase activity of chloroplast coupling factor 1. *Biochemistry* **37**(49): 17209-15.

Du, Z. and Z. Gromet-Elhanan (1999). Refolding of recombinant alpha and beta subunits of the Rhodospirillum rubrum F(0)F(1) ATP synthase into functional monomers that reconstitute an active alpha(1)beta(1)-dimer. *Eur J Biochem* **263**(2): 430-7.

Du, Z., W. C. Tucker, M. L. Richter and Z. Gromet-Elhanan (2001). Assembled F1-(alpha beta) and Hybrid F1-alpha 3beta 3gamma -ATPases from Rhodospirillum rubrum alpha, wild type or mutant beta, and chloroplast gamma subunits. Demonstration of Mg2+versus Ca2+-induced differences in catalytic site structure and function. *J Biol Chem* **276**(15): 11517-23.

Du, Z. Y. and P. D. Boyer (1990). On the mechanism of sulfite activation of chloroplast thylakoid ATPase and the relation of ADP tightly bound at a catalytic site to the binding change mechanism. *Biochemistry* **29**(2): 402-7.

Duan, Y. and P. A. Kollman (1998). Pathways to a protein folding intermediate observed in a 1-microsecond simulation in aqueous solution. *Science* **282**(5389): 740-4.

Duncan, T. M., Y. Zhou, V. V. Bulygin, M. L. Hutcheon and R. L. Cross (1995). Probing interactions of the Escherichia coli F0F1 ATP synthase beta and gamma subunits with disulphide cross-links. *Biochem Soc Trans* **23**(4): 736-41.

Dunn, S. D. and M. Futai (1980). Reconstitution of a functional coupling factor from the isolated subunits of Escherichia coli F1 ATPase. *J Biol Chem* **255**(1): 113-8.

Evron, Y. and R. E. McCarty (2000). Simultaneous measurement of deltapH and electron transport in chloroplast thylakoids by 9-aminoacridine fluorescence. *Plant Physiol* **124**(1): 407-14.

Fierz, B., H. Satzger, C. Root, P. Gilch, W. Zinth and T. Kiefhaber (2007). Loop formation in unfolded polypeptide chains on the picoseconds to microseconds time scale. *Proc Natl Acad Sci U S A*.

Fillingame, R. H., M. E. Girvin, W. Jiang, F. Valiyaveetil and J. Hermolin (1998). Subunit interactions coupling H+ transport and ATP synthesis in F1F0 ATP synthase. *Acta Physiol Scand Suppl* **643**: 163-8.

Fillingame, R. H., P. C. Jones, W. Jiang, F. I. Valiyaveetil and O. Y. Dmitriev (1998). Subunit organization and structure in the F0 sector of Escherichia coli F1F0 ATP synthase. *Biochim Biophys Acta* **1365**(1-2): 135-42.

Gao, F., B. Lipscomb, I. Wu and M. L. Richter (1995). In vitro assembly of the core catalytic complex of the chloroplast ATP synthase. *J Biol Chem* **270**(17): 9763-9.

Gibbons, C., M. G. Montgomery, A. G. Leslie and J. E. Walker (2000). The structure of the central stalk in bovine F(1)-ATPase at 2.4 A resolution. *Nat Struct Biol* **7**(11): 1055-61.

Groth, G. and E. Pohl (2001). The structure of the chloroplast F1-ATPase at 3.2 A resolution. *J Biol Chem* **276**(2): 1345-52.

Gumbiowski, K., D. Cherepanov, M. Muller, O. Panke, P. Promto, S. Winkler, W. Junge and S. Engelbrecht (2001). F-ATPase: forced full rotation of the rotor despite covalent cross-link with the stator. *J Biol Chem* **276**(45): 42287-92.

Hara, K. Y., Y. Kato-Yamada, Y. Kikuchi, T. Hisabori and M. Yoshida (2001). The role of the betaDELSEED motif of F1-ATPase: propagation of the inhibitory effect of the epsilon subunit. *J Biol Chem* **276**(26): 23969-73.

Hara, K. Y., H. Noji, D. Bald, R. Yasuda, K. Kinosita, Jr. and M. Yoshida (2000). The role of the DELSEED motif of the beta subunit in rotation of F1-ATPase. *J Biol Chem* **275**(19): 14260-3.

Hatch, L. P., G. B. Cox and S. M. Howitt (1995). The essential arginine residue at position 210 in the alpha subunit of the Escherichia coli ATP synthase can be transferred to position 252 with partial retention of activity. *J Biol Chem* **270**(49): 29407-12.

Hausrath, A. C., G. Gruber, B. W. Matthews and R. A. Capaldi (1999). Structural features of the gamma subunit of the Escherichia coli F(1) ATPase revealed by a 4.4-A resolution map obtained by x-ray crystallography. *Proc Natl Acad Sci U S A* **96**(24): 13697-702.

He, F., H. S. Samra, W. C. Tucker, D. R. Mayans, E. Hoang, Z. Gromet-Elhanan, C. L. Berrie and M. L. Richter (2007). Mutations within the C-Terminus of the gamma Subunit of the Photosynthetic F(1)-ATPase Activate MgATP Hydrolysis and Attenuate the Stimulatory Oxyanion Effect. *Biochemistry* **46**(9): 2411-2418.

Hightower, K. E. and R. E. McCarty (1996). Proteolytic cleavage within a regulatory region of the gamma subunit of chloroplast coupling factor 1. *Biochemistry* **35**(15): 4846-51.

Hirono-Hara, Y., K. Ishizuka, K. Kinosita, Jr., M. Yoshida and H. Noji (2005). Activation of pausing F1 motor by external force. *Proc Natl Acad Sci U S A* **102**(12): 4288-93.

Hisabori, T., A. Kondoh and M. Yoshida (1999). The gamma subunit in chloroplast F(1)-ATPase can rotate in a unidirectional and counter-clockwise manner. *FEBS Lett* **463**(1-2): 35-8.

Hisabori, T., K. Motohashi, P. Kroth, H. Strotmann and T. Amano (1998). The formation or the reduction of a disulfide bridge on the gamma subunit of chloroplast ATP synthase affects the inhibitory effect of the epsilon subunit. *J Biol Chem* **273**(26): 15901-5.

Hochman, Y., A. Lanir and C. Carmeli (1976). Relations between divalent cation binding and ATPase activity in coupling factor from chloroplast. *FEBS Lett* **61**(2): 255-9.

Hu, N., D. A. Mills, B. Huchzermeyer and M. L. Richter (1993). Inhibition by tentoxin of cooperativity among nucleotide binding sites on chloroplast coupling factor 1. *J Biol Chem* **268**(12): 8536-40.

Jackson, P. J. and D. A. Harris (1988). The mitochondrial ATP synthase inhibitor protein binds near the C-terminus of the F1 beta-subunit. *FEBS Lett* **229**(1): 224-8.

Johnson, C. K. (2006). Calmodulin, conformational states, and calcium signaling. A single-molecule perspective. *Biochemistry* **45**(48): 14233-46.

Johnson, E. A. and R. E. McCarty (2002). The carboxyl terminus of the epsilon subunit of the chloroplast ATP synthase is exposed during illumination. *Biochemistry* **41**(7): 2446-51.

Junge, W., O. Panke, D. A. Cherepanov, K. Gumbiowski, M. Muller and S. Engelbrecht (2001). Inter-subunit rotation and elastic power transmission in F0F1-ATPase. *FEBS Lett* **504**(3): 152-60.

Karplus, M. (2002). Molecular dynamics simulations of biomolecules. *Acc Chem Res* **35**(6): 321-3.

Kasson, P. M., N. W. Kelley, N. Singhal, M. Vrljic, A. T. Brunger and V. S. Pande (2006). Ensemble molecular dynamics yields submillisecond kinetics and intermediates of membrane fusion. *Proc Natl Acad Sci U S A* **103**(32): 11916-21.

Keis, S., A. Stocker, P. Dimroth and G. M. Cook (2006). Inhibition of ATP hydrolysis by thermoalkaliphilic F1Fo-ATP synthase is controlled by the C terminus of the epsilon subunit. *J Bacteriol* **188**(11): 3796-804.

Ketcham, S. R., J. W. Davenport, K. Warncke and R. E. McCarty (1984). Role of the gamma subunit of chloroplast coupling factor 1 in the light-dependent activation of photophosphorylation and ATPase activity by dithiothreitol. *J Biol Chem* **259**(11): 7286-93.

Ketchum, C. J., M. K. Al-Shawi and R. K. Nakamoto (1998). Intergenic suppression of the gammaM23K uncoupling mutation in F0F1 ATP synthase by betaGlu-381 substitutions: the role of the beta380DELSEED386 segment in energy coupling. *Biochem J* **330 (Pt 2)**: 707-12.

Ketchum, C. J. and R. K. Nakamoto (1998). A mutation in the Escherichia coli F0F1-ATP synthase rotor, gammaE208K, perturbs conformational coupling between transport and catalysis. *J Biol Chem* **273**(35): 22292-7.

Komatsu-Takaki, M. (1992). Energy-dependent changes in conformation and catalytic activity of the chloroplast ATP synthase. *J Biol Chem* **267**(4): 2360-3.

Larson, E., Umbach, A., Jagendorf, A.T., (1989). Sulfite stimulated release of ADP bound to chloroplast thylakoid ATPase. *Biochim. Biophys. Acta* **973**: 78-85.

Malyan, A. N. (2006). ADP and ATP binding to noncatalytic sites of thiol-modulated chloroplast ATP synthase. *Photosynth Res* **88**(1): 9-18.

McCarty, R. E. and E. Racker (1968). Partial resolution of the enzymes catalyzing photophosphorylation. 3. Activation of adenosine triphosphatase and 32P-labeled orthophosphate -adeno-sine triphosphate exchange in chloroplasts. *J Biol Chem* **243**(1): 129-37.

Menz, R. I., J. E. Walker and A. G. Leslie (2001). Structure of bovine mitochondrial F(1)-ATPase with nucleotide bound to all three catalytic sites: implications for the mechanism of rotary catalysis. *Cell* **106**(3): 331-41.

Mitchell, P. (1961). Coupling of phosphorylation to electron and hydrogen transfer by a chemi-osmotic type of mechanism. *Nature* **191**: 144-8.

Moroney, J. V., C. S. Andreo, R. H. Vallejos and R. E. McCarty (1980). Uncoupling and energy transfer inhibition of photophosphorylation by sulfhydryl reagents. *J Biol Chem* **255**(14): 6670-4.

Moroney, J. V., C. S. Fullmer and R. E. McCarty (1984). Characterization of the cysteinyl-containing peptides of the gamma subunit of coupling factor 1. *J Biol Chem* **259**(11): 7281-5.

Moroney, J. V. and R. E. McCarty (1979). Reversible uncoupling of photophosphorylation by a new bifunctional maleimide. *J Biol Chem* **254**(18): 8951-5.

Moroney, J. V. and R. E. McCarty (1982). Effect of proteolytic digestion on the Ca2+-ATPase activity and subunits of latent and thiol-activated chloroplast coupling factor 1. *J Biol Chem* **257**(10): 5910-4.

Moroney, J. V. and R. E. McCarty (1982). Light-dependent cleavage of the gamma subunit of coupling factor 1 by trypsin causes activation of Mg2+-ATPase activity and uncoupling of photophosphorylation in spinach chloroplasts. *J Biol Chem* **257**(10): 5915-20.

Moroney, J. V., K. Warncke and R. E. McCarty (1982). The distance between thiol groups in the gamma subunit of coupling factor 1 influences the proton permeability of thylakoid membranes. *J Bioenerg Biomembr* **14**(5-6): 347-59.

Murataliev, M. B. and P. D. Boyer (1994). Interaction of mitochondrial F1-ATPase with trinitrophenyl derivatives of ATP and ADP. Participation of third catalytic site and role of Mg2+ in enzyme inactivation. *J Biol Chem* **269**(22): 15431-9.

Nadanaciva, S., J. Weber and A. E. Senior (1999). Binding of the transition state analog MgADP-fluoroaluminate to F1-ATPase. *J Biol Chem* **274**(11): 7052-8.

Nakamoto, R. K., M. K. al-Shawi and M. Futai (1995). The ATP synthase gamma subunit. Suppressor mutagenesis reveals three helical regions involved in energy coupling. *J Biol Chem* **270**(23): 14042-6.

Nakamoto, R. K., M. Maeda and M. Futai (1993). The gamma subunit of the Escherichia coli ATP synthase. Mutations in the carboxyl-terminal region restore energy coupling to the amino-terminal mutant gamma Met-23-->Lys. *J Biol Chem* **268**(2): 867-72.

Nalin, C. M., R. Beliveau and R. E. McCarty (1983). Selective modification of coupling factor 1 in spinach chloroplast thylakoids by a fluorescent maleimide. *J Biol Chem* **258**(5): 3376-81.

Nalin, C. M. and R. L. Cross (1982). Adenine nucleotide binding sites on beef heart F1-ATPase. Specificity of cooperative interactions between catalytic sites. *J Biol Chem* **257**(14): 8055-60.

Noji, H., R. Yasuda, M. Yoshida and K. Kinosita, Jr. (1997). Direct observation of the rotation of F1-ATPase. *Nature* **386**(6622): 299-302.

Nowak, K. F. and R. E. McCarty (2004). Regulatory role of the C-terminus of the epsilon subunit from the chloroplast ATP synthase. *Biochemistry* **43**(11): 3273-9.

Nowak, K. F., V. Tabidze and R. E. McCarty (2002). The C-terminal domain of the epsilon subunit of the chloroplast ATP synthase is not required for ATP synthesis. *Biochemistry* **41**(51): 15130-4.

Ogilvie, I., R. Aggeler and R. A. Capaldi (1997). Cross-linking of the delta subunit to one of the three alpha subunits has no effect on functioning, as expected if delta is a part of the stator that links the F1 and F0 parts of the Escherichia coli ATP synthase. *J Biol Chem* **272**(26): 16652-6.

Ort, D. R., and Oxborough, K. (1992). In situ regulation of the chloroplast coupling factor activity. *Annu Rev Plant Mol Biol* **43**: 269-291.

Oster, G., H. Wang and M. Grabe (2000). How Fo-ATPase generates rotary torque. *Philos Trans R Soc Lond B Biol Sci* **355**(1396): 523-8.

Patrie, W. J. and R. E. McCarty (1984). Specific binding of coupling factor 1 lacking the delta and epsilon subunits to thylakoids. *J Biol Chem* **259**(17): 11121-8.

Penefsky, H. S. (1977). Reversible binding of Pi by beef heart mitochondrial adenosine triphosphatase. *J Biol Chem* **252**(9): 2891-9.

Racker, E. (1961). Mechanisms of synthesis of adenosine triphosphate. *Adv Enzyme Regul* **23**: 323-99.

Richter, M. L. (2004). Gamma-epsilon Interactions Regulate the Chloroplast ATP Synthase. *Photosynth Res* **79**(3): 319-29.

Richter, M. L. and F. Gao (1996). The chloroplast ATP synthase: structural changes during catalysis. *J Bioenerg Biomembr* **28**(5): 443-9.

Richter, M. L., R. Hein and B. Huchzermeyer (2000). Important subunit interactions in the chloroplast ATP synthase. *Biochim Biophys Acta* **1458**(2-3): 326-42.

Richter, M. L. and R. E. McCarty (1987). Energy-dependent changes in the conformation of the epsilon subunit of the chloroplast ATP synthase. *J Biol Chem* **262**(31): 15037-40.

Richter, M. L., W. J. Patrie and R. E. McCarty (1984). Preparation of the epsilon subunit and epsilon subunit-deficient chloroplast coupling factor 1 in reconstitutively active forms. *J Biol Chem* **259**(12): 7371-3.

Richter, M. L., H. S. Samra, F. He, A. J. Giessel and K. K. Kuczera (2005). Coupling proton movement to ATP synthesis in the chloroplast ATP synthase. *J Bioenerg Biomembr* **37**(6): 467-73.

Richter, M. L., B. Snyder, R. E. McCarty and G. G. Hammes (1985). Binding stoichiometry and structural mapping of the epsilon polypeptide of chloroplast coupling factor 1. *Biochemistry* **24**(21): 5755-63.

Rodgers, A. J. and M. C. Wilce (2000). Structure of the gamma-epsilon complex of ATP synthase. *Nat Struct Biol* **7**(11): 1051-4.

Rodgers, A. J., S. Wilkens, R. Aggeler, M. B. Morris, S. M. Howitt and R. A. Capaldi (1997). The subunit delta-subunit b domain of the Escherichia coli F1F0 ATPase. The B subunits interact with F1 as a dimer and through the delta subunit. *J Biol Chem* **272**(49): 31058-64.

Sambrook, J., E. F. Fritsch, T. Maniatis, N. Irwin and T. Maniatis (1989). Molecular cloning : a laboratory manual. Cold Spring Harbor, N.Y., Cold Spring Harbor Laboratory Press.

Samra, H. S., F. Gao, F. He, E. Hoang, Z. Chen, P. A. Gegenheimer, C. L. Berrie and M. L. Richter (2006). Structural analysis of the regulatory dithiol-containing domain of the chloroplast ATP synthase gamma subunit. *J Biol Chem* **281**(41): 31041-9.

Schulenberg, B., F. Wellmer, H. Lill, W. Junge and S. Engelbrecht (1997). Cross-linking of chloroplast F0F1-ATPase subunit epsilon to gamma without effect on activity. Epsilon and gamma are parts of the rotor. *Eur J Biochem* **249**(1): 134-41.

Schumann, J., M. L. Richter and R. E. McCarty (1985). Partial proteolysis as a probe of the conformation of the gamma subunit in activated soluble and membrane-bound chloroplast coupling factor 1. *J Biol Chem* **260**(21): 11817-23.

Schwem, B. E. and R. H. Fillingame (2006). Cross-linking between helices within subunit a of Escherichia coli ATP synthase defines the transmembrane packing of a four-helix bundle. *J Biol Chem* **281**(49): 37861-7.

Senior, A. E. (1990). The proton-translocating ATPase of Escherichia coli. *Annu Rev Biophys Biophys Chem* **19**: 7-41.

Shi, X. B., J. M. Wei and Y. K. Shen (2001). Effects of sequential deletions of residues from the N- or C-terminus on the functions of epsilon subunit of the chloroplast ATP synthase. *Biochemistry* **40**(36): 10825-31.

Shirakihara, Y., A. G. Leslie, J. P. Abrahams, J. E. Walker, T. Ueda, Y. Sekimoto, M. Kambara, K. Saika, Y. Kagawa and M. Yoshida (1997). The crystal structure of the nucleotide-free alpha 3 beta 3 subcomplex of F1-ATPase from the thermophilic Bacillus PS3 is a symmetric trimer. *Structure* **5**(6): 825-36.

Slaughter, B. D., R. J. Urbauer, J. L. Urbauer and C. K. Johnson (2007). Mechanism of Calmodulin Recognition of the Binding Domain of Isoform 1b of the Plasma Membrane Ca(2+)-ATPase: Kinetic Pathway and Effects of Methionine Oxidation. *Biochemistry*.

Snyder, B. and G. G. Hammes (1985). Structural organization of chloroplast coupling factor. *Biochemistry* **24**(9): 2324-31.

Sokolov, M., L. Lu, W. Tucker, F. Gao, P. A. Gegenheimer and M. L. Richter (1999). The 20 C-terminal amino acid residues of the chloroplast ATP synthase gamma subunit are not essential for activity. *J Biol Chem* **274**(20): 13824-9.

Soteropoulos, P., K. H. Suss and R. E. McCarty (1992). Modifications of the gamma subunit of chloroplast coupling factor 1 alter interactions with the inhibitory epsilon subunit. *J Biol Chem* **267**(15): 10348-54.

Spetzler, D., J. York, D. Daniel, R. Fromme, D. Lowry and W. Frasch (2006). Microsecond time scale rotation measurements of single F1-ATPase molecules. *Biochemistry* **45**(10): 3117-24.

Suzuki, T., T. Murakami, R. Iino, J. Suzuki, S. Ono, Y. Shirakihara and M. Yoshida (2003). F0F1-ATPase/synthase is geared to the synthesis mode by conformational rearrangement of epsilon subunit in response to proton motive force and ADP/ATP balance. *J Biol Chem* **278**(47): 46840-6.

Taussky, H. H. and E. Shorr (1953). A microcolorimetric method for the determination of inorganic phosphorus. *J Biol Chem* **202**(2): 675-85.

Tozer, R. G. and S. D. Dunn (1986). Column centrifugation generates an intersubunit disulfide bridge in Escherichia coli F1-ATPase. *Eur J Biochem* **161**(2): 513-8.

Tsunoda, S. P., A. J. Rodgers, R. Aggeler, M. C. Wilce, M. Yoshida and R. A. Capaldi (2001). Large conformational changes of the epsilon subunit in the bacterial F1F0 ATP synthase provide a ratchet action to regulate this rotary motor enzyme. *Proc Natl Acad Sci U S A* **98**(12): 6560-4.

Tucker, W. C., Z. Du, Z. Gromet-Elhanan and M. L. Richter (2001). Formation and properties of hybrid photosynthetic F1-ATPases. Demonstration of different structural requirements for stimulation and inhibition by tentoxin. *Eur J Biochem* **268**(7): 2179-86.

Tucker, W. C., A. Schwarz, T. Levine, Z. Du, Z. Gromet-Elhanan, M. L. Richter and G. Haran (2004). Observation of calcium-dependent unidirectional rotational motion in recombinant photosynthetic F1-ATPase molecules. *J Biol Chem* **279**(46): 47415-8.

Uhlin, U., G. B. Cox and J. M. Guss (1997). Crystal structure of the epsilon subunit of the proton-translocating ATP synthase from Escherichia coli. *Structure* **5**(9): 1219-30.

Wilkens, S. and R. A. Capaldi (1998). Solution structure of the epsilon subunit of the F1-ATPase from Escherichia coli and interactions of this subunit with beta subunits in the complex. *J Biol Chem* **273**(41): 26645-51.

Wilkens, S., F. W. Dahlquist, L. P. McIntosh, L. W. Donaldson and R. A. Capaldi (1995). Structural features of the epsilon subunit of the Escherichia coli ATP synthase determined by NMR spectroscopy. *Nat Struct Biol* **2**(11): 961-7.

Xiong, H., D. Zhang and S. B. Vik (1998). Subunit epsilon of the Escherichia coli ATP synthase: novel insights into structure and function by analysis of thirteen mutant forms. *Biochemistry* **37**(46): 16423-9.

Yasuda, R., H. Noji, K. Kinosita, Jr., F. Motojima and M. Yoshida (1997). Rotation of the gamma subunit in F1-ATPase; evidence that ATP synthase is a rotary motor enzyme. *J Bioenerg Biomembr* **29**(3): 207-9.

Yasuda, R., H. Noji, M. Yoshida, K. Kinosita, Jr. and H. Itoh (2001). Resolution of distinct rotational substeps by submillisecond kinetic analysis of F1-ATPase. *Nature* **410**(6831): 898-904.

Yoshida, M., E. Muneyuki and T. Hisabori (2001). ATP synthase--a marvellous rotary engine of the cell. *Nat Rev Mol Cell Biol* **2**(9): 669-77.

Younis, H. M., G. D. Winget and E. Racker (1977). Requirement of the delta subunit of chloroplast coupling factor 1 for photophosphorylation. *J Biol Chem* **252**(5): 1814-8.

Zhou, Y., T. M. Duncan and R. L. Cross (1997). Subunit rotation in Escherichia coli FoF1-ATP synthase during oxidative phosphorylation. *Proc Natl Acad Sci U S A* **94**(20): 10583-7.